Postsynaptic actions of excitatory amino acids investigated with flash photolysis

A thesis submitted for the degree of
Doctor of Philosophy in the University of London

by

Kamran Khodakhah

Division of Neurophysiology and Neuropharmacology
National Institute for Medical Research
Mill Hill, London NW7 1AA
and
Department of Pharmacology
University College London

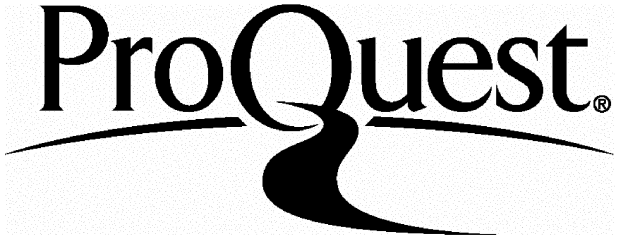

Abstract

Flash photolysis and whole cell patch clamp technique were combined with microspectrofluorimetry of calcium to study the role of inositol trisphosphate as a second messenger, and the role of L-glutamate as a neurotransmitter.

Inactive photolabile analogous of inositol trisphosphate, caged $InsP_3$, and fluorescent calcium indicators, Fluo-3 or Furaptra, was introduced into single cells *via* the whole-cell patch pipette. Astrocytes and neurones from primary cultures of cerebellar granule cells, hippocampal pyramidal cells, striatal neurones, and dorsal root ganglion neurones, and Purkinje cells from acutely prepared thin slices of the cerebellum were voltage clamped (holding potential -70mV). A 1ms pulse of near UV (300-350nm, 100mJ) was used to photolytically release a known concentration of $InsP_3$ in the cytosol, and the changes in the intracellular free calcium concentration, $[Ca^{2+}]_i$, and conductance monitored. The results may be summarised as follows: (1) Photolytic release of $InsP_3$ (100nM-30μM) in cultured neurones did not alter $[Ca^{2+}]_i$ or the membrane conductance. In glial cells from the same preparations, however, a rise in $[Ca^{2+}]_i$ was observed following intracellular release of $InsP_3$ (0.2-5μM). The concentrations of $InsP_3$ required to mobilise calcium in astrocytes is similar to that found in peripheral tissue. (2) Photolytic release of $InsP_3$ (9-76μM) in voltage clamped Purkinje neurones in acutely prepared thick slices of the cerebellum resulted in a large increase in $[Ca^{2+}]_i$, often reaching 30μM when calibrated with Furaptra, and at the same time an outward current (200-900pA) in the presence or absence of external calcium. The outward current was the result of an increase of the membrane conductance to potassium ions, and under current clamp conditions hyperpolarised the cell to approximately -85mV. The responses occurred with a latency that decreased from a few hundred ms at low (9μM) to <15ms at high (76μM) $InsP_3$ concentration. The time to peak also decreased from 900ms to <20ms over this concentration range, indicating increased calcium efflux from stores at high $InsP_3$ concentration. The concentrations of $InsP_3$ required to mobilise calcium in Purkinje neurones is higher than that required in astrocytes and peripheral tissue. The kinetics of calcium release is also faster than that in astrocytes and peripheral tissue, indicating an adaptation of $InsP_3$ signalling in Purkinje cells.

Photolabile analogues of L-glutamate would be useful to produce controlled pulses of L-glutamate to study synaptic transmission in the central nervous system. Several photolabile analogues of L-glutamate were characterised using whole cell patch clamp recording with granule cells and dorsal root ganglion neurones in culture. Five photolabile analogues of glutamate were dismissed due to low quantum yield, instability, or having activity at glutamate receptor sites. One photolabile analogue of glutamate, N(1,(2-nitrophenyl)ethoxycarbonyl)-L-glutamate, satisfied most of the criteria required for a caged neurotransmitter. Compared with L-glutamate, 1mM caged glutamate in its un-photolysed form was >10000X less potent at the NMDA, and >50X at the non-NMDA receptors. When irradiated with a 1ms pulse of near UV light (300-350nm, 100mJ) it cleaved to release L-glutamate, 2-nitrosoacetophenone, and carbon dioxide with a quantum yield of 50%. Neither caged glutamate (1mM) nor its photolysis by-products had any potency as an antagonist at the excitatory amino acid sites. The rate of photolysis was found to have a half time of about 50ms at pH7, too slow to allow for studies of rate of receptor activation. The rate of photolysis, however, is pH dependent increasing 10 fold with one pH unit drop.

The ability of the squid giant synapse to withstand acidic conditions was taken advantage of, and L-glutamate was photolytically released from caged glutamate equilibrated with the synapse at pH5.5. This abrupt release of L-glutamate elicited action potentials in the 3rd order fibre of the giant synapse providing good evidence of the role of L-glutamate as a neurotransmitter at this synapse.

This work is dedicated to my father;
maybe one day he will appreciate my love for science.

Acknowledgement

I should like to thank David Ogden, to whom I am greatly indebted. I am particularly grateful to him for two reasons. First, his admirable insistence in conceptualising thoughts based on first principles . This forced me to read and try to understand papers written, and principles established before my conception was even feasible; an exercise that I truly enjoyed and consider invaluable. Second, his desire for me to learn how to properly make, modify, and set up experimental apparatus. I spent many happy days modifying perfusion taps, altering the microscope, melting fibre optic light guides, building video-contrast enhancement circuits, and playing around with op-amps, resistors, and capacitors. I sincerely enjoyed my research.

I should like to thank Glaxo Group Research for their generous scholarship; Drs John Corrie, Amadeo De Santis, Yoshiki Katayama, John Messenger, and David Trentham for their collaboration in some of the experiments, and Drs Steve Smith, Thiery Capiod, and Tom Carter for their support.

Last, but not least, I should like to thank Kimberley for her love and tolerance.

Table of contents

List of Tables

List of Figures

List of Photographs

Chapter 1
Introduction

1. Excitatory amino acids as neurotransmitters

The excitatory effects of L-glutamic and L-aspartic acid on cerebral cortical neurones were first demonstrated by direct intracarotid injections by Japanese workers studying epilepsy some forty years ago (Okamoto, 1951; Hayashi, 1952). However it was not until several years latter that systematic ionophoretic application of a variety of amino acids on spinal cord and cortical neurones (Curtis *et al*, 1959, 1960; Curtis and Watkins, 1960, 1963; Krnjevic and Phillis, 1963) provided strong evidence in support of the role of excitatory amino acids as neurotransmitters. Since then the excitatory actions of acidic amino acids has been demonstrated in a variety of tissues and the role of L-glutamate as a neurotransmitter in the central nervous system (CNS) is well established (cf Watkins and Evans, 1981). L-glutamate or L-aspartate are thought to be the endogenous neurotransmitter substance and in the CNS they mediate fast synaptic transmission by activating ligand-gated cation channels and modulate postsynaptic excitability function by activating second messenger linked 'metabotropic' receptors.

As early as 1963 it was shown that of a large number of dicarboxylic amino acids tested on spinal cord neurones (Curtis and Watkins, 1963) the synthetic analogue of aspartate *N*-methyl-D-aspartate (NMDA) (Watkins, 1962) was the more potent. Subsequently other analogues of glutamate and aspartate, kainic (Shinozaki and Konishi, 1970; Johnston *et al*, 1974), and quisqualic acids (Takemoto *et al*, 1972, Shinozaki and Shibuya, 1974; Biscoe *et al*, 1975) were discovered and shown to posses excitatory potencies. The use of these various agonists, together with the development of antagonists has indicated that there are at least five different classes of glutamate receptor in the mammalian central nervous system (CNS) (cf Foster and Fagg, 1984; Nicoll *et al*, 1990). Three of these receptors are ligand gated cation channels and are the main receptors mediating fast synaptic transmission in the central nervous system. These receptors, on the basis of their activation by selective agonists, have been classified as NMDA, (S)-α-amino-3-hydroxy-5-methyl-4-isoxazole propionic acid (AMPA), and kainate. The other two glutamate receptors are those which do not directly modulate a plasma membrane ion channel, but exert their action *via* a second messenger. These include a family of receptors activated by quisqualate, collectively called the glutamate metabotropic receptors (mGluR), and a presynaptic glutamate receptor selectively activated by 2-amino-4-phosphonobutyrate (AP4).

1.2. Ion channels activated by glutamate

Of the three glutamate gated ion channels NMDA is the most widely studied and characterized, probably because of early synthesis of selective antagonists such as D-2-amino-5-phosphonovalerate (AP5 or APV) (Davies *et al*, 1981). Activation of this receptor results in the opening of a channel to several different conductance levels (Cull-Candy and Usowicz, 1987), with the channel permeable to both Na^+ and Ca^{2+} ions with a permeability ratio Ca^{2+}:Na^+ of about 10.6 (Mayer and Westbrook, 1987). This receptor is particularly interesting because it has a current voltage relationship strongly dependent on the concentration of magnesium ions bathing the channel, so that in the presence of low concentrations of magnesium an area of negative slope conductance is observed. This is because of an open channel block of the NMDA receptors with magnesium ions between about -60 to -30mV (Nowak *et al*, 1984; Mayer *et al*, 1984). The voltage dependence of the NMDA channels with magnesium ions, and the presence of about 1mM Mg^{2+} in the cerebrospinal fluid results in production of a very small current due to activation of the NMDA receptors at membrane resting potentials. The NMDA receptors are also modulated by glycine in a strychnine independent manner, so that the activation of the receptors is greatly potentiated in the presence of nanomolar concentrations (Johnson and Ascher, 1987), and indeed is dependent on the presence of glycine (Klenecker and Dingledine, 1988). NMDA receptors also have a high probability of opening by L-glutamate so that following binding glutamate and glycine 70% of them open before glutamate unbinds, and of those channels that do open 60% open before 20ms after binding glutamate (Jahr, 1992). Furthermore these receptors are shown to be inhibited by physiological concentrations of protons (Traynellis and Cull-Candy, 1990; Tang *et al*, 1990).

The complementary DNAs encoding distinct and alternatively spliced forms of the NMDA receptor subunits have been cloned and characterized (Moriyoshi *et al*, 1991; Kumar *et al*, 1991; Nakanishi *et al*, 1992; Kutsuwada *et al*, 1992; Sugihara *et al*, 1992). These subunits form heteromeric NMDA receptor channels (Meguro *et al*, 1992; Monyer *et al*, 1992) which are functionally distinct (for a review see Nakanishi, 1992). The amino acids controlling the sensitivity of the NMDA channel to block by Mg^{2+} and its permeation to Ca^{2+} have been identified (Mori *et al*, 1992; Burnashev *et al*, 1992; Sakurada *et al*, 1993).

The classification of the non-NMDA receptors have been more difficult than that of the NMDA. It has been only recently that selective non-NMDA antagonists, the quinoxalinediones 6-cyano-7-nitroquinoxaline-

2,3-dione (CNQX), and 6,7-dinitroquinoxaline-2,3-dione (DNQX) have become available (Honore *et al*, 1988). In contrast to NMDA receptors these receptors have little permeability to divalent cations (Mayer *et al*, 1987), activate rapidly with a rise time as low as <100μs (Silver *et al*, 1992; see also Hesterin et al, 1990; Keller *et al*, 1991; Jonas and Sakmann, 1992; Stern *et al*, 1992; Colquhoun *et al*, 1992) and mediate fast synaptic transmission in the CNS. Non-NMDA receptors desensitize rapidly, time constant between 9.3-11.3ms (Colquhoun *et al*, 1992), with the decay of the current faster after a brief pulse compared to a long pulse of glutamate (Dudel *et al*, 1990; Colquhoun *et al*, 1992; but see also Trussel and Fischbach, 1989).

Following cloning of the complementary DNA by functional expression of kainate-gated ion channels (Hollman *et al*, 1989), non-NMDA glutamate subunit genes GluR1, GluR2, GluR3 (Boulter *et al*, 1990), and GluR5 (Bettler *et al*, 1990) have been cloned and functionally expressed in Xenopus oocytes. Hetromultimeric receptors composed of different subunits have distinct channel properties (Nakanishi *et al*, 1990), so that Ca^{2+} permeability of kainate-AMPA-gated receptors depends on their subunit composition (Hollman *et al*, 1991; Burnashev *et al*, 1992). Single amino acids in the glutamate receptor subunits that control the current-voltage behaviour (Verdoorn *et al*, 1991; Curutchet *et al*, 1992) and Ca^{2+} permeability (Hume *et al*, 1991; Mishina *et al*, 1991) have been identified by site directed mutagenesis. A cDNA for a glutamate receptor subunit activated by kainate but not AMPA has also been cloned (Egebierg *et al*, 1991).

1.3. Excitatory amino acids and synaptic transmission

Although a great deal is known about the single channel properties of glutamate gated receptors, most of this information has been obtained by the study of these channels in xenopus oocytes or neuronal culture preparations where synaptic contact between cells is often absent or greatly modified. Therefore much less is known about the role of these receptors during synaptic transmission. The advances in preparation of slices with relatively intact synaptic connections from the nervous system in which individual neurones could be visually identified (Takahashi, 1978), and high resolution patch clamp recordings obtained (Edwards *et al*, 1989) has allowed the study of the function of glutamate gated ion channels during synaptic transmission (see for example Hestrin *et al*, 1990; D'Angelo *et al*, 1990; Llano *et al*, 1991, Stern *et al*, 1992; Silver *et al*, 1992). Co-localization of NMDA and non-NMDA receptors at the same synapse results

in the presence of two pharmacologically distinct synaptically evoked currents. Activation of non-NMDA receptors results in a current with rapid onset (<1ms to peak) and fast decay (<10 ms) though that of the NMDA receptors are slower to peak (rise time of about 8ms) and decay in hundreds of milliseconds. The long time course of the NMDA component, about 100 times longer than its mean open time (Cull-Candy and Usowicz, 1987), is not as the result of continuous presence of the neurotransmitter but is solely determined by the channel kinetics of NMDA receptors (Lester *et al*, 1990). The time course of free glutamate in the synaptic cleft, estimated by kinetic analysis of the displacement of a rapidly dissociating competitive antagonist from NMDA receptors, suggests that during synaptic transmission glutamate peaks at 1.1mM and decays with a time constant of 1.2s (Clements *et al*, 1992), in agreement with estimates obtained from other experiments (see for example Silver *et al*, 1992; Colquhoun *et al*, 1992). Although millimolar concentration of L-glutamate results in saturation of the NMDA receptors the much faster dissociation of glutamate from non-NMDA receptors suggests that dissociation contributes to the decay of these currents. Experiments during which the neurones in slices were well-clamped, for example in stellate cells of the visual cortex (Stern *et al*, 1992) and granule cells of the cerebellum (Silver *et al*, 1992) have found that excitatory post synaptic currents in the presence of NMDA receptor antagonists have rise times of about 0.2ms and decay time constants of 2.4 or 1.3ms. These data are in agreement with those reported from outside-out patches obtained from hippocampal pyramidal cells in slices following 1ms application of glutamate (Colquhoun *et al*, 1992).

To study the processes involved in synaptic transmission in more detail it is necessary to be able to mimic the action of the neurotransmitter during synaptic transmission by rapid application of active compounds to the synaptic cleft. This has been particularly fruitful at the neuromuscular junction where the post synaptic region is easily identifiable and approachable for the rapid application of compounds with a pressure pulse or ionophoretic microelectrode (see for example Kuffler and Yoshikami, 1975). However the complex morphology of the synapses at the central nervous system combined with the short distance across the synaptic cleft (about 0.1µm) results in the presence of an effective diffusion barrier for the compounds applied to the synaptic region. This diffusion barrier results in the delayed and nonuniform arrival of compounds applied to the postsynaptic region, yielding ambiguous information.

1.4. The technique of flash photolysis

One approach to this problem has been the use of light-activated compounds. The quaternary ammonium compound bis-Q was the first photo-sensitive compound to be used in physiology. Bis-Q is a potent cholinergic agonists in its *trans* form, but void of any potency as its *cis* isomer. The *cis*-bis-Q, however, is light sensitive and following a pulse of UV light isomerises to produce the biologically active *trans*-bis-Q. The process of transition from the inactive isomer to the active isomer following a pulse of light is rapid, thus permitting the production of a rapid jump in the concentration of a cholinergic agonist. By allowing a solution containing a known concentration of *cis*-Bis-Q to equilibrate with a voltage clamped electrophorus electroplaque preparation, and converting it to *trans*-bis-Q with a pulse of light, Lester was able to follow the kinetics of activation of the nicotinic ACh receptors (Lester, 1977). Although this type of photo-sensitive compounds is no longer used, the principles and method of use of caged compounds is the same. A known concentration of a biologically inactive, photolabile analogue of compound of interest (caged compound) is allowed to equilibrate with the preparation, and a known concentration of the biologically active compound is photolytically released following a pulse of UV light (Figure 1.1). The result is a spatially uniform rapid concentration step, with kinetics only dependent on the photolysis reaction, and independent of diffusion. The caged compound has often the additional advantage of not being a substrate for the uptake mechanisms or metabolic pathways due to the presence of the protective group. These compounds can therefore be introduced into the cells by injection or via the whole cell patch pipette and used with the same ease intracellularly as they would be extracelluarly (Figure 1.1).

A number of photolabile analogues of active molecules have been synthesised and used to elucidate diverse physiological mechanisms. These compounds include the nicotinic acetylcholine receptor agonist caged carbamoyl choline (Walker *et al*, 1986), caged intracellular messengers such as cyclic nucleotide cGMP and cAMP (Nerbonne *et al*, 1984) or nucleotide phosphate ATP (Goldman *et al*, 1982), $InsP_3$ (Walker *et al*, 1989), and caged divalent cations the nitr series compounds and DM-nitrophen (Tsien and Zucker, 1986; Kaplan and Ellis-Davies, 1988). To be able to take advantage of the technique of flash photolysis when studying glutamatergic synaptic transmission in the CNS several photolabile analogues of caged glutamate were synthesized by Drs John Corrie, Yoshiki Katayama, Gordon Reid, and David Trentham at the Division of Physical Biochemistry, National Institute for Medical Research, London. To be used as a caged glutamate, however,

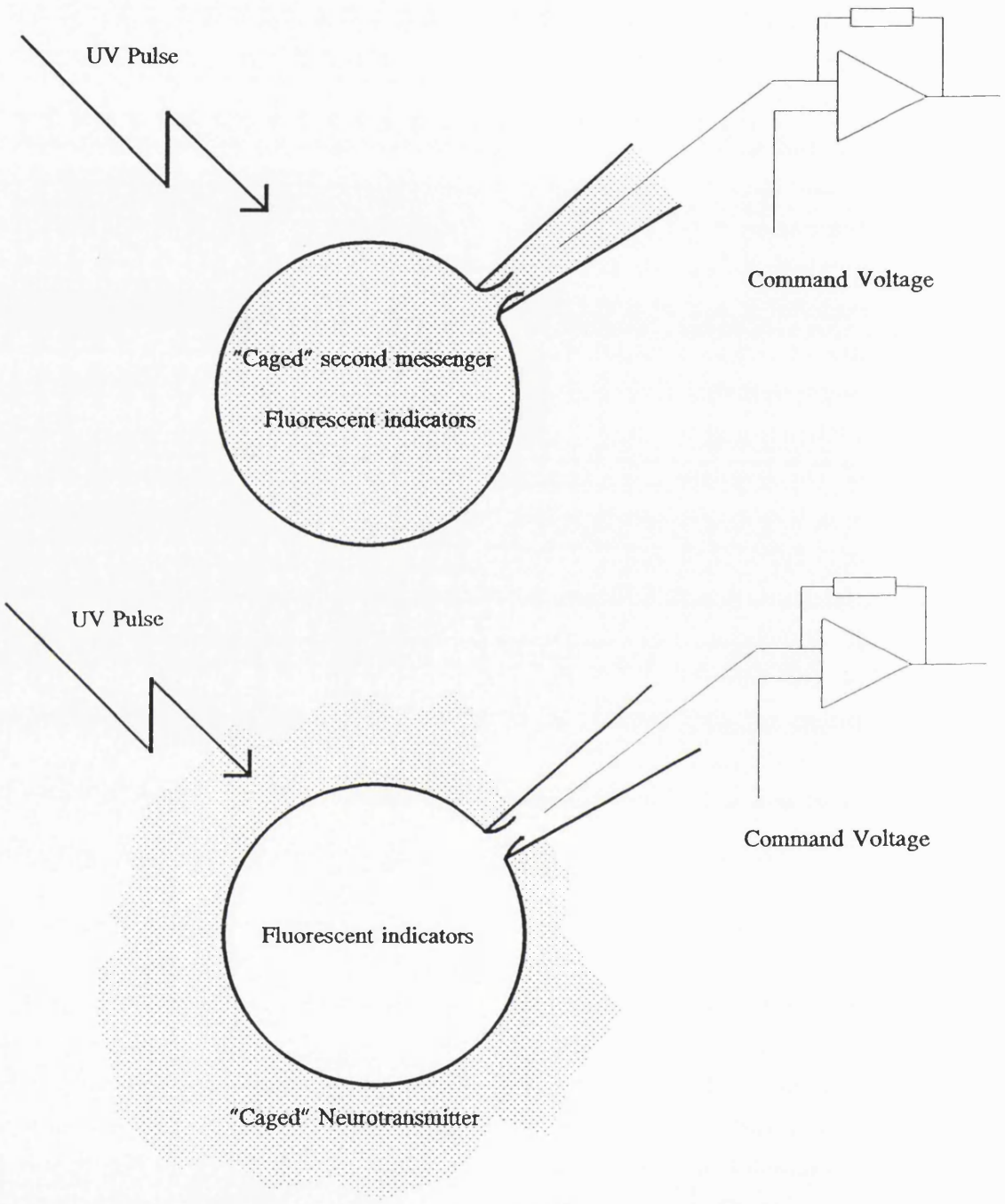

Figure 1.1 The technique of flash photolysis

The biologically inactive caged compound is allowed to equilibrate with the preparation. A short pulse of near UV light results in the spatially uniform photolytic release of the biologically active compound, with kinetics only dependent on the photolysis reaction and independent of diffusion.

the photochemical and pharmacological properties of each compound need to be characterized and its suitability as a caged neurotransmitter established. Specifically neither the photolabile compound, nor the byproducts and intermediates of photolysis should activate, nor interfere with the activation of glutamate receptors or its uptake mechanism. Furthermore the rate of photolysis of the compound, and the kinetics of release of glutamate should be faster than the rate of activation of glutamate receptors. Chapter 3 outlines the principles and experiments necessary for characterization of a caged neurotransmitter by providing data for *N*(1,(2-nitrophenyl)-ethoxycarbonyl)-L-glutamate, the only photolabile analogue of glutamate synthesized that satisfied most of the criteria required for a caged neurotransmitter. Chapter 4 demonstrates the use of this compound to show that abrupt application of glutamate to the squid giant synapse results in production of postsynaptic action potentials, providing good evidence for the glutamatergic nature of fast synaptic transmission at this synapse. This phenomenon had not been possible to demonstrate because of the complex and inaccessible nature of the synapse. Although the experiments described demonstrate the use of technique of flash photolysis in studying synaptic transmission they point out that in order to take full advantage of the technique it is necessary to restrict the area illuminated by the pulse of UV light so that the caged compound is photolyzed only in the synapse. The technical requirements for this are discussed in chapter 6.

1.5. Glutamate 'metabotropic' receptors

Stimulation of glutamate 'metabotropic' receptors trigger, *via* a G protein, the activation of intracellular second messenger systems. The second messenger pathway most predominantly activated by these receptors is the hydrolysis of phosphotidylinositol bisphosphate resulting in the generation of inositol 1,4,5 trisphosphate ($InsP_3$) and diacylglycerol (DAG). The stimulation of phosphoinositide hydrolysis by glutamate and formation of inositol 1,4,5-trisphosphate was first demonstrated in striatal neurones in culture (Sladeczek *et al*, 1985). The presence of a G protein linked receptor activated by glutamate, mediating inositol phospholipid metabolism was demonstrated by characterisation of responses of xenopus oocytes injected with the rat-brain messenger RNA to quisqualate and kainate (Sugiyama *et al*, 1987). The cDNA for a metabotropic glutamate receptor, mGluR1, was isolated and characterized in 1991 (Masu *et al*, 1991; Houamed *et al*, 1991) and since then four other receptors, mGluR2-4 (Tanabe *et al*, 1992) and mGluR5 (Abe *et al*, 1992) have been characterized.

These receptors form a family of related, but distinct genes that have a unique structural architecture with a large amino-terminal sequence preceding the seven membrane-spanning domains and share no sequence similarity with other members of G-protein linked receptors (Masu *et al*, 1991; Houamed *et al*, 1992; Tanabe *et al*, 1992; Abe *et al*, 1992). Although both mGluR1, and mGluR2 modulate phosphoinositide metabolism, mGluR5, unlike mGluR1, is not capable of inducing stimulation of the cAMP cascade (Masu *et al*, 1991; Abe *et al*, 1992). These receptors are differentially expressed in neuronal cells; Purkinje cells of the cerebellar cortex, for example, show selective expression of mGluR1 mRNA whereas hippocampal CA1 pyramidal cells show selective expression of mGluR5 (Abe *et al*, 1992). mGluR2 is not involved in phosphoinositide metabolism but mediates inhibition of forskolin-stimulated cAMP formation in cDNA transfected cells (Tanabe *et al*, 1992). It is not clear yet which second messenger system is activated by mGluR3 and mGluR5.

An increase in phosphoinositide metabolism following stimulation with glutamate, quisqualate, or what might be a selective metabotropic agonist, trans-1-amino-cyclopentyl-1,3-dicarboxylic acid (trasn-ACPD), (Palmer *et al*, 1989) has been shown in cells originating from many neuronal tissues such as hippocampal (Nicoletti *et al*, 1986a; Schoepp and Johnson, 1988), and cortical (Godfrey *et al*, 1988, Challiss *et al*, 1988) slices, primary cultures of striatal neurones (Sladeczek *et al*, 1985), cerebellar granule cells (Nicoletti *et al*, 1986b), astrocytes (Pearce *et al*, 1986; Nicoletti *et al*, 1990), and rat brain synaptosomes (Recasens *et al*, 1987). However despite the presence of the extensive literature on activation of phosphoinositide signal transduction by glutamate in neurones a rigorous characterization of the subsequent effects of the activation of this pathway on the membrane excitability and intracellular free calcium concentration, $[Ca^{2+}]_i$, has not been done. Therefore although it is likely that phosphoinositide metabolism is not the only second messenger system activated by metabotropic glutamate receptors it was the second messenger system selected for further study in this thesis.

From experiments carried mainly on peripheral tissues it is believed that the hydrolysis of phosphotidylinositol bisphosphate results in the generation of inositol 1,4,5 trisphosphate ($InsP_3$) and diacylglycerol (DAG). DAG enhances the activity of protein kinase C (PKC) by making it more sensitive to stimulation by Ca^{2+} (Nishizuka, 1988), while low micromolar concentrations of $InsP_3$ mediates calcium mobilization (Berridge, 1987; Berridge and Irvine, 1989) by activating a calcium channel present in the membrane of the intracellular stores, the $InsP_3$ receptor. In the central

nervous system it is believed that stimulation of $InsP_3$ production and the subsequent release of calcium from intracellular stores by glutamate may be important in modifying the excitability of neurones and may be involved in processes such as neurotransmitter release or long term potentiation (for reviews see Henzi and MacDermott, 1992; Ferris and Snyder, 1992). The data in support of these hypotheses, however, is limited. There is good evidence for the heterogeneous presence of $InsP_3$ receptor binding sites in the rat brain (Worly *et al*, 1987; Worly *et al*, 1989; Mignery *et al*, 1990; Maeda *et al*, 1991), with the Purkinje cells of the cerebellum having the highest density of $InsP_3$ receptor binding sites. Furthermore in Purkinje cells $InsP_3$ receptors are shown to be localized to the calcium stores, the endoplasmic reticulum, (Ross *et al*, 1989; Satoh *et al*, 1990; Otsu *et al*, 1990). Molecular cloning has shown the presence of several different $InsP_3$ receptor mRNAs in the brain, each heterogeneously distributed (Dannof *et al*, 1991; Nakagawa *et al*, 1991; Ross *et al* 1992) and different from that in the periphery, although there is no information regarding the functional properties of these receptors. Rapid mixing experiments using $^{45}Ca^{2+}$ with tissue derived from the CNS indicate that low micromolar concentrations of $InsP_3$ mediates release of calcium (Finch *et al*, 1991). Furthermore $InsP_3$ receptors from canine cerebellum reconstituted in lipid bilayers activate with low concentrations of $InsP_3$ (Bezprozvanny *et al*, 1991). However in both experiments the neuronal origin of the $InsP_3$ receptor can not be ascertained since the possibility that the receptors arise from glia can not be overlooked. Chapter 5 describes experiments during which the functional properties of $InsP_3$ mediated calcium release from intracellular stores in cultured cerebellar astrocytes, hippocampal pyramidal cells, striatal neurones, dorsal root ganglion neurones and Purkinje cells in acutely prepared slices of the cerebellum were studied. In these experiments $InsP_3$ was rapidly released in the cytosol of single cells by photocleavage of caged $InsP_3$, $[Ca^{2+}]_i$ monitored with microspectrofluorimetry, and the whole cell conductance with the whole cell clamp amplifier. These experiments provide the first direct evidence for calcium mobilization by $InsP_3$ in intact mammalian neurones, and bring to light interesting differences between $InsP_3$ signalling in non-excitable tissue and that of Purkinje cells.

It is necessary to provide an overview of the mechanism by which intracellular free calcium is regulated, and its role in cell physiology. The following sections aim to provide such background.

1.6. Calcium as a second messenger

Calcium is one of the second messengers used by physiological systems to link events that occur at the cell membrane, such as membrane depolarisation and ligand-receptor interaction, with intracellular mechanisms, such as contraction, transmitter and hormone release, or activation of biochemical and molecular processes. The total amount of intracellular calcium varies from cell to cell; brain cells contain 1.5mM calcium (Widdowson & Dickerson, 1964), Heart cells 4mM (Widdowson & Dickerson, 1964), and axons 200-400µM (Keynes & Lewis, 1956). In higher organisms the concentration of calcium in the blood plasma is regulated to approximately 3mM by movement of calcium from bones and teeth (Ames *et al*, 1964). A calcium concentration of about 1.7mM (Ames *et al*, 1964) is achieved in the cerebrospinal fluid, the solution bathing the cells in the nervous system, by diffusional leak and active transport across the blood-brain barrier (Graziani *et al*, 1967; Wright, 1972). The essential difference between intracellular and extracelluar calcium is that in the blood plasma and the CSF more than half of the total calcium is ionised resulting in a free calcium concentration of approximately 1.5mM, whereas within cells only 0.1% or less of the total calcium is ionised. The low concentration of free intracellular calcium, $[Ca^{2+}]_i$, was demonstrated by Hodgkin and Keynes when they injected radioactive Ca^{2+} into the giant axon of a squid, and found that the diffusion of Ca^{2+} when a voltage gradient was applied was very limited over a period of hours. By comparing the rate of diffusion of Ca^{2+} in the axoplasm and in solution Hodgkin and Keynes (1957) concluded that the ionised Ca^{2+} in the axoplasm was less than 0.022% of the total calcium, ie less than 0.1 µM.

The regulation and maintenance of Ca^{2+} ions at low concentrations intracellularly is done by presence of special Ca^{2+}-binding proteins and pumps, the first of which, troponin C, was described by Ebashi almost 30 years ago (Ebashi, 1963). These belong to two groups, the membrane-intrinsic proteins which act as pumps, and the nonmembranous proteins. Two types of membrane-intrinsic calcium binding proteins have been found; first Ca^{2+} ATPase calcium pumps which export Ca^{2+} from the cell (Schatzmann, 1966), or into intracellular organelles such as endoplasmic (sarcoplasmic) reticulum (MacLennan, 1970), and second Na^+/Ca^{2+} exchangers in the plasma membrane (Reuter & Seitz, 1968; Blaustein & Hodgkin, 1968) which transports Ca^{2+} out of the cells down the electrochemical gradient of Na^+. The membrane-intrinsic proteins provide an almost nonsaturable buffering capacity; they bind Ca^{2+} on one side of the membrane (the plasma membrane, or the membrane of organelles), transport it across, and

return either uncomplexed or carrying a Na^+ to repeat the transport cycle.

The nonmembranous calcium binding proteins such as troponin C, parvalbumin, and calmodulin which reversibly bind Ca^{2+} have a limited buffering capacity. The main role of these proteins is not that of calcium buffering but is mainly the shaping and transmission of the calcium signal. These proteins bind two to four Ca^{2+} and upon binding Ca^{2+} acquire the ability to interact with enzyme targets. The most studied of these proteins is calmodulin which after binding four Ca^{2+} ions with a high affinity interacts with a large number of cellular enzymes a few of which are adenylate cyclase, the nucleotide phosphodiesterase, phospholamban, and the Ca^{2+}-pumping ATPase of plasma membranes.

1.7. The measurement of the intracellular free calcium

The investigation of the role of intracellular calcium in cell function has lead to the development and use of several techniques for its measurement. Techniques such as radioactive tracers and flame photometry were employed as early as mid-fifties for the measurement of the total intracellular calcium. However, the effective concentration of calcium which drives mass action reactions and quantitatively balances them is the hydrated, ionized species which exist in much less concentrations compared to the total, largely bond calcium. Ideally a technique used for the measurement of the free intracellular calcium concentration, $[Ca^{2+}]_i$, should be able to detect Ca^{2+} in low nM concentrations, in the presence of a large excess of Mg^{2+} and other physiological cations, and should be able to report transient changes in $[Ca^{2+}]_i$ (with millisecond resolution) without modifying calcium buffering capacity of the cytosol. Techniques utilized include the use of ion selective microelectrodes, $^{45}Ca^{2+}$ flux measurements, optical indicators, and nmr spectroscopy. It is not the purpose of this script to review these techniques, and is sufficient to point that no one method used so far satisfies all of the requirement listed above. The principle and limitation of use of fluorescent optical indictors, however, will be discussed since it forms the basis of the experiments reported here.

1.8. Fluorescent calcium indicators

Fluorescent calcium indictors are chemicals that following binding calcium ions rearrange increasing or decreasing their fluorescent quantum yield. These compounds are introduced into the cytosol and the fluorescence emitted is measured by a photomultiplier or photodiode,

capable of detecting changes in the calcium concentration with millisecond time resolution. The range of detectable calcium concentration depends on the affinity, concentration, and the change in the quantum efficiency of the dye following binding calcium, as well as the efficiency of the experimental apparatus used.

The first rationally designed high affinity fluorescent Ca^{2+} indicators were synthesised by altering the structure of the Ca^{2+} chelator ethylene glycol bis(ß-aminoethyl ether)-N,N,N',N',-tetraacetic acid, EGTA (Tsien, 1980); resulting in compounds with great selectivity for calcium against magnesium ions. Fluo-3, based on the calcium chelator BAPTA, is one such fluorescent indicator with excitation and emission wavelengths in the visible spectrum (506, 526 nm excitation & emission fluorescence maxima with excess Ca^{2+}) that increases its quantum efficiency upto 40 fold with increasing [Ca^{2+}] (effective K_D 0.40 µM) in solution (Minta *et al*, 1989). The fact that this indicator does not require excitation at the UV range allowed its use in flash photolysis experiments, where UV illumination results in unwanted photolysis. However, as discussed in chapter 2, the high affinity of this dye results in local saturation and a gross deviation from linearity, so cannot be used for quantitative measurements of large calcium transients. For this purpose the fluorescent indicator Furaptra, which has a much lower affinity for calcium, was used. Furaptra was developed from the magnesium chelator APTRA (Raju *et al*, 1989), has a K_D of 44µM for Ca^{2+} and 5.3mM for Mg^{2+}, (Konishi *et al*, 1991), and can be used, with care, to measure large calcium transients.

The effect of these indicators on the rate of diffusion and buffering of intracellular calcium is discussed in chapter 2.

Chapter 2
Experimental methods and underlying theory

2. Introduction

In this chapter a description of the experimental apparatus and preparations will be given and the principles of the techniques and their limitations will be discussed.

2.1. Preparations

All chemicals were purchased from Sigma, UK unless otherwise stated.

2.2. Explant cultures of cerebellar granule cells

Cerebella were removed from Wistar rat pups (6- to 8-days-old) killed by decapitation and transferred to Eagle's essential medium (Flow Laboratories) containing 10% fetal calf serum (heat inactivated; Imperial Laboratories), penicillin (100units/ml; Flow Laboratories) and streptomycin (100units/ml; Flow Laboratories). The meninges were removed, and the cerebella were chopped (0.4mm) with a McIlwian tissue chopper in two perpendicular directions. The slices were collected and medium was added to obtain a 15ml suspension. This suspension was drawn into a syringe, and gently passed through 1.1mm and 0.8mm diameter needles successively. The resulting explants were allowed to settle for a few minutes and the upper 12ml was plated onto cover-slips (No 1, 13mm & 40mm diameter) which had previously been coated with poly-l-lysine (10µg/ml in distilled water for 2 hours), poly-ethylene-imine (0.1% in borate buffer, pH 8.6 for one hour), or laminin (20µg/ml in borate buffer, pH 8.6; > half an hour on previously poly-l-lysine coated coverslips). A ratio of one cerebellum to five 13mm cover-slips was used. Explants were maintained in culture medium at 37°C in a humidified incubator gassed with 5% CO_2:95% air. The medium was replaced three times a week. For experiments individual cover-slips were fixed to the bottom of a recording chamber with vaseline (Glisseal, Borer Chemicals).

2.3. Explant cultures of the hippocampus and the striatum

Seventeen to eighteen days after mating a pregnant Wistar rat was anaesthetized with diethyl-ether and decapitated. Following an incision in its lower abdomen the gravid uterus was removed and placed in serum free medium. All the embryos were dissected from the uterus, separated from their amniotic sac and decapitated. The brains were removed and the

hippocampi and striatum were dissected and placed in individual petri dishes containing serum free medium. The tissue was chopped, triturated and plated following the same procedure as that of cerebellar explant cultures. For these explants, however, one hippocampus, or striatum was used per two 13mm cover-slips.

2.4. Explant cultures of Dorsal root ganglion neurones

Spines were removed from 1-day or 6- to 8-day-old neonatal rats, cut open and the spinal cord was taken out allowing the visualization of ganglions embedded in the cavities. The dorsal root ganglia were pooled and incubated in 1ml of dissociation culture media containing 0.2% collagenase (Worthington Biochemical), 0.1% hyaluronidase , 0.02% trypsin inhibitor, for two hours at 37°C in a water-saturated incubator gassed with 5% CO_2:95% air. The solution containing the tissue was triturated using a polished pastor pipette and centrifuged at 1000rpm for 5 minutes. The supernatant was aspirated, the tissue was re-suspended in 10ml of medium, and was plated onto glass cover-slips coated with laminin. The cells were kept in the incubator and usually used within two days of culture.

2.5. Excised cerebellar Purkinje cells

The cerebellum from a 25-28g Wistar rat (12-15 days old) anaesthetized with diethyl-ether were removed following cervical dislocation, and the vermis dissected. The pia was removed and the vermis was cut to four pieces in Hank's solution which was supplemented with the following (mM): 2 $CaCl_2$, 1 $MgCl_2$, 1.7 glucose, 5 NaHEPES at pH 7.4 (all the solutions were warmed to 37°C unless otherwise stated). The tissue was transferred to 10ml of a cold (4°C) enzyme solution containing (mM): 81.4 Na_2SO_4, 30 K_2SO_4, 5.8 $MgCl_2$, 0.25 $CaCl_2$, 20.4 glucose, 1 NaHEPES (pH 7.4), and 1.5mg/ml protease XXIII (Sigma) for five minutes. The solution was allowed to warm in a water bath (37°C) for 5 minutes, and was shaken for a further 7 minutes in the shaking water bath. The enzyme solution was aspirated, and the tissue was agitated gently for 2 minutes in 10ml of a solution containing (mM): 150 NaCl, 2.8 KCl, 2 $MgSO_4$, 10 NaHEPES (pH 7.4), 1mg/ml trypsin inhibitor (from soya bean), and 1mg/ml BSA. The solution was aspirated, the tissue resuspended in 5ml of Eagle's minimum essential medium (the Eagle's minimum essential medium used was modified by addition of 15mM glucose and 10mM NaHEPES, pH7.4) supplemented with 1mg/ml trypsin inhibitor and 1mg/ml BSA, and gently triturated with a fire polished pasteur pipette. The large lumps were allowed to settle and the

supernatant was gently poured over 5ml of a solution in a narrow centrifugation tube containing Eagle's essential medium supplemented with 10mg/ml trypsin inhibitor, and 10mg/ml BSA. The solution was centrifuged for 1 minute at 800rpm, the superfusate aspirated, and the pellet gently resuspended in 5ml of Eagle's essential medium containing 1mg/ml trypsin inhibitor. The suspension was allowed to settle for 10-12 minutes and the top 4ml of the suspension was added to 3-4 poly-L-lysine/laminin coated coverslips. The cells were used within 3-4 hours.

2.6. Optimization of the thin brain slice procedure

A procedure for preparation of thin slices of tissues (Edwards *et al*, 1989) allows the application of the patch clamp technique to visually identified cells with intact synaptic input *in situ*. This method comprises two steps: first cutting thin slices (about 120-300µm) with a tissue slicer, and second cleaning the surface membrane of individual cells for application of the patch clamp technique. Fluorescence microscopy and vital staining of cells were used to optimize the procedure for the preparation of rat brain slices.

2.7. Preparation of thin brain slices

Brains from Wistar rats (8-45 days old) anaesthetized with diethyl-ether were removed very rapidly following cervical dislocation and decapitation (less than 1 minute) and incubated in cold (0-4°C) slicing solution, low calcium containing bicarbonate solution (see section 2.11. Solutions), for at least 3 minutes. To obtain mechanical stability, a large block of tissue containing the region of interest was cut by hand, with a surface parallel to the desired orientation of slices, and was glued to the stage with a thin layer of cyanoacrylate glue. Subsequent vital staining (see below) of the slices demonstrated the importance of keeping the temperature of the tissue low during slicing to maximize survival of neurones. To achieve this the sectioning and slicing was performed in a cold room (4°C) as follows. After sectioning roughly down to the required level it was often necessary to discard a few slices before uniform slices could be obtained. The slicing was continuously monitored and the vibratome variables (forward speed, amplitude of vibration, and frequency of vibration of the blade) were adjusted so that the tissue was never pushed but always cut by the blade. Using the blunt-end of a pasteur pipette each slice was transferred to a incubation chamber (Edwards *et al*, 1989), containing calcium enriched incubation solution. After slicing, the

temperature of the incubation chamber was allowed to reach either the room temperature (about 22-27°C), or 37°C by placing it in an incubator for the first hour following sectioning. In either case the slices were kept at room temperature after the first hour. One slice at a time was placed in a glass or quartz bottomed recording chamber and held in place with a grid of parallel nylon threads (Konnerth *et al*, 1987) made from stockings. This chamber was placed on the microscope stage and was continuously perfused with gassed solution at a rate of 2ml per minute.

For cutting the slices an Oxford Vibratome was modified to produce larger amplitude of vibration (about 1.2mm) and was used together with single edged 'valet' blades supplied by the Campden Instruments. Table 2.1 summarises the procedure that resulted in the maximum survival of the neurones as determined by vital staining of slices prepared under different conditions. After initial incubation, no further deterioration was seen for upto 6-8 hours. After 8-10 hours fewer cells seemed to survive, with the majority of live cells deep in the slice. It was found, however, progressively more difficult to clean the surface of the slices with a cleaning pipette when the slices were kept longer than 7-9 hours. The age of the animals used was not found to be very critical for the survival of cells when damage to the cells was minimized by choosing the right slicing orientation. The age, however, did limit the maximum thickness of the slices since it was often more difficult to see individual cells in slices from older animals.

Most laboratories working with brain slices incubate the slices at 37°C for at least one hour before use. No proper explanation is given for this. Experiments were performed to see whether this incubating temperature had any effect on the viability of slices. Horizontal hippocampal slices were cut and the viability of the cells examined before and after incubation at 37°C (see next section). It was found that more cells on the surface of the slices incubated at 37°C were alive and fewer damaged. This could be due to "washing off" of the dead cells from the surface of the slice. Indeed in support of this possibility less cleaning of neurones was found to be required after incubation at 37°C.

2.8. Estimation of the slice thickness and vital staining

The slice thickness was estimated by focusing on the bottom of the slice chamber and measuring the distance travelled by an indicator on the fine focus knob of the microscope when the surface of the slice was brought into focus. The fine-focus knob of the microscope was calibrated by refocusing from the upper edge of a 150μm glass coverslip to its lower

** Decapitate and remove the brain as quickly as possible (<60s)*

** Place the brain in cold (<4°) saline for at least 3 minutes, paying particular attention to the pH and ionic composition of the solution*

** Stick down a larger block of tissue with the desired orientation*

** Gently pour cold saline over the tissue*

** Adjust the amplitude of vibration, and the speed of forward motion so that the tissue is never pushed, but always cut*

** Transfer the slices with the back end of a pasteur pipette to an incubation chamber*

** Keep at 37° for about 1 hour before use*

** Transfer to the recording chamber and continuously perfuse with gassed saline*

Table 2.1 Procedure for preparation of thin slices of the CNS

edge. Slices were incubated in a gassed bicarbonate solution containing 10µg/ml Fluorescein diacetate for 15 minutes, and were then either counter stained with 0.2mg/ml ethidium bromide in bicarbonate solution for 2 minutes or transferred directly to the slice chamber for viewing. Fluorescein diacetate is not fluorescent but is enzymatically broken down to fluorescein inside the cells. The cells thus stained were considered to be viable when the slices were viewed using the fluorescein filter set since they had the ability to cleave fluorescein diacetate to fluorescein and keep it within their outer membrane. Ethidium bromide is a membrane impermeable nuclear stain which stains the nucleus only when the cell wall is damaged. Cells with stained nuclei, when the slice was viewed with the rhodamine filter set, had damaged cell membranes and were assessed as dead. Images obtained with a CCD camera were stored on video tape (Videostar, Ferguson).

2.9. Orientation of slicing

Experiments were performed to test whether the orientation of slicing had any correlation with the survival of neurones in regions of interest. Hippocampal slices were prepared in four different orientations, namely coronal, sagittal, horizontal, and in a 45° angle to the midbrain (Figure 2.1). Slices were stained with fluorescein diacetate and ethidium bromide immediately after sectioning and cell survival in different regions of each slice assessed. Within each orientation a particular part of the pyramidal cell layer survived better than the rest, although no major differences were observed in the survival of granule cells in the dentate gyrus. The majority of the CA1 pyramidal cells did not survive if the hippocampus was sliced with the 45° orientation, although very little damage was done to the CA3 pyramidal cells. With the same orientation, however, live cells could be found deep inside the CA1 region (about 45µm from the surface), if the thickness of the slice was greater than 150µm (Figure 2.2). Longer incubation of the slices at room temperature did not greatly effect the survival of the different regions. In contrast to the 45° orientation, in coronal and sagittal sections the CA1 pyramidal cells survived better than the CA3 pyramidal cells (Figure 2.3). In the horizontal orientation the entire pyramidal cell layer survived uniformly (Figure 2.4) and slices as thin as 75µm could be made without any major cell loss. It is likely that the preferential survival in different regions in sections cut with different orientations is related to the geometry of the dendritic tree; sectioning in an orientation across the dendritic tree causes cell damage and increases the possibility of cell death. This idea was

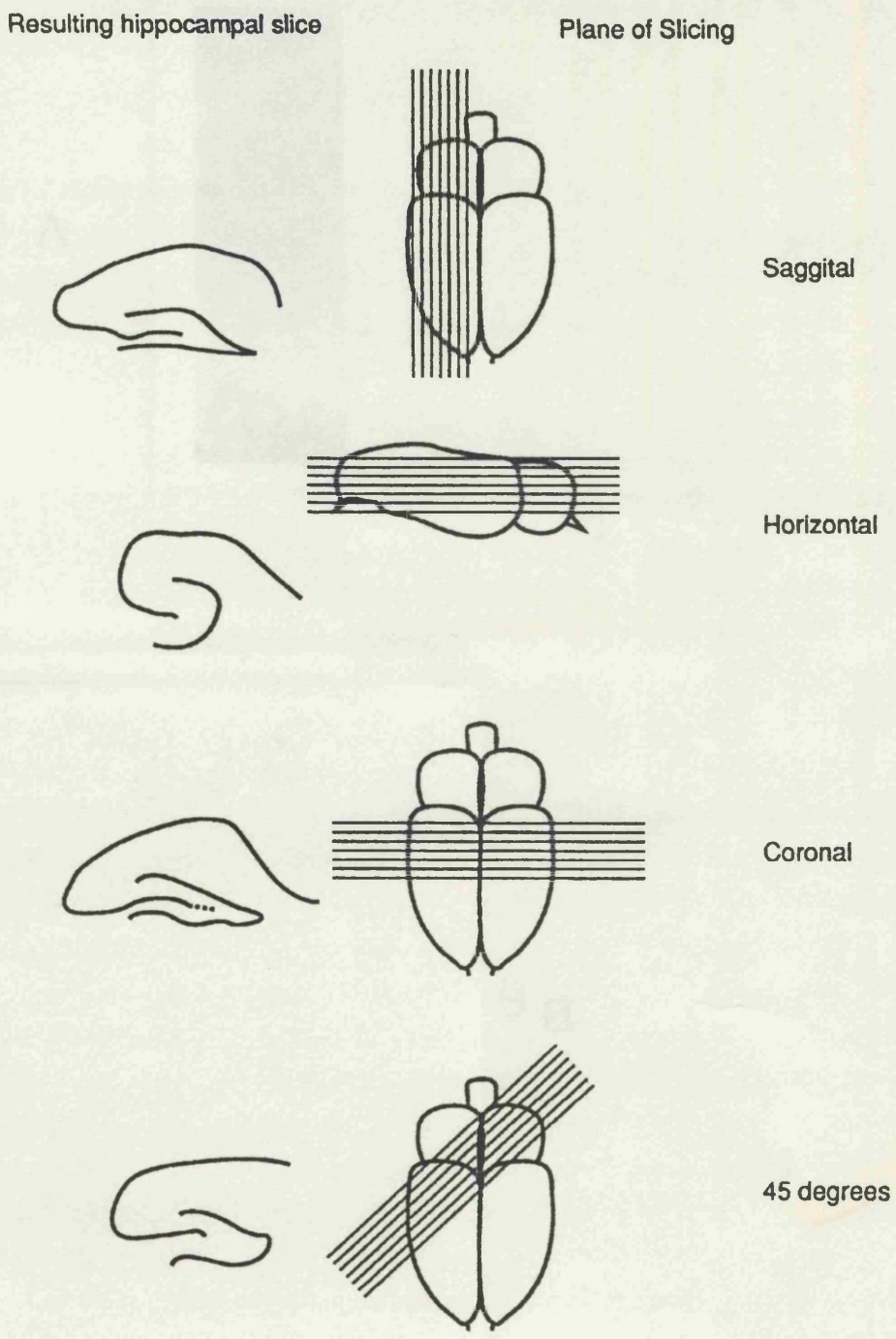

Figure 2.1 Orientations used to slice the rat hippocampus

The diagram shows different orientations used when slicing the rat hippocampus and the shape of their resulting slices. Neurones from different regions survived preferentially depending on the orientation (see text).

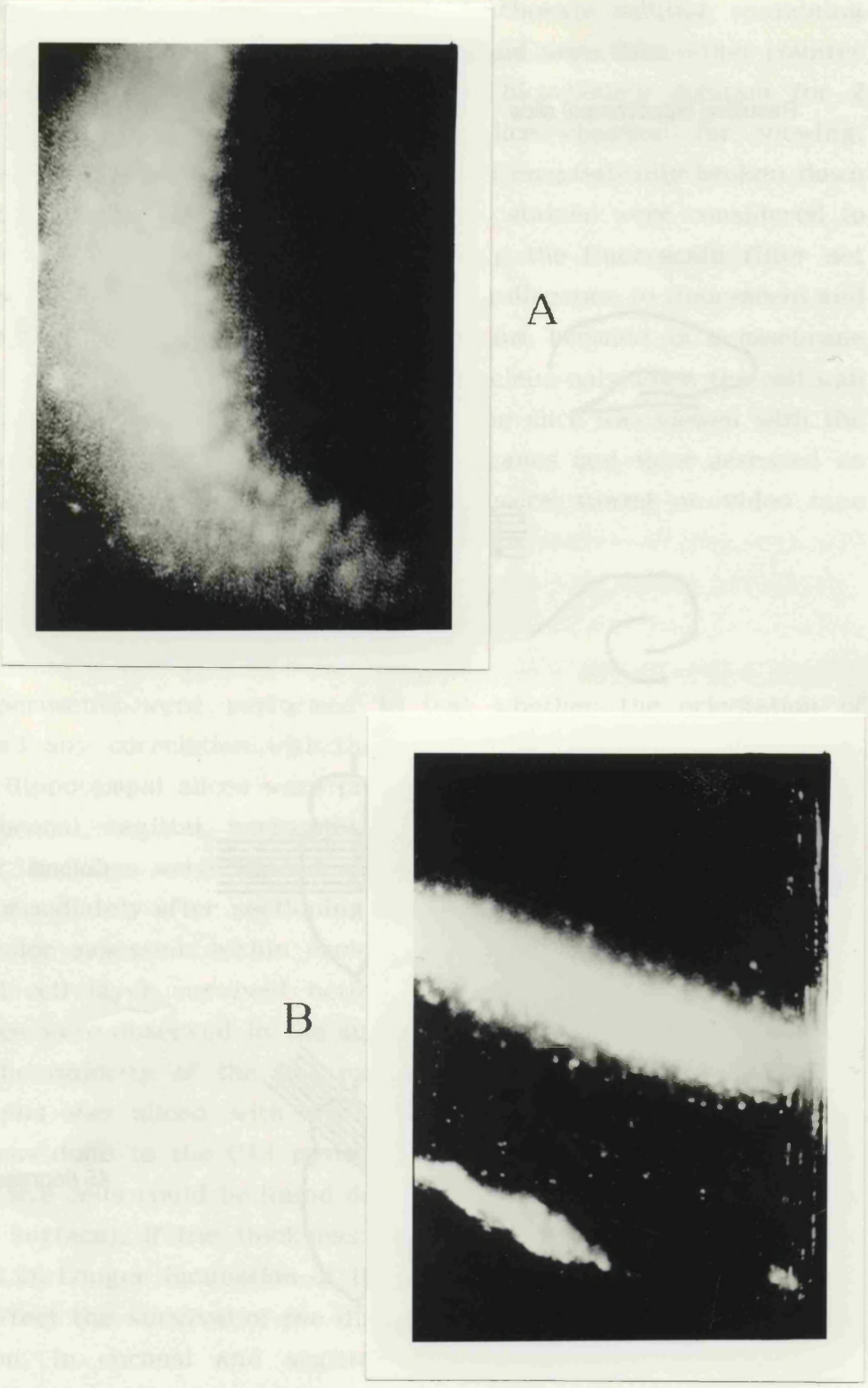

Figure 2.2 Vital Staining of 45° hippocampal slice

120μM thick slices of the rat hippocampus sliced at 45°. Slices were stained with Fluorescein diacetate (FDA) or Ethidium Bromide (EB) after 1 hour incubation at 37°. A) CA3 region of the slice stained with FDA for live cells; B) CA1 region of the same slice stained with EB for dead cell.

A

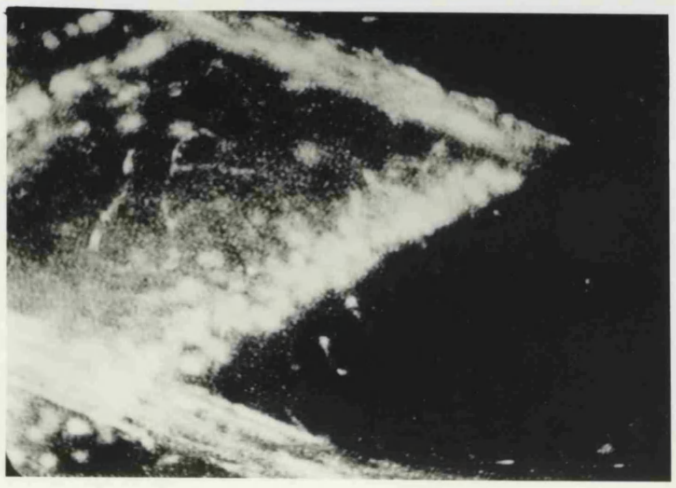

B

Figure 2.3 Vital Staining of coronal and sagital hippocampal slices

120μM thick slices of the rat hippocampus sliced at coronal and sagital orientations. Slices were stained with Fluorescein diacetate (FDA) or Ethidium Bromide (EB) after 1 hour incubation at 37°. A) CA1 region of a coronal slice stained with FDA for live cells; B) CA1 region of a sagital slice stained with EB for dead

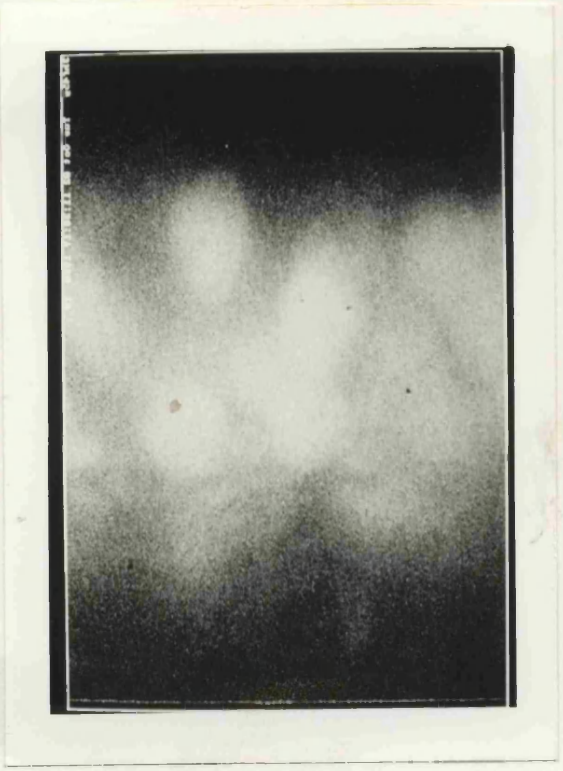

A

B

Figure 2.4 Vital Staining of a horizontal hippocampal slice

120µM thick slices of the rat hippocampus sliced at horizontal orientation. Slices were stained with Fluorescein diacetate (FDA) or Ethidium Bromide (EB) after 1 hour incubation at 37°. A) CA1 region of stained with FDA for live cells, note individual cell bodies (scale 50µm/cm); B) CA3 region of the same slice stained with FDA for live cells (scale 35µm/cm).

A

B

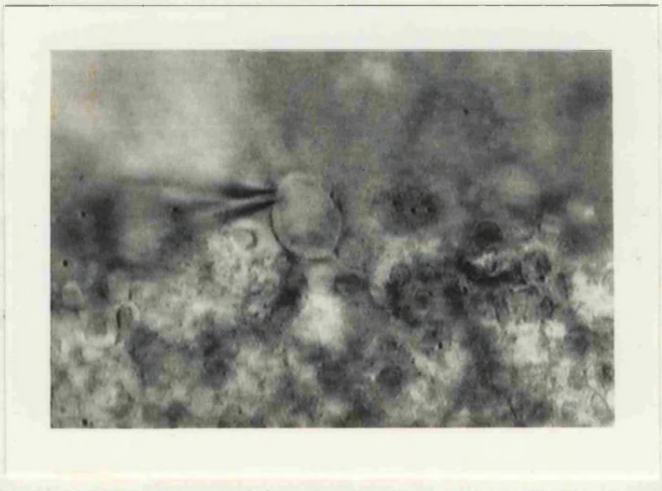

Figure 2.5 Cleaning of a Purkinje cell in a slice of cerebellum

Photographs show a 200µM thick slice of rat cerebellum viewed with a 40X water immersion objective. Panel (A) shows the cleaning pipette (slightly out of focus) and outline of a Purkinje cell (centre of micrograph). Positive pressure at the back of the cleaning pipette results in a stream of saline which 'cleans' the surface of the cell from debris. Panel (B) shows the same cell after it has been cleaned. Note the whole cell patch pipette (top left of the cell) and the axon of the Purkinje cell (bottom right of the cell). Scale is 20µm/cm.

supported by the fact that in thick slices live neurones could be found deep in the regions in which superficial neurones did not survive. The granule cells of the dentate gyrus, however, are very small, in great numbers, and without an extensive dendritic tree. This could explain the lack of variation in the survival of granule cells in sections cut at different orientations.

2.10. Thin slices of the cerebellar Cortex

Purkinje neurones in thin slices of the cerebellum were used to investigate the calcium mobilising actions of $InsP_3$. The cerebellum was dissected from brain rapidly excised from a Wistar rat (25-55g), the midbrain removed, and cut sagitally at the vermis into two pieces. One of the blocks was fixed on the stage so that sagittal 300µm thick slices of the vermis were obtained. This orientation was parallel to the extensive dendritic tree of Purkinje neurones and resulted in the maximum survival of these cells as tested with vital staining of the slices. Figure 2.5 shows consecutive photographs of a thin cerebellar slice during which a Purkinje cell was cleaned and patch clamped.

2.11. Solutions

The minimal intracellular patch pipette solution contained (mM) 153 K-Gluconate, 3 Na-ATP, 3 $MgSO_4$, and 8 HEPES buffered to pH 7.2 with KOH, with osmolarity of 293mosmol/l. Some intracellular patch pipette solutions also contained 50µM GTP. The 'ATP regenerating' intracellular patch pipette solution contained (mM): 140 K-Gluconate, 3 Na-ATP, 3 $MgSO_4$, 8 K-HEPES, 0.1 leupeptin, 0.05 GTP, 10 phosphocreatine, and 10mg/ml creatine phosphokinase (240units/mg) adjusted to pH 7.2 with osmolarity of 297mosmol/l. The chloride containing internal solution used was (mM): 120 KCl, 2 KH_2PO_4, 5 CH_3COONa, 20 K-HEPES, 6 $MgSO_4$, 5 Na-ATP, and 0.05 EDTA adjusted to pH 7.2 with osmolarity of 294mosmol/l.

The extracelluar solution for cultured cells contained (mM): 150 NaCl, 2.8 KCl, 1 $CaCl_2$, 2 $MgSO_4$, and 10 Na-HEPES adjusted to pH 7.4, osmolarity 299mosmol/l. For activation of NMDA channels magnesium was omitted and 5µM glycine added. The calcium free solutions contained no added calcium with 0.5mM EGTA.

Fluo-3 (200µM or 1.2mM; Molecular Probes) or Furaptra (500µM, Molecular Probes) were included in the intracellular patch pipette solution when changes in the $[Ca^{2+}]_i$ were monitored.

The 1-(2-Nitrophenyl)ethyl ester of inositol (1,4,5) trisphosphate

(Walker *et al*, 1989), Caged $InsP_3$, (gift from Dr D Trentham, Division of Physical Biochemistry, NIMR) was used in experiments during which the calcium mobilising action of $InsP_3$ was studied. Depending on the phosphate residue esterified, caged $InsP_3$ exists in P1, P4 and P5 isomers. P4 and P5 caged $InsP_3$ are biologically inactive with the exception that P5 caged $InsP_3$ inhibits the soluble $InsP_3$ 3-kinase of bovine brain (Walker *et al*, 1989). For experiments on cultured neurones and astrocytes P4 caged $InsP_3$ was added to the intracellular solution (1-100 μm). P4 caged $InsP_3$ was used for all the experiments on Purkinje cells when Fluo-3 was used as an indicator, and 3 Purkinje cells when Furaptra was used as the calcium indicator. However due to lack of availability of P4 caged $InsP_3$ the majority of experiments on the Purkinje cells when Furaptra was used as the indicator was with P5 caged $InsP_3$. No difference was observed between the responses recorded in the 3 Purkinje cells loaded with Furaptra and P4 caged $InsP_3$ and those loaded with Furaptra and P5 caged $InsP_3$.

For thin brain slices the slicing solution contained (mM): 125 NaCl, 2.5 KCl, 1 $MgSO_4$, 26 $NaHCO_3$, 1.25 NaH_2PO_4, 0.5 $CaCl_2$, and 11 Glucose. The incubation solution was the same with 1.5mM calcium chloride, and the experimental solution had either 2mM calcium chloride, or 4mM magnesium sulphate with 0.5mM EGTA. The pH of all the bicarbonate based solutions was close to 7.4 when bubbled with 95%O_2:5%CO_2 gas. These solutions had an osmolarity of about 298mosmol/l.

For experiments on the squid giant synapse artificial sea water of the following composition was used (mM): 470 NaCl, 10 KCl, 11 $CaCl_2$, 11 $MgCl_2$, 30 $MgSO_4$, 50 HEPES; pH 7.8. Experiments in acid pH were made in artificial seawater buffered with 50mM 2-phosphoglycerate (pK_a=6.2) or MES (pH 5.5).

2.12. Experimental apparatus

Two sets of apparatus were used for the experiments reported in this thesis, and for ease in reference they have been termed "Inverted" and "Slice" microscopes.

2.13. Inverted microscope

Figure 2.6 shows the schematic diagram, and Photograph 2.1 the actual Inverted microscope sets of apparatus. This apparatus allowed simultaneous microspectrofluoremitry, flash photolysis and patch clamp recordings from single cultured neurones or glia. It consisted of a fixed stage Nikon Diaphot microscope mounted on an anti-vibration table inside

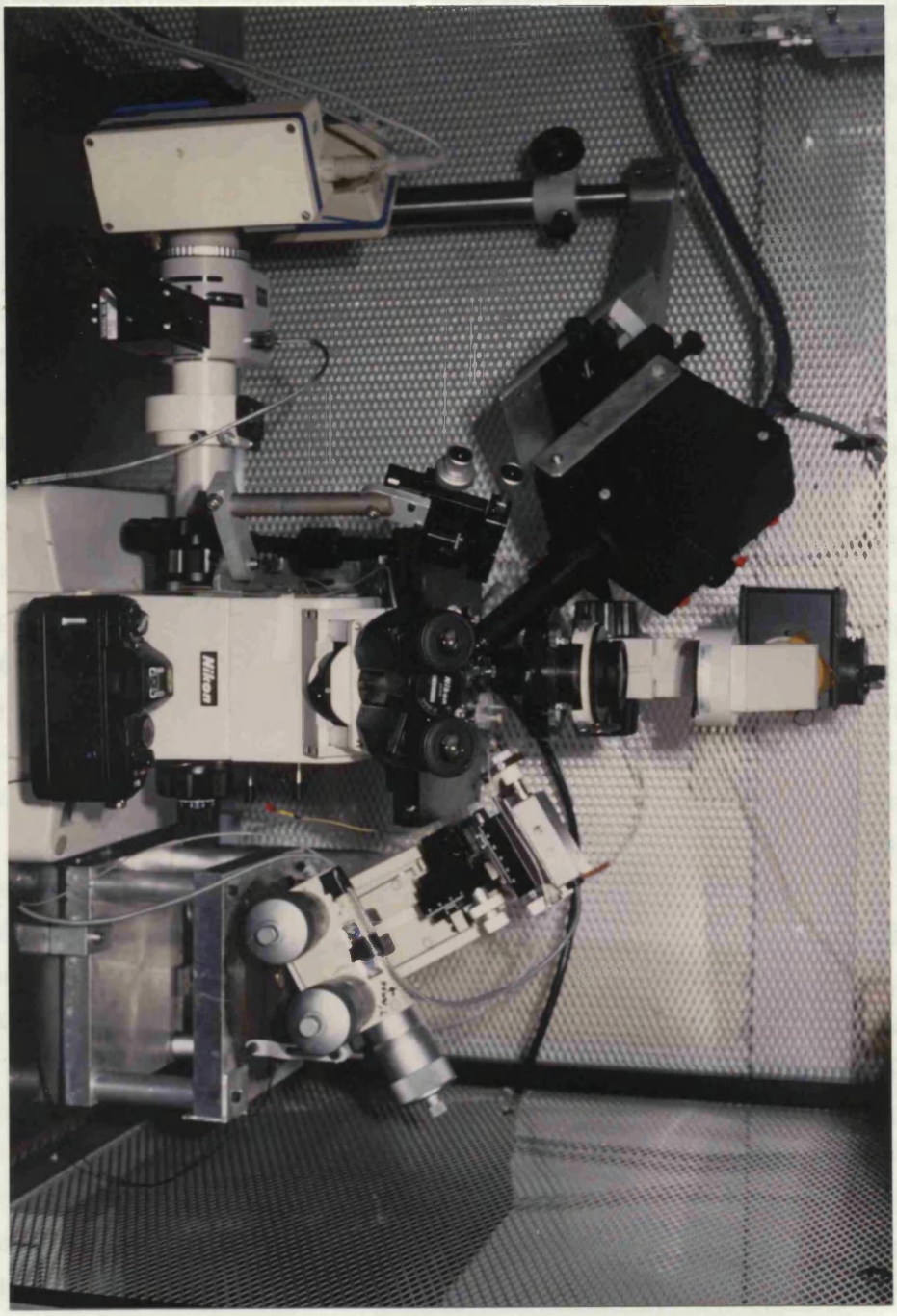

Photograph 2.1 The Inverted microscope

Opposite page

Figure 2.6 The schematic diagram of the Inverted microscope

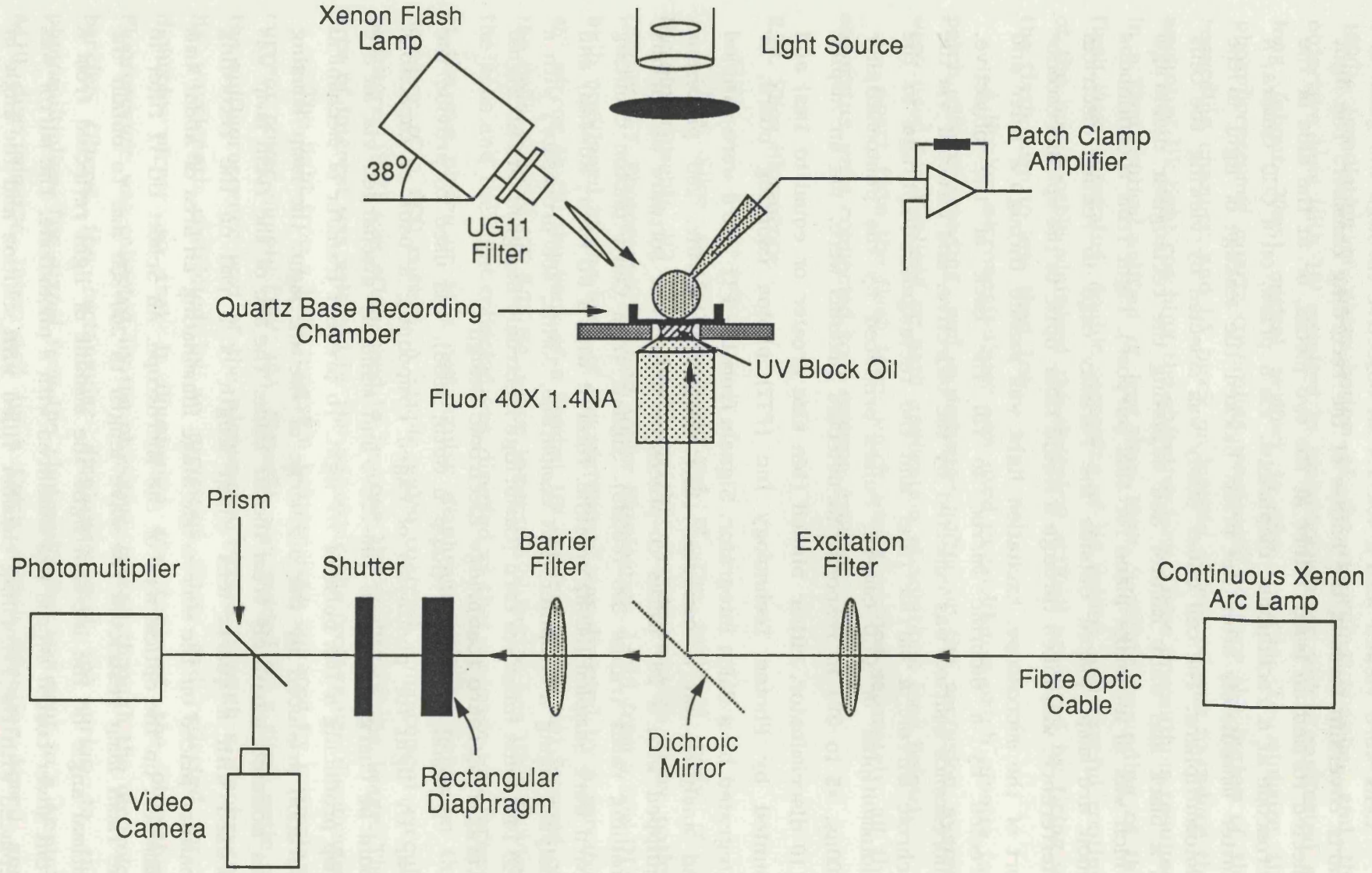
Xenon Flash Lamp
Light Source
38°
Patch Clamp Amplifier
UG11 Filter
Quartz Base Recording Chamber
UV Block Oil
Fluor 40X 1.4NA
Prism
Photomultiplier
Shutter
Barrier Filter
Excitation Filter
Continuous Xenon Arc Lamp
Fibre Optic Cable
Dichroic Mirror
Rectangular Diaphragm
Video Camera

a Faraday cage.

Cells were viewed with a 40X 1.4 NA objective through the glass or quartz coverslip forming the bottom of the recording chamber. The light collected formed an image either at the eye pieces, or at the side of the microscope at a rectangular diaphragm, *via* a prism, on a CCD camera. A shutter immediately after the prism blocked the leakage of light to the photomultipliers. The cell under study was selected by viewing the cells on a black and white monitor and adjusting the rectangular diaphragm (which was in an image plane for this purpose). Light from a continuous xenon arc-lamp, placed outside the Faraday cage to reduce electrical interference, was taken through a liquid fiber optic to the epifluorescence port of the microscope. Excitation light was passed through a filter and directed by a dichroic mirror to fill the back of the objective. Fluorescence emitted was collected by the objective, and directed *via* the dichroic mirror, a barrier filter and the rectangular diaphragm to the photomultiplier or CCD camera. Pulses produced by the photomultiplier (200ns, +5 to 0V) in response to detected photons were, *via* an Amptek A110 discriminator, either binned (bin size greater or equal to 1ms) and counted by Photon Technology Inc (PTI) photon counting board, or integrated by a Cairn integrator. Signals from the PTI board were sampled and analyzed on a computer (IBM compatible, 20MHz, 286 processor equipped with a 287 maths co-processor using PTI software at various sampling rates (range 300-1000Hz). Signals from Cairn photon counting board were sampled (300Hz or 1kHz, filtered with a RC filter, RC=4ms) and analyzed using a computer (IBM compatible, 33MHz, 486 processor) with a CED 1401-plus interface card (Cambridge Electronic Design) and CED Signal Averager software (Cambridge Electronic Design).

A xenon flash lamp (Rapp & Guth, 1988), was used to provide the near UV light for photolysis of caged compounds; a bank of capacitors could be charged between 100-300V, and manually discharged via an arc lamp producing a 1ms pulse of UV light. To prevent transfer of mechanical vibration produced by the discharge of the arc lamp, the lamp housing was mounted separately from the air table. The arc of the flash lamp was focused with a quartz lens (focal length of 3 cm) on the recording chamber placed on the microscope stage illuminating an area of about 4mm diameter, on the optical axis of the microscope. An Schott UG-11 filter in the flash lamp restricted the wave length to 300-350 nm. To obtain the optimal angle of the incident light the amount of light reflected from a front silver coated mirror was measured with a photodiode. The mirror was replaced with the recording chamber filled with solution and the angle of the incident light was varied so that minimal light was reflected from the

solution. An incident angle of 38° was set at which only 13% of the light reflected by the mirror was reflected by the solution (see Ogden *et al*, 1990). Irradiation of glass bottom of the recording chamber and the objective lens with UV resulted in phosphorescence which manifested as long (about 30ms) optical artifact in the records. To minimize the phosphorescence quartz coverslips were used to form the bottom of the recording chamber, and UV block oil instead of lens oil was to reduce the amount of UV light reaching the objective lens. These precautions resulted in a flash optical artifact of less than 15ms. Separate grounding of the flash lamp apparatus, double screening of its cables, and careful routing of the power cable minimized the electrical artifact produced by firing of the flash lamp to less than 1ms.

A Huxley micromanipulator was used to position a patch pipette for patch clamp recording, and a pressure puffer or the perfusion system were used for localised or bath application of solutions (see below).

Apart from the flash lamp, which was grounded separately, all the apparatus were connected to a common ground.

2.14. Slice Microscope

The Slice microscope comprised of the modified body of a Microinstruments M2 fixed stage upright microscope with Zeiss optics (Figure 2.7, Photograph 2.2) and Kohler illumination. Light from a 50W QTM bulb positioned at the back of the microscope was directed by a movable 45° mirror to fill the back of a Reichat UV condenser (0.9 NA) focused on the cells. A Zeiss 40X 0.75 NA, water immersion objective was used to view the cells and the light collected was directed so that an image was formed at the eye pieces or at a rectangular diaphragm and *via* prism on the detector of a CCD camera. A simple video contrast enhancement circuit (Ashmore, 1987) was often used to improve the quality of the image. The area of interest was selected by the adjusting the rectangular diaphragm.

The light from a 150W tungsten halogen lamp powered by a constant current power supply (15V, 10A, Farnell), was guided by a fiber optic to the epifluorescence port of the microscope, passed through a diaphragm, its wavelength restricted by an excitation filter, and reflected by a dichroic mirror so that it illuminated the back of the objective. Fluorescence was collected by the objective, passed through the dichroic, barrier filters, the rectangular diaphragm and the prism to the photomultiplier. The signal from the photomultiplier was sent to a Amptek A110 discriminator, integrated by a Cairn photon counting board and recorded on FM tape.

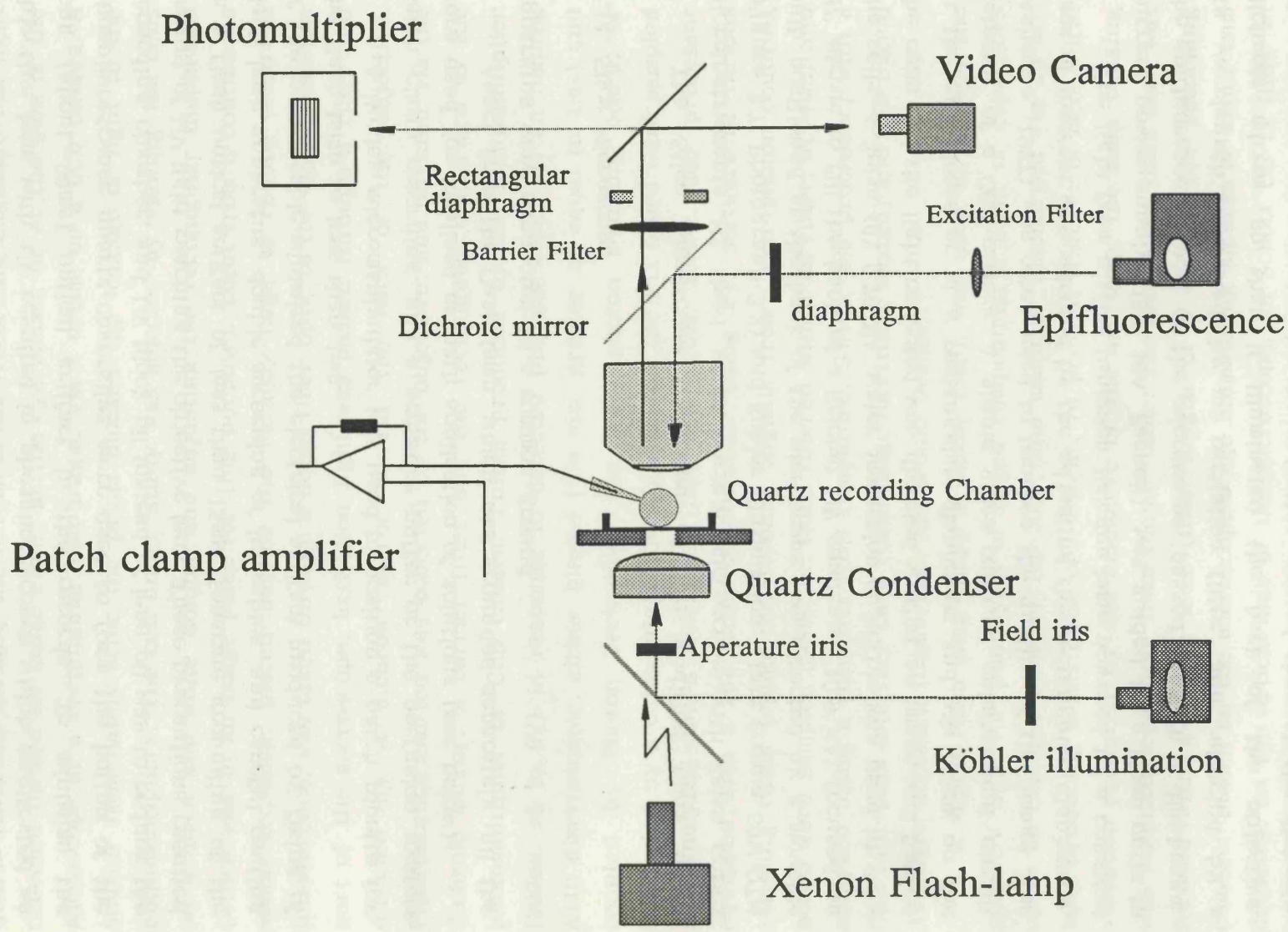
Photomultiplier
Video Camera
Rectangular diaphragm
Barrier Filter
Excitation Filter
Dichroic mirror
diaphragm
Epifluorescence
Quartz recording Chamber
Patch clamp amplifier
Quartz Condenser
Aperature iris
Field iris
Köhler illumination
Xenon Flash-lamp

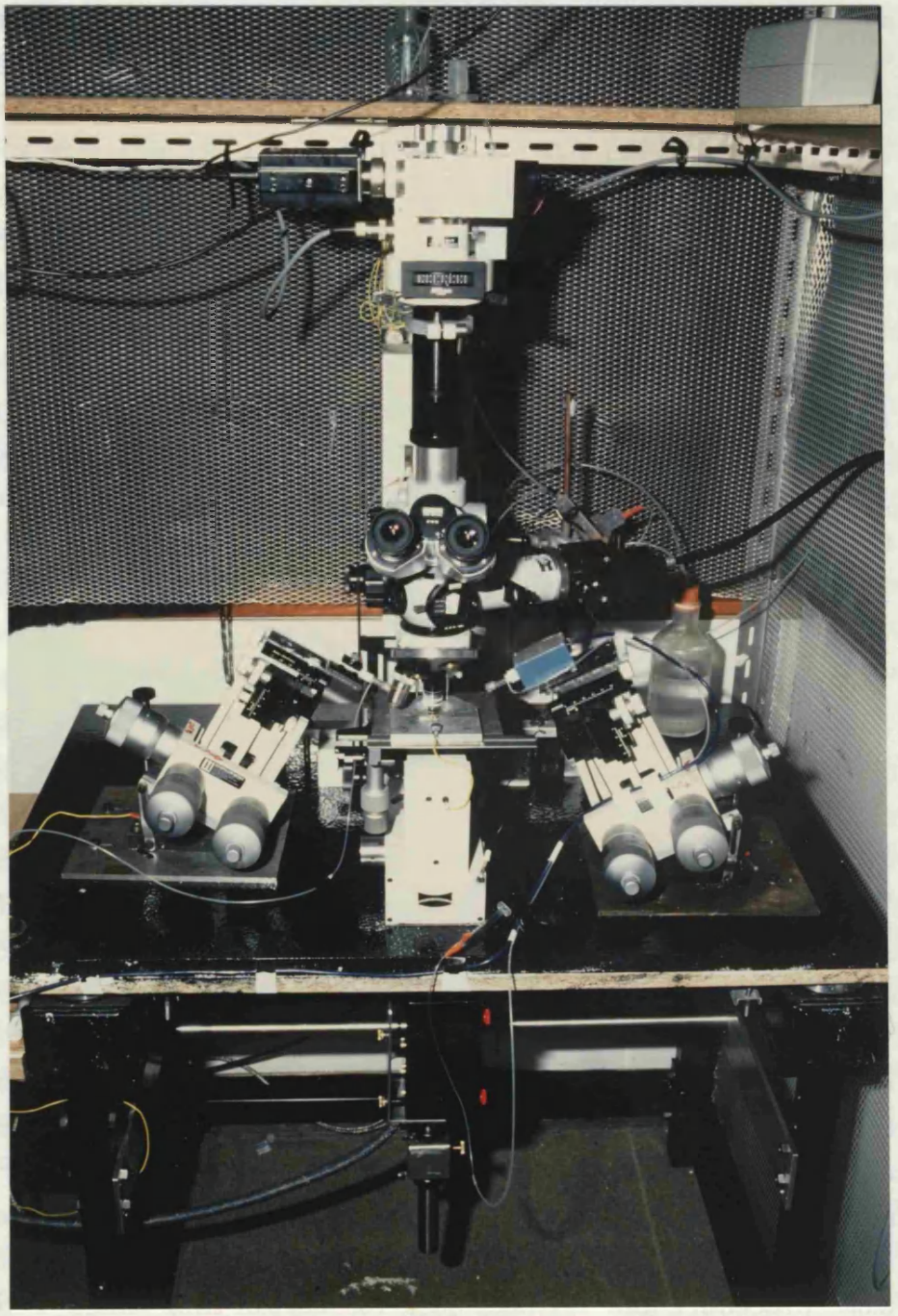

Photograph 2.2 The Slice microscope

Opposite page

Figure 2.7 The schematic diagram of the Slice microscope

The use of the water immersion objective prevented the application of the UV pulse from above. The flash lamp was positioned vertically under the base plate on the optical axis of the microscope, and the light path was through a hole in the base-plate, pulling back the movable mirror, so that the UV pulse filled the back of the UV condenser. The flash lamp was focused on the cells by adjusting the condenser so that the flash arc was in focus when the cells were viewed with a low power objective. The condenser and the recording chamber were made from silica to minimize energy loss of the UV light and to reduce the optical artifact due to phosphorescence.

Two Huxley micromanipulators were used to position the cleaning and patch pipettes, and a third small manipulator was used to position the pressure puffer pipette.

2.15. Bath and puffer application of solutions

Two types of perfusion systems were used, with the solution removed by a vacuum pump via a suction tube and three traps to reduce electrical interference. With the inverted microscope a 4 way manual tap was mounted near the stage and was arranged so that the perfusing solution could be altered rapidly between two solutions, with the dead time being that of the length of fine tubing used to connect the tap to the stage (volume <200µl). The solutions were gravity fed and the perfusion rate was about 4ml per minute changing the bath solution in about 15s.

With the slice microscope two tubes were attached to the water immersion objective, allowing rapid change of two solutions. Solutions were gravity fed and each solution could be turned On or Off with electrically operated pinch valves. Perfusion rate was about 2 ml per minute.

A Huxley manipulator was used to position a puffer pipette two cell diameters away from the cells under study. Puffer pipettes were made using the same procedure and settings used for normal thin-walled whole cell patch pipettes. The back end of the puffer pipette was connected to an electronically gated electrically switched two way valve, and was arranged so that the puffer was subject to either normal atmospheric, or 1 kPa air pressure. The output signal of the tap circuitry was arranged so that it switched from 0 to -1.5 volt when the tap was turned on, thus marking the onset and length of application of solutions. The On and Off lag times of the valve used are reported to be 3 and 5 ms respectively.

2.16. Electrical Recordings

In all experiments, apart from those performed on the squid giant fibre, the whole-cell voltage clamp configuration of the patch clamp technique was utilised (Hamill *et al*, 1981). Patch pipettes were made from thin-walled (0.16mm) and thick-walled (0.32mm) borosilicate glass capillary tubing containing a filament (1.5mm outside diameter, Clark Electromedical) with a vertical pipette puller (Kopf). To reduce their electrical capacitance, pipettes were coated with sylgard (Dow Corning) or dipped in melted parafilm wax and mineral oil (50/50 parafilm melted in mineral oil) while applying positive pressure. Pipettes were back-filled with various intracellular solutions and had a resistance between 3-8MΩ. Tight seals were formed and the membrane under the patch pipette was either broken by suction or perforated by the haemolytic staphylococcal α-toxin (see next section) to achieve whole cell configuration. The series resistance in the whole cell recordings was typically between 8-15MΩ. The patch clamp amplifier used was an Axopatch-1B (Axon Instruments) with a conventional resistor feedback head-stage. Signals were stored on wide band FM tape (Racal Store 4; bandwidth: DC 2.5 or 5kHz). The data obtained during characterisation of 'caged' glutamate analogues were captured at 10kHz and analyzed using SCAN, a software written by Dr John Dempster, in conjunction with a LabMaster analogue to digital converter and a computer (IBM compatible, 386 processor, 25MHz) equipped with a 387 maths coprocessor. The data obtained while studying the effect of intracellular release of $InsP_3$ were also stored on FM tape, but were captured and analyzed using Signal Averager (cambridge Electronic Design) in conjunction with a CED 1401-plus (Cambridge Electronic Design) interface board and a computer (IBM compatible, 486 processor, 33MHz).

To estimate the junction potential present during the whole cell recordings a whole cell patch pipette was filled with intracellular patch pipette solution and placed in a recording chamber containing the external solution. A junction potential of 3.5mV was measured by recording the offset produced when the bath solution was replaced with the internal solution. Membrane potentials are not corrected for the estimated junction potential.

2.17. Experiments on the giant synapse

The stellate ganglion from small specimens of the squid *Alloteuthis subulata* or *Loligo forbesii* were mounted above a quartz window in a bath of total volume 500µl containing oxygenated artificial seawater maintained

at 16°C and viewed on the Slice microscope, with the UV pulse delivered from underneath as described. In one set of experiments the synapse was viewed with a binocular microscope and photolysis was with a xenon arc lamp focused from above as described for the Inverted microscope. Presynaptic stimulation of the pallial nerve (second order giant fibre) was by a suction electrode and postsynaptic recording was with an intracellular microelectrode inserted close to the synapse in the largest third order giant fibre. Microelectrodes were pulled from the thick-walled glass described, using a Kopf puller and had resistance of 8-12MΩ when filled with 3M KCl. An Axoclamp-2A amplifier (Axon Instruments) was used to record the membrane potential and the signals were recorded on a wideband FM tape. The data were captured either with a storage oscilloscope for looking or on a Medelec to obtain photographic permeant records.

2.18. Use of the haemolytic α-toxin for patch perforation

For conventional tight-seal whole cell recordings electrical continuity of the patch pipette with the cytosol is obtained by disruption of the membrane under the patch pipette with suction or a large (1.5V) voltage pulse (Hamill *et al*, 1981). Although this method has the advantage of allowing the control of the intracellular cytosolic composition (Hamill *et al*, 1981; Marty and Neher, 1983), the cytosolic dialysis that occurs via the patch pipette (Marty and Neher, 1983) has been reported to result in the modification or loss of function of ion channels or second messenger mediated processes (Fernandez *et al*, 1984; Trautmann and Marty, 1984; Dufy *et al*, 1986; Horn and Marty, 1988; Korn and Horn, 1989; Carter and Ogden, 1992). Two methods have been used to prevent, or slow, the 'wash out' phenomenon; either a cytosolic extract is added to the intracellular patch pipette solution (Dufy *et al*, 1986), or the electrical continuity between the patch pipette and cytosol is achieved in a more controlled manner by increasing the membrane permeability by inclusion of ATP in the patch pipette solution (Bennett *et al*, 1981), or permeabilising the membrane under the patch with a membrane pore forming antibiotic, nystatin (Horn and Marty, 1988). The use of nystatin to form pores has advantages over ATP-permeabilisation of the membrane that it does not require ATP receptors present on a limited number of cell types, and that voltage control of the cytosol is greatly improved because of smaller access resistance. The disadvantage in the use of nystatin as a membrane perforant is that the pores formed by this antibiotic are permeable only to monovalent cations such as Na^+, and therefore do not allow introduction

of dyes and caged second messengers from the patch pipette. It would be useful, therefore, if similar patch perforation could be achieved with a perforant which results in the formation of larger pores in the membrane.

The haemolytic α-toxin released from strain Wood-46 (variant NCTC 10344) of *Staphylococcal aureus* (Kjems, 1963) is a monomeric protein of 34kDa (Lind *et al*, 1987) which has been used for permeabilisation ('skinning') of smooth (Kitazawa *et al*, 1989) and skeletal muscle membranes (Torok *et al*, 1990) permitting access to molecules of molecular weight up to 1kDa (Fussle *et al*, 1981). A similar technique to that for nystatin perforation of the cell-attached-patches was developed with the α-toxin as the membrane perforant.

Dorsal root ganglion neurones were use to investigate the properties of the α-toxin as a perforant. An aliquot of α-toxin (800U/ml or 10000U/ml; gift from Dr K Torok, Division of Physical Biochemistry, NIMR) was diluted into the intracellular patch pipette at 50-200U/ml, spun to remove debris and kept on ice for up to 3 hours during the experiments. 0.5-0.75µl was put in the tip of the patch pipette by back-filling and the rest of the pipette filled with normal solution. High resistance tight seals were obtained by gentle suction within three minutes of entering the bath solution; longer delays resulted in a reduced chance of obtaining a good tight seal. Series resistance was monitored by measuring the peak currents during capacitance spikes when a 5ms 2mV voltage step was applied. Good access to the cytosol was developed over the course of several minutes; usually small fluctuations in the membrane conductance were observed followed with a sudden increase in the membrane conductance (Figure 2.8). Occasionally after the sudden increase in the membrane conductance there were fluctuations in the membrane conductance (Figure 2.8) which settled to provide a low access resistance between 10-16MΩ and did not change during the course of experiments (upto 1 hour). Increasing the concentration of the toxin reduced the time taken to achieve a series resistance of less than 30MΩ (Table 2.2). Increasing the concentration of α-toxin also decreased the success rate in obtaining a good tight seals so that with 100U/ml of α-toxin the success rate was about 80%. During some experiments the calcium indicator Fluo-3 was also included in the patch pipette. Equilibration of the indicator between the cell and pipette, monitored by the increase and subsequent levelling of the whole cell fluorescence, was achieved 2-4 minutes following membrane permeabilisation by α-toxin.

α-toxin was also used at 100U/ml to permeabilise the membrane of cell attached patches of cells in the primary cultures of hippocampus, striatum, astrocytes, and pig aortic endothelial cells, as well as Purkinje

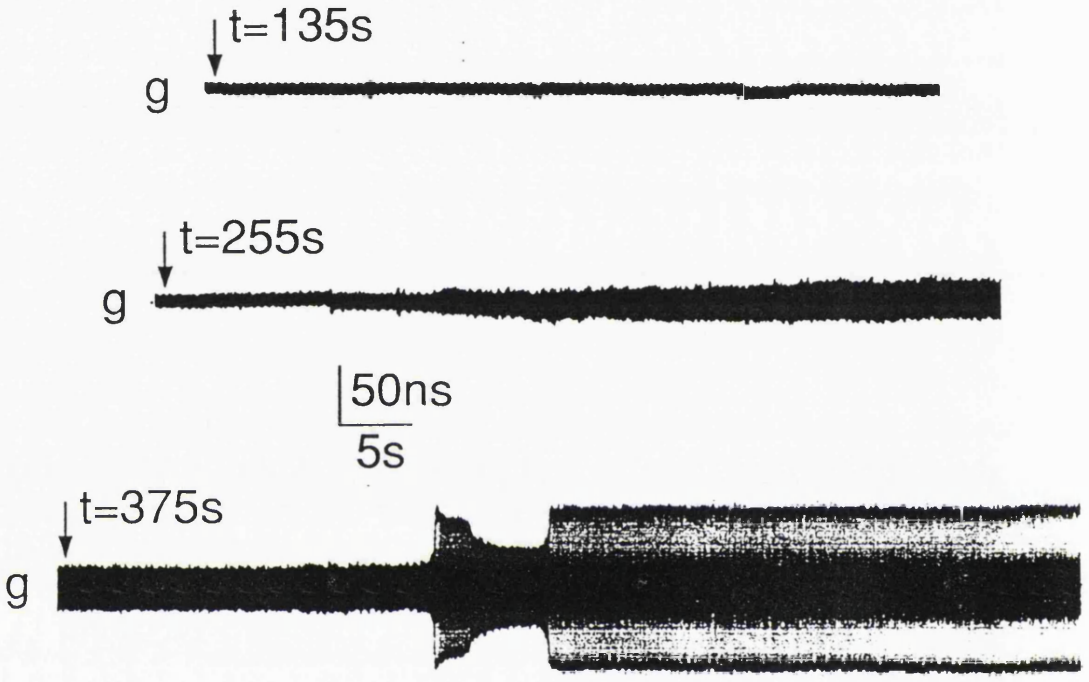

Figure 2.8 Patch perforation with α-toxin

The records show the conductance of a DRG neuron patch clamped at -70mV (pipette potential). A tight seal was formed at t=0 and 2mV, 5ms long voltage steps were applied at 100Hz. The patch pipette contained 100 Units/ml α-toxin. Conductance of the patch under the pipette increased gradually after 3 minutes. After about 7 minutes the conductance suddenly increased, fluctuated for a few seconds, and stabilised to result an access resistance of 15MΩ. The access resistance did not alter during the course of experiment (about 45 minutes).

α-toxin concentration / Units ml^{-1}	Time taken to achieve access resistance <15MΩ / minutes
50	20
60	15
80	10
100	6
200	2

Table 2.2 Concentration dependance of patch perforation by α-toxin

Approximate time taken to achieve whole cell configuration with a series resistance less than 15MΩ with varying concentration of α-toxin in the patch pipette. Rat DRG neurones.

cells in acutely prepared thin slices of the cerebellum; and proved to be essential for reproducible responses of endothelial cells to ATP when recording conductance and $[Ca^{2+}]_i$ with fluorescent calcium indicators (Khodakhah *et al*, 1992, Carter and Ogden, 1992).

2.19. Estimation of the extent of photolysis under the experimental conditions

To ensure reproducible and maximum illumination of the cells with the UV light the flash lamp was aligned and its arc focused on the cells before experiments. On the Inverted microscope the arc was focused with a silica lens (3cm focal length) so that burn patterns (about 4mm diameter) obtained on a piece of UV sensitive photographic paper (Kodak) placed on the stage were concentric with the optical axis of the microscope. On the Slice microscope the flash lamp was aligned and the UV condenser adjusted in the continuous mode so that the flash arc could be visualised on the cells when viewed with a low power objective.

The power output of the flash lamp could be altered by selecting 3 or 7 capacitors before the experiment and charging to various potentials of 100, 150, 200, and 300V with 7 capacitors, and 150, 300V with three capacitors. The power output of the flash lamp measured with a bolometer in the range 300-350nm was 100mJ (7 capacitors charged to 300V), and varied less than 10mJ from pulse to pulse.

The extent of photolysis in the Inverted microscope was estimated as follows. A small droplet (5µl) containing caged ATP (500 µM) was placed on the microscope stage, and irradiated by firing the flash lamp. The area illuminated by the UV light was greater than that occupied by the droplet, and the maximum pathlength of the light through the droplet was less than 1.5mm[1] resulting in underestimation of the extent photolysis by less than 5%[2]. The droplet was collected, the concentrations of free and caged ATP measured with ionic exchange HPLC, and the percent photolysis of caged ATP calculated. The percentage photolysis obtained for caged ATP was used to calculate the amount of $InsP_3$ released photolytically since caged ATP and caged $InsP_3$ have the same extent of photolysis under these conditions (Walker *et al*, 1989).

---

[1] The droplet was assumed to form a hemisphere, the radius of which was calculated to be 1.47mm.

[2] Using the Beer-Lambert law, the maximum reduction in the intensity of the UV light by the sample, assuming an average extinction coefficient of $550M^{-1}cm^{-1}$ for the wavelength 300-350nm ($\varepsilon_{347}=660M^{-1}cm^{-1}$; Walker et al, 1989), and a pathlength of 1.5mm would be 4.3%.

One essential prerequisite of the method described above was that the irradiated area was greater than that occupied by the sample. This was difficult to achieve with accuracy on the slice microscope because the arc of the flash lamp was focused with the silica condenser to irradiate a very small area (about 500µm diameter). One approach to this problem would be the use of a caged fluorophore that is normally quenched and fluoresces after photolysis. The area from which light is collected is restricted to an area smaller than that irradiated by the flash, and the concentration of the free fluorophore photolytically released estimated from an empirical calibration curve of fluorescence versus concentration. The advantage of this approach would be that the caged fluophore can be included in the patch pipette to directly estimate the extent of photolysis of the caged fluophore inside a cell. The extent of photolysis of other caged compounds can be estimated by comparing their photolytic efficiency with that of the caged fluophore in larger volumes in cuvette experiments. Attempts made to employ this technique using caged fluorescein allyl-ether or allyl-maleiamide were not successful because of problems with the chemistry and slow photolysis of the caged compound.

An alternative approach for estimation of the extent of photolysis was implemented using the fluorescent pH indicator 2',7'bis(2-carboxyethyl)-5(6)-carboxyfluorescein, BCECF, (pK_a=6.89) exploiting the stoichiometric photolytic release of a proton with ATP during the photolysis of caged ATP (Walker *et al*, 1988). Using BCECF an increase in the concentration of protons was detected as a decrease in the fluorescence emitted by the indicator since the fluorescence quantum efficiency of BCECF is greatly reduced when it is protonated. One millilitre of a solution containing 40µM BCECF (approximate concentration), 3mM $MgCl_2$, 1mM dithiotrietol, and 137µM caged ATP at pH 7 was placed in a quartz-base recording chamber on the Slice microscope. The surface of the recording chamber was viewed with a 40X 0.75NA water immersion objective, and the UV condenser was adjusted so that the arc of the flash lamp could be visualised at the same place. Fluorescence emitted from a 400µm^2 area (20µm square) was measured, and flash lamp was fired at various intensities (Figure 2.9). Following each pulse of UV light the fluorescence was reduced demonstrating an increased proton concentration. The fluorescence signal recovered over several seconds as protons or dye diffused away because only a small fraction (<0.5%) of the total volume of the solution was irradiated and the protons released could not significantly alter the proton concentration of the total solution. Mixing the solution resulted in the full recovery of the fluorescence to its pre-flash background level, allowing the calibration procedure to be carried out

Figure 2.9 Calibration of photolysis with the fluorescent proton indicator BCECF

Figure shows fluorescence measured from a 20μm square of a solution containing 40μM BCECF, 137μM caged ATP, 3mM $MgCl_2$, and 1mM dithiotrietol at pH 7. The flashlamp was aligned and focused so that the arc could be visualised in the plane of focus. The xenon arc lamp was discharged at various potentials (a=100V, b=150V, c=200V, and d=300V; all with 7 capacitors) irradiating a 500μm diameter circle. Photolysis of caged ATP results in the stoichiometric release of one proton for each molecule of ATP. The rise in the proton concentration following each pulse was detected by the indicator and is reflected in the signal by a decrease in the fluorescence. A relatively small volume of the solution was illuminated (<0.5%), and the protons released could not significantly alter the proton concentration of the solution. Mixing of the solution following each pulse resulted in the recovery of the signal to its pre-flash levels (dots). The same solution was titrated by addition of small volumes of 5mM HCl and a calibration curve constructed (see Figure 2.10, opposite page). The amount of protons released with each flash was estimated from the calibration curve, and the extent of photolysis in the solution calculated.

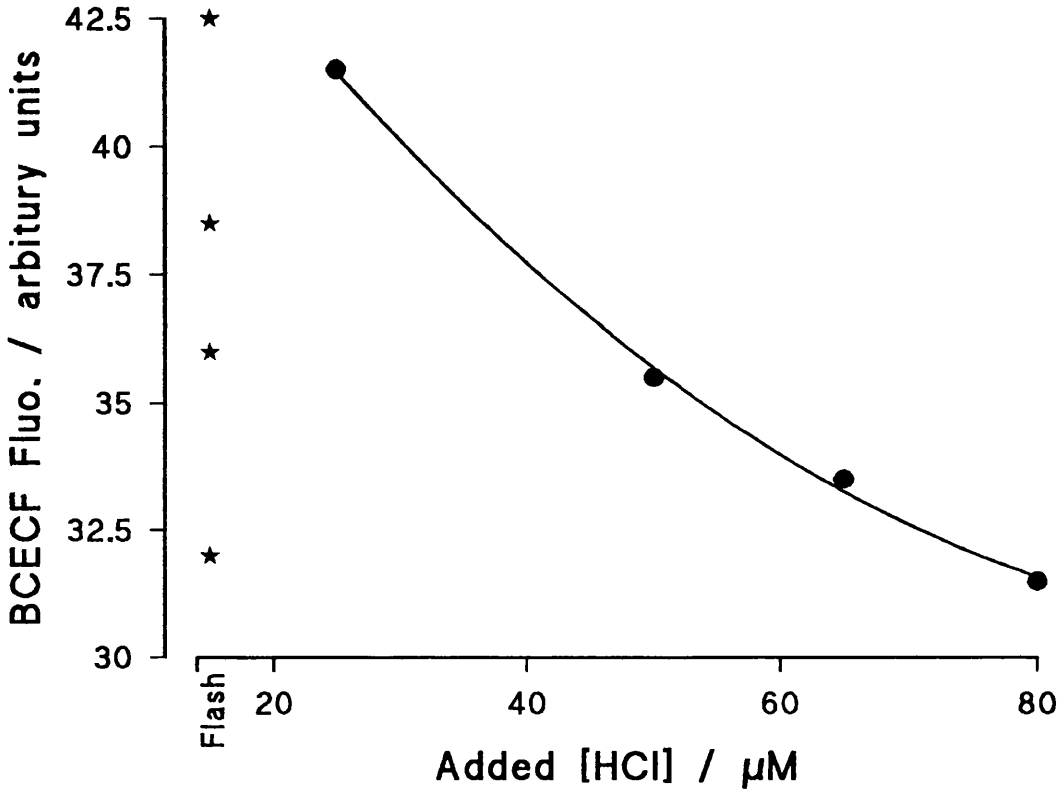

Figure 2.10 Photolysis calibration curve

The change in the fluorescence emitted by the fluorescent pH indicator BCECF was measured following addition of small amounts of HCl and a calibration curve constructed. The percent photolysis was estimated by reading from the calibration curve the equivalent proton released with each pulse of UV light (stars, 300, 200, 150, and 100V).

Flash Intensity / V	100	150	200	300
Slice Microscope (SM)	15	26	35	53
SM corrected for Slice	10	19	25	38
Inverted Microscope	NA	15	NA	30

Table 2.3 Extent of photolysis achieved in the experimental apparatus

The extent photolysis estimated from the BCECF calibration on the Inverted and Slice Microscopes. The corrected values for a 300μM thick slice on the Slice Microscope is also reported.

without the need to change the solution with the obvious advantage that the pathlength, area, and light intensity were unaltered throughout the experiment. The change in the fluorescence when small volumes of 5mM HCl was added to the solution was measured, and a calibration curve constructed (Figure 2.10). The amount of protons released with each flash was estimated from the calibration curve, and the extent of photolysis in the solution calculated.

The extent of photolysis was corrected for the loss in intensity of UV light due its passage through brain slices. The extinction coefficient of CNS slices at 316nm was estimated to be $10cm^{-1}$ by measuring transmission of light through various slices of known thickness in the experimental microscope, and the extent of photolysis corrected for the loss of the UV light intensity due to the passage of the light through the slice using the Beer-Lambert law. The loss of the intensity of the UV light after passing through a slice of 300µm was estimated to be 26%. Table 2.3 lists the extent photolysis achieved on the Inverted and Slice microscopes with various intensities of illumination measured by caged ATP photolysis with HPLC or proton release calibrations.

It should be noted that the extent of photolysis can be estimated by an alternative way if the exact concentration of the fluorescent proton indicator, BCECF, is known. The free $[H^+]$ can be calculated from the fluorescence emitted by BCECF from the equation:

$$[H^+]=K_D\cdot\frac{(F-F_{min})}{(F_{max}-F)}$$

where K_D is the dissociation constant of the dye, F is the fluorescence of the dye at free proton concentration $[H^+]$, and Fmin and Fmax are the fluorescence of the indicator at zero and saturating concentrations of H^+ (see appendix 1 for the derivation). By quantitative measurement of the fluorescence emitted from a solution containing BCECF and caged ATP after a pulse of UV light, the change in the free proton concentration can be obtained from the above equation. If the concentration of the indicator, D_{tot}, is known the change in the concentration of protonated indicator can also be obtained:

$$[D]+[DH]=D_{tot}$$

$$[DH]=\frac{[H^+].[D]}{K_D}$$

where $[DH]$ and $[D]$ are the concentration of protonated and unprotonated dye. The total amount of protons released, $[H^+]_r$ is given by:

$$[H^+]_r=\Delta[H^+]+\Delta[DH]$$

From the total amount of protons released after each flash the extent photolysis can be calculated and corrected for the loss of light by its passage through the tissue as discussed above. A disadvantage of calculation of the extent photolysis by this method is that it is important to know the exact concentration and K_D of the indicator at the ionic strength and temperature of the experimental solution and therefore direct calibration was preferred.

Although theoretically the extent photolysis in the solution could be estimated accurately and corrected for the loss of energy due to the tissue appropriately, between experiments the errors due to lamp alignment, loading of caged $InsP_3$ in the cell, and true cell to cell variations are more difficult to estimate. However the mean latency of onset of the increase in Fluo-3 fluorescence when 38μM $InsP_3$ (submaximal concentration) was photolytically released in 15 cells was 22.1+3.2ms (mean and SEM). If it is assumed that close to this concentration of $InsP_3$ an inverse linear correlation exists between the concentration of $InsP_3$ released and latency of calcium release (supported by the data described in chapter 5), coefficient of the variation in the concentration of $InsP_3$ released photolytically is less than 40%.

2.20. Estimation of calcium with fluorescent indicators

The relation between the fluorescence emitted by the fluorescent calcium indicator and $[Ca^{2+}]$ is:

$$[Ca^{2+}]=K_D.\frac{(F-F_{min})}{(F_{max}-F)} \quad \ldots\ldots\ldots\ldots \quad (1)$$

where K_D is the dissociation constant of the dye, F is the fluorescence of the calcium indicator at free calcium concentration $[Ca^{2+}]$, and F_{min} and F_{max}

are the fluorescence of the indicator in zero and saturating[1] concentrations of Ca^{2+} (see appendix 1). The calcium concentration of a well-stirred homogenous solution of an indicator and calcium ions can also be obtained from the above equation, if it is assumed that there is negligible loss of the excitation light and the fluorescence emitted due to absorption by the solution. The relationship between the fluorescence emitted and $[Ca^{2+}]$ can be approximated to a linear function ($F=[Ca^{2+}]/K_D$) only when the concentration of free calcium is much less than the K_D of the dye. The average calcium concentration of a non-homogenous solution of calcium ions, assuming homogenous distribution of the fluorescent dye, can only be determined if the rate of change in the fluorescence of dye at each point with change in the free calcium concentration is the same.

The high affinity of Fluo-3 for calcium ions (K_D=0.4μM), and the large increase in its quantum efficiency following binding calcium makes it ideal for measuring small changes in the calcium ion concentration around the resting levels of $[Ca^{2+}]_i$. However the non-linearity of Fluo-3 at low μM concentrations of Ca^{++} renders estimation of large intracellular calcium transients impractical since these transients are often associated with existence of large calcium gradients in the cytosol resulting in local saturation of the dye. Consequently measurement of higher $[Ca^{2+}]_i$, and large calcium transients requires an indicator with lower affinity for calcium, such as Furaptra (K_D=44μM). These indicators were selected because the use of caged compounds during experiments prevented the use of indicators requiring an excitation wavelength in the UV range. During the experiments Fluo-3 was excited at 450-490nm and the fluorescence emitted was measured at 515-565nm, and Furaptra was excited at 395-440nm and the fluorescence emitted measured at the wavelengths >470nm.

2.21. Additional calcium buffering and increase in calcium mobility by calcium indicators

The extent of additional buffering introduced into the cell by the calcium indicator can be calculated from the ratio of the bound calcium to free obtained by rearranging the law of mass action equation describing the reaction process at equilibrium;

---

[1] If the binding of calcium ions with the indicator result in a molecule with greater fluorescent quantum efficiency, such as Fluo-3, the F_{min} and F_{max} would be the minimum and maximum fluorescence emitted by the indicator. However if the binding of the calcium ions with the indicator result in a molecule with lower fluorescent quantum efficiency, such as Furaptra, then the F_{min} and F_{max} would correspond to the maximum and the minimum fluorescence of the dye respectively.

$$\frac{[DCa]}{[Ca]} = \frac{[D]}{K_D}$$

$$[DCa]+[D]=[D]_{tot}$$

where, $[DCa]$ and $[D]$ are the concentrations of dye in calcium bound and unbound forms, $[D]_{tot}$ and K_D are the total concentration and the dissociation constant of the dye, and $[Ca]$ is the concentration of free calcium ions. The reported endogenous cell buffering at resting free calcium concentration of 0.1μM is of the order of 50 bound calcium ions to 1 free in the axons of *Loligo* (Baker & Umbach, 1987) and 75 bound to 1 free in bovine chromaffin cells (Neher & Augustine, 1992). In the experiments where Fluo-3 was used to monitor the average cytosolic change of the $[Ca^{2+}]_i$ the concentration of dye, D_{tot}, was 200 μM. By substituting for the K_D=0.4μM (Minta et al, 1989) and the concentration used in the above equation it is apparent that at a free calcium concentration of 0.1μM Fluo-3 would introduce a substantial additional buffering in the cytosol, of an order of 400 bound calcium ions to 1 free. In experiments where the lower affinity dye Furaptra was used, despite the higher concentration (500 μM), the additional buffering introduced is only that of 11 bound to 1 free calcium ions at a free calcium concentration of 0.1μM. Therefore when the results obtained are interpreted it is important to consider the substantial buffering of Fluo-3 compared to the endogenous buffers, although that of Furaptra may be neglected.

The influence of mobile buffer on the distribution of calcium ions can be illustrated by the following considerations. Dyes are soluble and the calcium bound to the dye is able to diffuse in the cytosol, effectively increasing the rate of diffusion of free calcium ions in the cytosol. The diffusion in one dimension is given by Fick's second law:

$$\frac{dC}{dt} = D.\frac{d^2C}{dx^2}$$

where C is the concentration of the diffusing substance along the x-axis, t is time, and D is the diffusion coefficient. The diffusion of a substance is slowed by binding to immobile compounds and Fick's second law is modified to:

$$\frac{dC}{dt} = \frac{D}{R+1} \cdot \frac{d^2C}{dx^2}$$

where R is the number of molecules of the substance bound to the immobile compound for every free molecule (Crank, 1975). The diffusion of calcium, assuming an endogenous cytosolic calcium buffering of 1 free to 75 bound calcium ions at 0.1μM free calcium, is therefore reduced by 1/(75+1) in the cytosol. The effect of introducing 200μM Fluo-3 in the cytosol would be an additional buffering of 400 bound to 1 free calcium ions at a free calcium concentration of 0.1μM. Calcium ions bound to the dye are able to diffuse at the same rate as the dye. Therefore in the presence of Fluo-3 for every 75 immobile calcium ions there exists 401 mobile calcium ions, and the diffusion of calcium in solution would be 401/(75+401), effectively increasing 60 fold. Similarly the increase in the rate of diffusion of calcium with introduction of 500μM Furaptra in the cytosol may be calculated and, in contrast to that brought about by Fluo-3, neglected. In practice the increase in the rate of diffusion is not as high as that estimated, because of binding of dyes to intracellular proteins in the cytosol (Konishi et al, 1991). The effect of calcium buffering and the alteration of the rate of diffusion of calcium on the interpretation of the data obtained will be considered in detail in the discussion.

2.22. Calibration of the fluorescence signal in terms of calcium concentration

Some attempt was made but Fluo-3 cannot be calibrated because it is likely that during the transients recorded the concentration of free calcium exceeded the range at which the dye fluorescence was proportional to concentration. The background fluorescence of the cell was recorded before proceeding to the whole-cell configuration. The extent of equilibration achieved between the patch pipette solution and the cell soma was monitored by recording the fluorescence emitted from the soma of the cells; the signal increased during the 5-8 minutes subsequent to obtaining a whole cell configuration and was usually constant after 10 minutes. Experiments were performed only after the fluorescence emitted did not change with time, with the minimum 'equilibration waiting time' of 10 minutes. To compare signals from different cells the intensity of the excitation light, and the area from which light was collected were kept constant. The intensity of the illumination light was adjusted by applying a constant voltage across the tungsten-halogen lamp, or by measuring the

intensity of the light directly using a photodiode. The epifluorescence aperture placed was set to the minimum required for illumination of the area under study to reduce the background fluorescence. Throughout the thesis Fluo-3 data are given either as the ratio of the change of the fluorescence measured divided by the fluorescence in the resting cell, or simply as the change in the fluorescence.

The low K_D (44μM) of Furaptra for calcium (Konishi *et al*, 1991) allowed calibration of the fluorescence signal to free calcium concentration. Figure 2.11 is the emission spectra for Furaptra at free calcium concentrations 0-1000μM. However because Furaptra has an affinity for magnesium ions (K_D=5.3mM, Konishi *et al*, 1991) as well for calcium ions it is necessary to consider the binding of Furaptra with magnesium ions present in the cytoplasm. The concentration of free ionized magnesium in the axoplasm of the squid axon was estimated to be between 2-3mM (Baker and Crawford, 1972; Bringley and Scarpa, 1975). During experiments with Furaptra the intracellular patch pipette solutions contained 3mM $MgSO_4$ as well as 3mM NaATP which is known to have a high affinity for magnesium ions (pK=4.1 at 25°C and ionic strength of 0.1, Martel and Smith, 1982). If it is assumed that the intracellular magnesium concentration was determined by that of the patch pipette due to dialysis of the cytosol during the whole cell recording, then the proportion of dye bound to magnesium would be 5% when the concentration of free calcium was zero. Furthermore the proportion of unbound dye when $[Ca^{2+}]$ is increased in a solution containing 500μM Furaptra, 3mM NaATP and 3mM MgSO4 is not significantly different in the presence or the absence of magnesium ions (see Figure 2.12 for an estimate of the error). Calibration of the fluorescence signal requires knowledge of F_{min} and F_{max} for each cell, that is the fluorescence emitted when the concentration of free ions in the cytoplasm was zero and saturating, respectively. This was difficult to obtain for the cells in thin slices. However since the resting free calcium concentration of neurones is less than 0.2μM the Furaptra fluorescence of the resting cell was used as an approximation to F_{min}. This, together with the reduction in the proportion of free dye due to presence of magnesium ions, resulted in the underestimation of calcium concentration when the free concentration was less than 2μM, without significantly altering that of high concentrations (Figure 2.12).

In order to obtain F_{max} concentration of free calcium ions in the cytosol needed to be raised to saturate the dye. This is usually done with calcium ionophores such as ionomycin or A23187 in the presence of high extracelluar calcium. This was difficult to do with Purkinje cells in slices because of mechanical difficulty in local application without losing the cell,

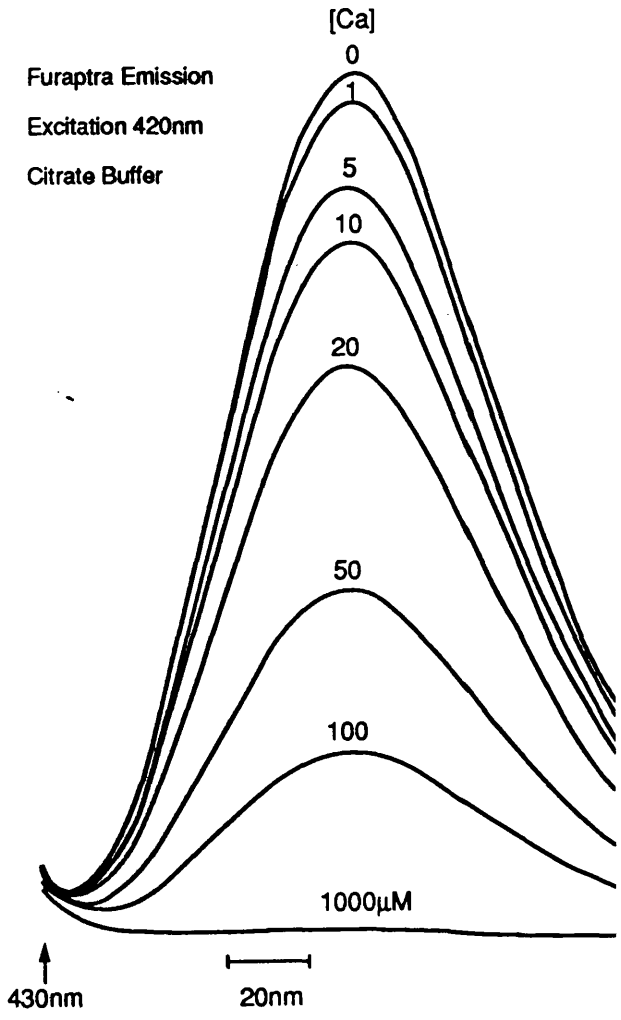

Figure 2.11 The emission spectra of Furaptra with varying concentrations of free calcium

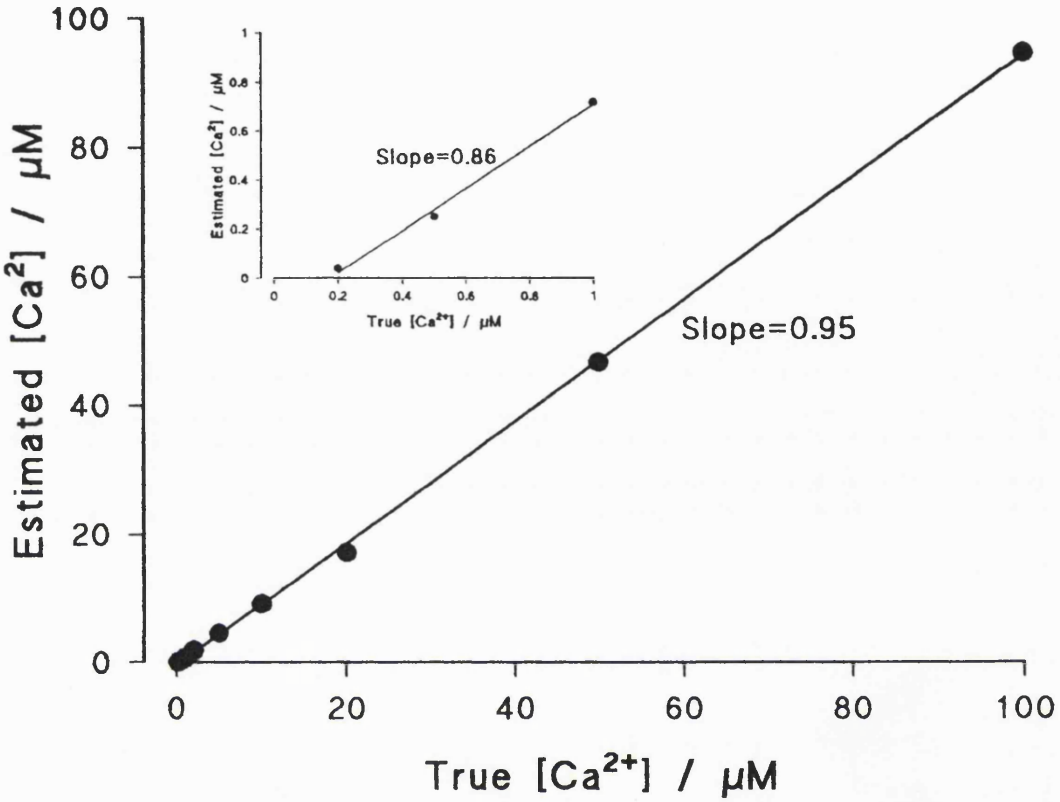

Figure 2.12 Underestimation of $[Ca^{2+}]_i$ by Furaptra under the experimental conditions

Concentration of free calcium reported by Furaptra in presence of magnesium ions was calculated using the procedure used for calibration of the experimental data (Estimated calcium) and is plotted against the actual concentration of free calcium (True calcium). To calculate 'Estimated calcium' it was assumed that F_{max} was zero, F_{min} was the fluorescence of the dye when free calcium concentration was 100nM, and that the solution contained 3mM NaATP, as well as 3mM $MgSO_4$. The K_D of Furaptra for calcium and magnesium were assumed to be 44µM and 5.3mM respectively. A pk=4.1 was assumed for the affinity of ATP for magnesium ions.

Note that the underestimation of free calcium concentration is larger when the free calcium concentration is low (Inset). However for concentrations of free calcium larger than 1µM the 'Estimated calcium' concentration is close to the 'True calcium' concentration.

the existence of diffusion barriers limiting the extent of permeabilisation of the entire cell. Therefore the calibration was done with excised cerebellar Purkinje cells which were whole cell voltage clamped and dye and caged $InsP_3$ present in the patch pipette allowed to equilibrate with the cell cytosol. A known concentration of $InsP_3$ was photolytically released and the change in the fluorescence emitted by the dye recorded. At the end of the experiment 10μM ionomycin, or 10μM A23187 in a calcium rich solution (2mM calcium chloride) was applied to the cells via the pressure puffer (Figure 2.13). Although this resulted in a decrease in the Furaptra fluorescence due to influx of calcium from the extracelluar solution into the cytosol through the permeabilised plasma membrane, maximum reduction in the fluorescence was only achieved when membrane holding potential was switched between +200 and -200mV several times. The minimum fluorescence thus obtained, corresponding to saturation of the dye with calcium (F_{max}), was not significantly different from the background fluorescence of the cell. Therefore for calibration of the fluorescence signal recorded from cells in slices, where F_{max} was not determined experimentally, the background fluorescence of each cell was considered as their F_{max}.

The background signal was offset, the signal amplified, filtered with a time constant of 4ms, and digitised together with the membrane current by a CED 1401-plus analogue to digital converter. The accuracy of analogue to digital conversion was examining by digitizing records of ±20mV pulses applied to the input of the tape recorder. The maximum reduction in the Furaptra fluorescence following the pulse of UV light was measured from the digitized data using CED software, Signal Averager (Cambridge Electronic Design). The fluorescence change was subtracted from F_{max} to obtain F, and was substituted in equation (1) together with the corresponding values of F_{max}, F_{min}, and K_D to yield an estimate of the peak calcium concentration during each fluorescence transient. For this the K_D of Furaptra *in vivo* was assumed to be the same as its K_D *in vitro* (44μM), although it is possible that the apparent affinity of the dye for calcium ions is larger *in vivo* than *in vitro* due to binding of the dye to intracellular proteins (see Konishi et al, 1991), resulting in the underestimation of calcium concentration. This possibility was not investigated in these experiments.

The area under the calcium transient was estimated by calculating the mean fluorescence during the transient, calculating $[Ca^{2+}]$ from equation (1) and multiplying by the duration of the transient. This probably underestimates the total mobilised calcium because the calcium concentration was close to or larger than the K_D of the dye. A more accurate procedure would have been to convert each point of the

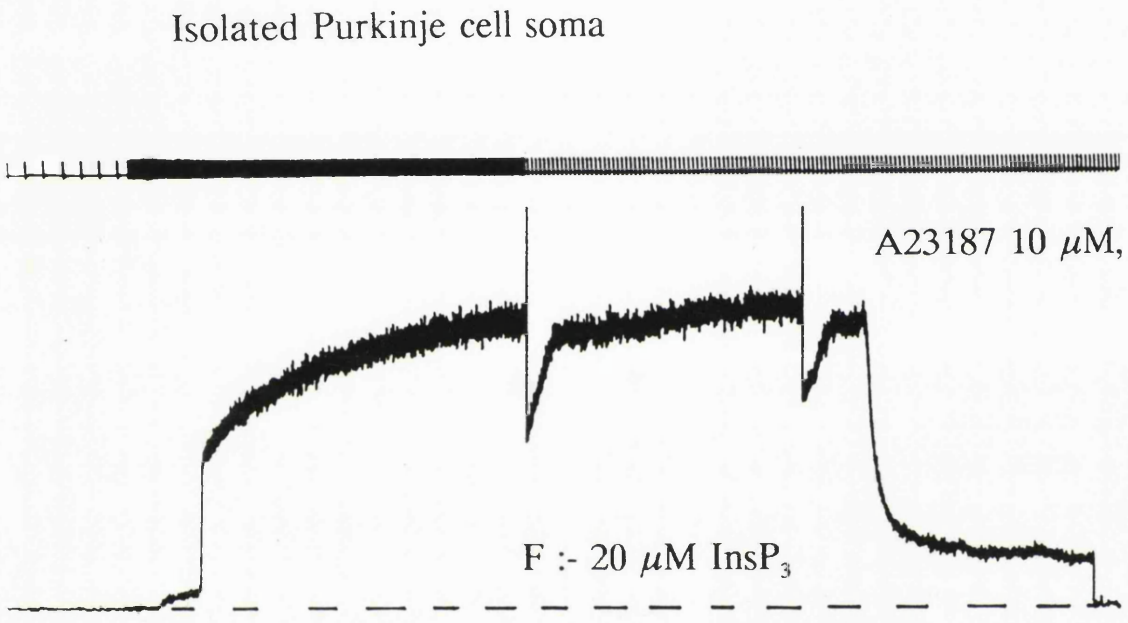

Figure 2.13 Use of excised Purkije cells for calibration of Furaptra fluorescence records

Figure shows fluorescence measured from the soma of an excised Purkinje cell patch clamped with a pipette containing 200μM Furaptra, 100μM caged $InsP_3$, 3mM $MgSO_4$, 3mM NaATP, 153mM K-Gluconate, and 10mM K-HEPES pH 7.2. Following obtaining whole cell configuration, Furaptra and caged $InsP_3$ diffused into the cytosol (the sudden increase in fluorescence record is due to an improvement of the access resistance). After about 10 minutes no further increase in the fluorescence signal was observed (at this time equilibrium between the contents of patch pipette and cytosol was assumed). As an approximation, this value of the signal was used as F_{min}.

Following discharge of the xenon arc lamp (150V) releasing an estimated 25μM $InsP_3$, a rise in $[Ca^{2+}]_i$ was detected as a decrease in the Furaptra signal. F_{max}, the fluorescence of Furaptra in saturating concentrations of free calcium, was obtained by application of 10μM A23187 in presence of 2mM $CaCl_2$ *via* a pressure puffer.

fluorescence response to calcium concentration before integration. The area under the current trace was digitized and integrated directly. Latency of the onset of fluorescence and current responses were estimated from records digitized at 1kHz.

Chapter 3
Caged L-glutamate

3. Characterisation of 'caged' glutamate

Several photolabile analogues of L-glutamate synthesised by Drs John Corrie, Yoshiki Katayama, Gordon Reed, and David Trentham (Division of Physical Biochemistry, National Institute for Medical Research, Mill Hill, London) were studied to establish their suitability as caged neurotransmitters (Figure 3.1). From the compounds listed in Figure 1 only the first compound, *N*(1,(2-nitrophenyl)-ethoxycarbonyl)-L-glutamate, satisfied the pharmacological and photochemical properties required from a caged neurotransmitter, although its rate of photolysis under physiological conditions was too slow to allow the study of the rate of activation of the glutamate-gated-ion-channels. The principles and methods for characterisation of any caged neurotransmitter are similar to those decribed here, and this compound (hereafter referred to as caged glutamate) was used to provide evidence for the role of L-glutamate as a neurotransmitter at the squid giant synapse. Details of the synthesis are given in Corrie *et al*, 1993. The experiments to determine the rate and efficiency of photolysis was made by Dr David Trentham.

3.1. Photochemistry of *N*(1,(2-nitrophenyl)-ethoxycarbonyl)-L-glutamate (caged glutamate)

Figure 3.2 outlines the reaction processes that caged glutamate undergoes following a pulse of UV light in the pH range 5.5 to 8, demonstrating the presence of one light and two dark reaction steps. During the light reaction the molecule absorbs photons and rearranges to release a proton and an *aci*-nitro intermediate. The *aci*-nitro intermediate decays to release 2-nitroso-acetophenone, the main photolysis byproduct, and a carbamate which absorbs two protons to release L-glutamate and carbon dioxide.

The rate of formation and decay of the *aci*-nitro intermediate was measured by following the spectral changes at 406nm (Figure 3.3). A solution at 20°C containing (mM) 0.2 caged glutamate, 50 KCl, 2 dithiothreitol, 100 MES at pH 5.8 was placed in an absorbance spectrophotometer linked to a frequency doubled ruby laser (347nm) (Walker *et al*, 1988), and photolysed with a pulse of light providing the rate constants $k_1 > 10^5 s^{-1}$ (faster than the time resolution of the equipment) and $k_2 = 180 s^{-1}$. The release of a proton in step one, and the subsequent absorption of two protons at step three were monitored by recording the spectrophotometric changes of the proton indicator chlorophenol red at 579nm (Figure 3.3). A solution containing (mM) 0.2 caged glutamate, 100

Photolabile Glutamate Analogue

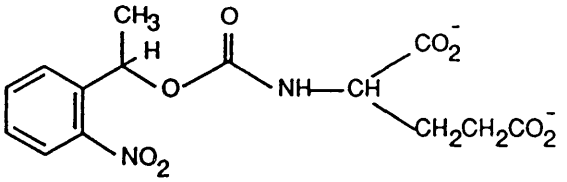

N-[1-(2-Nitrophenylethoxy)carbonyl]glutamate

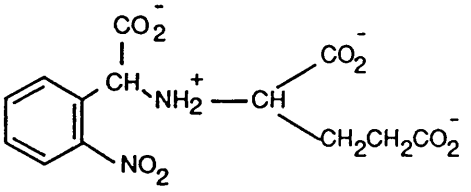

N-(α-carboxy-2-nitrobenzyl)glutamate

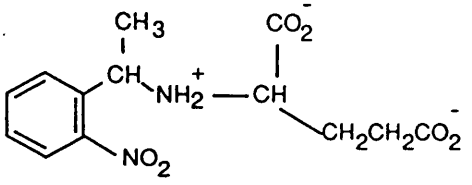

N-[(2-nitrophenyl)ethyl]glutamate

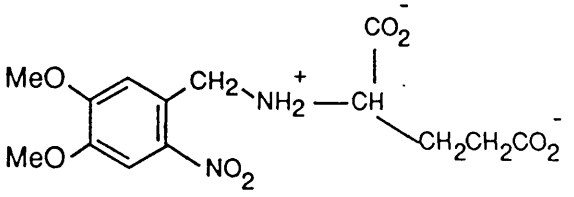

N-(4,5-dimethoxy-2-nitrobenzyl)glutamate

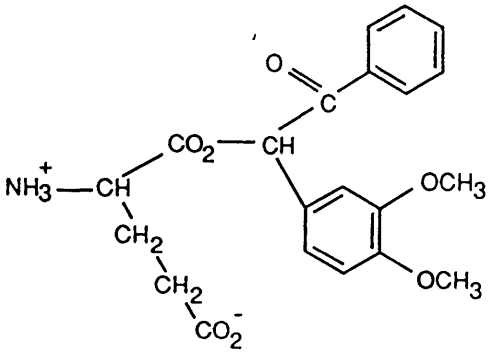

Glutamate α-(3',5'-dimethoxybenzoin ester)

Figure 3.1 The structure of photolabile analogues of L-glutamate.

The structure of several photolabile analogues of L-glutamate. Only the compound on the top of the page satisfied the criteria required from a caged neurotransmitter, although its rate of photolysis at physiological pH is too slow.

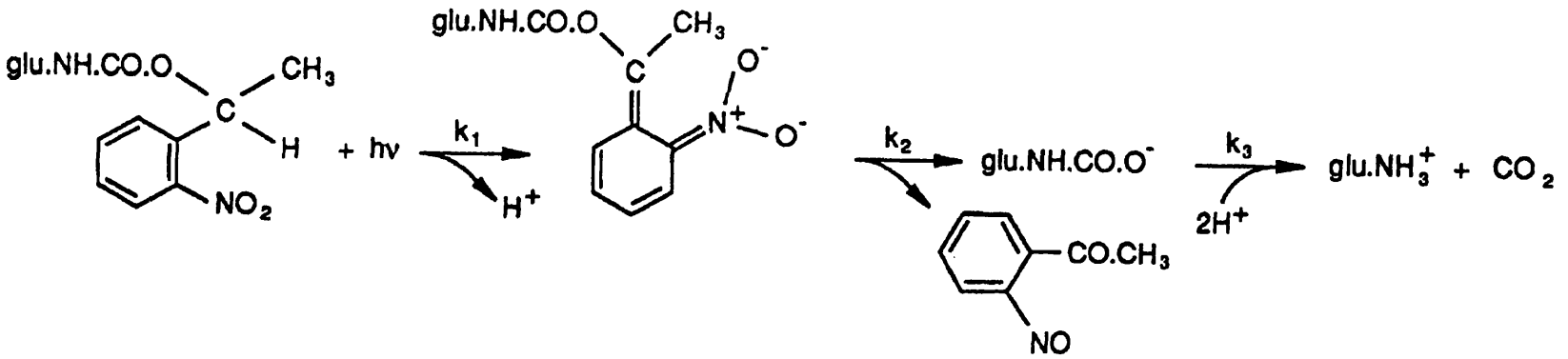

Figure 3.2 The equation describing the photolysis of caged glutamate.

Caged glutamate absorbs the energy of near-UV light to rapidly form an aci-nitro intermediate (the light reaction step), which decays to form a nitrosoketone, and a carbamate. The carbamate decays further to release L-glutamate and carbon dioxide (see text for details).

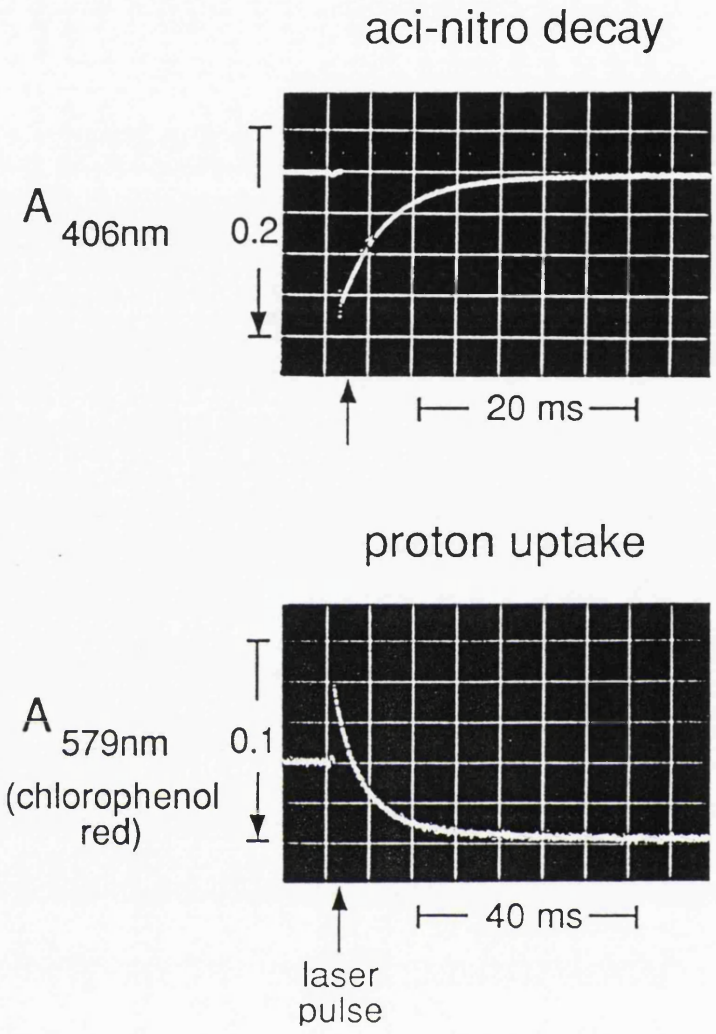

Figure 3.3 Kinetics of photolysis of caged glutamate.

The top trace shows the absorbance spectral changes at 406nm of a solution at 20°C containing (mM): 0.2 caged glutamate, 50KCl, 2 dithiothreitol, 100 MES at pH 5.8 irradiated at the time indicated by the arrow with a pulse of frequency doubled ruby laser. Following the pulse of light the *aci*-nitro intermediate is formed rapidly ($>10^5 s^{-1}$), but decays more slowly ($180 s^{-1}$). The release of one proton, and the subsequent uptake of two protons (see Figure 3.2) is demonstrated in the lower trace which is a record of the proton indicator chlorophenol red spectral changes at 529nm. During the later experiment the solution at 20°C contained (mM): 0.2 caged glutamate, 100 KCl, 1 dithiothreitol, chlorophenol red (concentration adjusted to give A=0.75 at 4mm pathlenght), and 1 mES at pH 5.8.

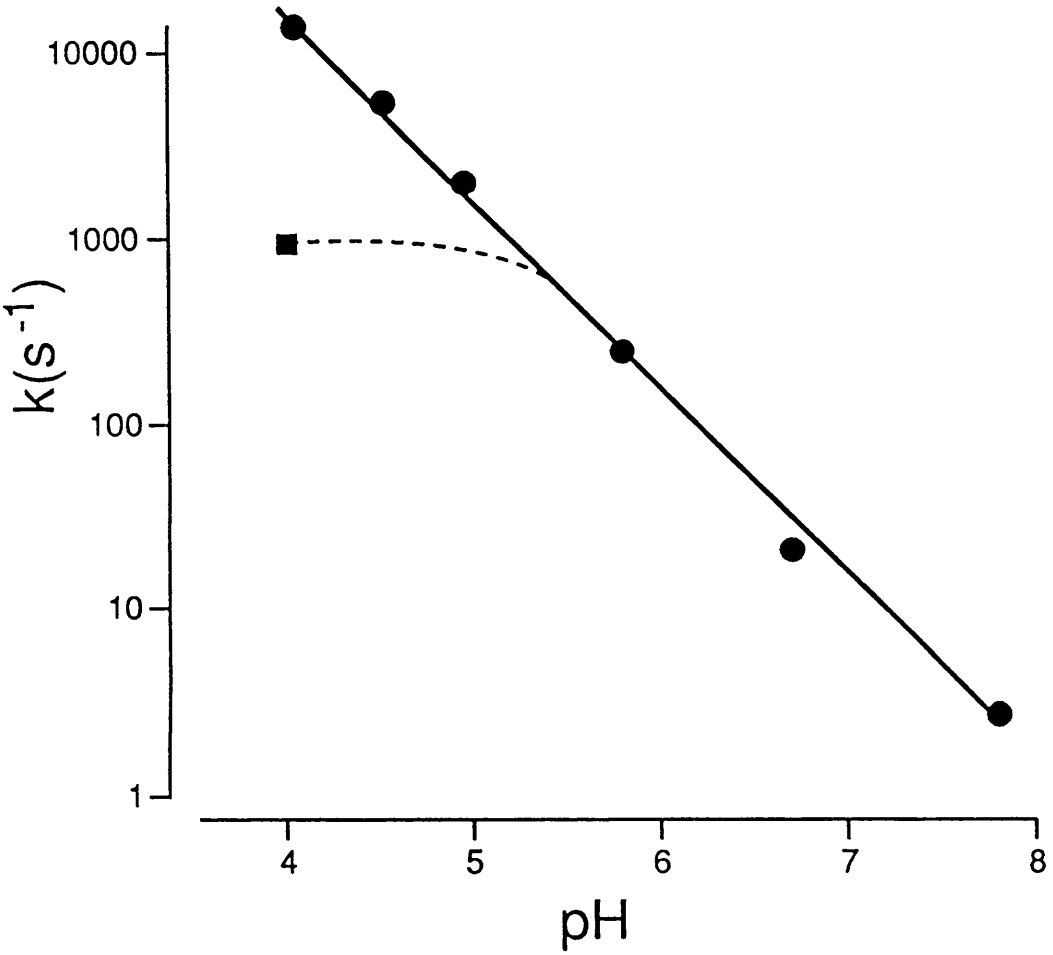

Figure 3.4 The dependence on pH of the rate of photolysis of caged glutamate.

The rate of decay of the *aci*-nitro intermediate (k_1, circles on the graph) is dependent on pH, increasing 10 fold with one pH unit drop. The rate of photolysis of caged glutamate is that of the rate of decay of the *aci*-nitro intermediate above pH 5, and is limited by the rate of decay of the carbamate (step 3) below pH 5 (filled square).

KCl, 1 dithiothreitol, chlorophenol red (A=0.75, 4mm path cell), and 1 MES adjusted to pH 5.8 was placed in the described apparatus. Following the pulse of UV light the indicator detected rapid release of protons followed by a slower absorption with a proton-stoichiometry of one H^+ release to two H^+ uptake as expected from the photolysis equation. From the spectrophotometric change of chlorophenol red the rate constant of the absorbtion of the protons appeared to be the same as that of the decay of the *aci*-nitro intermediate, indicating that $k_3 > k_2$ with k_2 as the rate limiting step. The decay of the *aci*-nitro intermediate was pH dependent and Figure 3.4 demonstrates the proportionality of the rate constant k_2 with pH. The rate constant of proton uptake matched that of the *aci*-nitro intermediate decay above pH 5, however, proton uptake was biphasic below pH 5; the fast phase resembled that of the *aci*-nitro intermediate decay and was attributed to H^+ uptake in step 2, and the slow phase was associated with step 3 (filled square in Figure 3.4).

3.2. Pharmacology of caged glutamate

Whole cell patch clamp recordings from cerebellar granule cells were utilized to investigate the efficiency of the protective group in reducing the potency of caged glutamate at the glutamate activated ion-channel receptors. These cells express L-glutamate activated ion channels (Cull-Candy and Ogden, 1985) of the NMDA and at least two non-NMDA types (Cull-Candy *et al*, 1988; Howe *et al*, 1988, 1991; Wyllie *et al*, 1992). The relative potency of caged glutamate to L-glutamate at NMDA and non-NMDA receptors was estimated. Ideally this is achieved by comparison of the log dose-response curves of the compounds under study. In order to determine log-dose-response curves several concentrations of glutamate and caged-glutamate would need to be tested on the same cell, because the maximum drug-induced conductance vary from cell to cell. However desensitisation of the receptors and short duration of individual whole cell recordings prevented elaborate experimental design. An alternative experimental protocol based on the comparison of the minimum concentration of ligands effective in producing a detectable response was implemented (see appendix 2 for a mathematical treatment). This took advantage of the fact that cerebellar granule cells are small spherical cells (5-10 µM in diameter) with a simple bipolar structure which are efficiently voltage clamped (Cull-Candy *et al*, 1985) and in the whole cell configuration activation of single glutamate channels can be easily resolved (Cull-Candy *et al*, 1988). The effective block of the NMDA receptors with extracellular magnesium ions at hyperpolarised membrane potentials (Nowak *et al*, 1984)

was used to selectively record from the non-NMDA or both NMDA and non-NMDA receptors. Minimum concentration of L-glutamate needed to produce activation of glutamate gated channels in the absence and presence of 2.5mM extracellular Mg^{2+} ions was compared to that of 1mM caged glutamate to yield the low concentration potency of the two compounds. In the absence of magnesium block of the NMDA channels, activation of glutamate gated channels was detected in whole cell voltage clamped granule cells (holding potential -70mV) with 125nM but not 60nM L-glutamate (Figure 3.5). In the presence of magnesium a much higher concentration, 50μM L-glutamate, was needed to produce activation of the channels. Application of solutions containing 1 mM caged glutamate seldom resulted in the activation of an ion channel in the absence of 2.5mM Mg^{2+} ions (Figure 3.6), and never in the presence of Mg^{2+} ions. It was concluded that compared to L-glutamate, caged glutamate is at least 10000 times less potent at the NMDA, and at least 50 times less potent at the non-NMDA receptor sites.

The possibility that addition of the protective group to L-glutamate had resulted in a compound with potency as an antagonist at the glutamate sites was examined. L-glutamate (50μM) was applied to the cells *via* the perfusion in absence of external magnesium ions and the effect of puffer application of a solution containing 50μM glutamate and 1mM caged glutamate on the sustained response was examined. No alteration in the responses were detected (Figure 3.7) indicating that 1mM caged glutamate did not block the NMDA receptor-channel site. Block at the non-NMDA sites was studied by comparing the response of the cells to rapid application of L-glutamate in the presence and absence of 1 mM caged glutamate. No change in the amplitude or kinetics of the response was observed.

The experiments outlined above examined the potency of 1mM caged glutamate as an agonist or antagonist at the glutamate activated ion-channel sites. No attempts were made to investigate the action of caged glutamate on glutamate 'metabotropic' receptors or the glutamate uptake sites. Such experiments should be carried out if caged glutamate is to be used in preparations where functional 'metabotropic' receptors exist, or when caged glutamate is used to study synaptic processes *in situ* where uptake of glutamate by glial cells and neurones plays an important role in maintaining the extracellular glutamate at low concentrations (Hertz, 1979). The possible actions of caged glutamate on the glutamate uptake system can be investigated by taking advantage of the stoichiometry of glutamate uptake. During each cycle of the transport system at least two sodium ions are cotransported into the cytosol with a glutamate molecule, and a potassium ion and possibly bicarbonate ion is extruded out of the cell

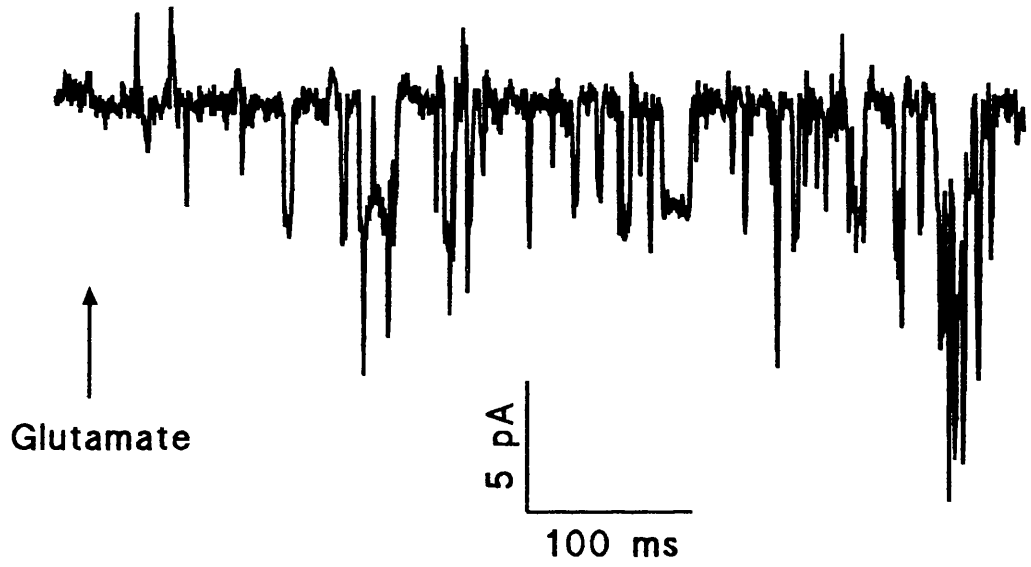

Figure 3.5 Effect of 125nM L-glutamate on the whole cell conductance of a granule cell.

125nm L-glutamate was applied *via* a pressure puffer at the time indicated by the arrow to a voltage clamped (-70mV) cerebellar granule cell in primary culture. The external solution did not contain any Mg^{2+} ions.

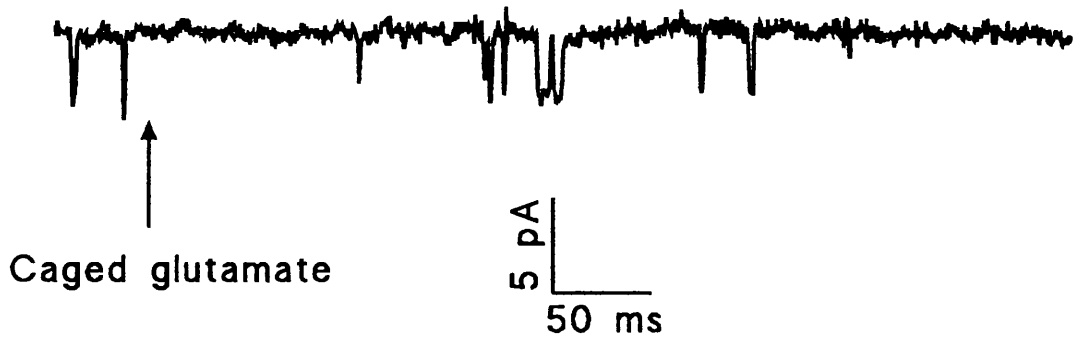

Figure 3.6 Effect of 1mM caged glutamate on the whole cell conductance of a granule cell.

1mM caged glutamate applied *via* a pressure puffer did not result in the activation of multiple glutamate gated ion channels. The record shows the whole cell conductance of a voltage clamped cerebellar granule cell in a solution with no added Mg^{2+} ions.

(Stallcup *et al*, 1979; Barbour *et al*, 1988; Bouvier *et al*, 1992), resulting in a net influx of positive charges easily detectable as an inward current with a whole cell patch pipette (Brew and Attwell, 1987). Design of experiments to study the possible actions of caged glutamate on the 'metabotropic' receptors is more difficult due to the ill-defined physiological processes activated by these receptors.

3.3. Pharmacology of the byproduct, 2-nitroso-acetophenone

It is important to characterise the pharmacology of the photolysis intermediates and the photolysis byproduct, 2-nitroso-acetophenone, since they are formed and released concurrently with L-glutamate following the pulse of UV light, a fact that also makes their study difficult. An alternative approach was therefore the use of 1-(2-nitrophenyl)ethyl phosphate, (caged phosphate), which with the same photolytic efficiency as caged glutamate photolyses to form the same intermediates and nitrosoketone with inert phosphate (Walker *et al*, 1988). Caged phosphate (1 mM) was added to the solution bathing the granule cells and photolysed (1 ms pulse, 300-350nm, 100 mJ) in the absence of any added magnesium without altering the cell conductance (data not shown). It was concluded that the photolysis intermediates and byproducts of 1mM caged phosphate did not posses any glutamatergic potency. To test whether the byproduct interfered with the activation of ion-channels by L-glutamate 2mM caged phosphate was applied with the puffer together with 50µM L-glutamate onto the cells and responses recorded. A mercury lamp (300-350nm, 1W) was used to produce continuous photolysis of caged phosphate and the response of the cells to rapid application of glutamate and the released byproducts was compared to those obtained previously. No change in the response was observed, indicating the lack of action of the photolysis byproduct on the glutamate activated ion-channels.

The possible actions of the released nitrosoketone and the photolysis intermediates on the glutamate 'metabotropic' receptors or the glutamate uptake site was not tested.

3.4. Photolysis of caged glutamate

The percentage photolysis of caged glutamate under our experimental conditions was determined by flashing a 10µl drop of 1mM caged glutamate on the microscope stage with full light intensity (300-360 nm, 100 mJ), and estimating the concentration of glutamate released with reversed phase

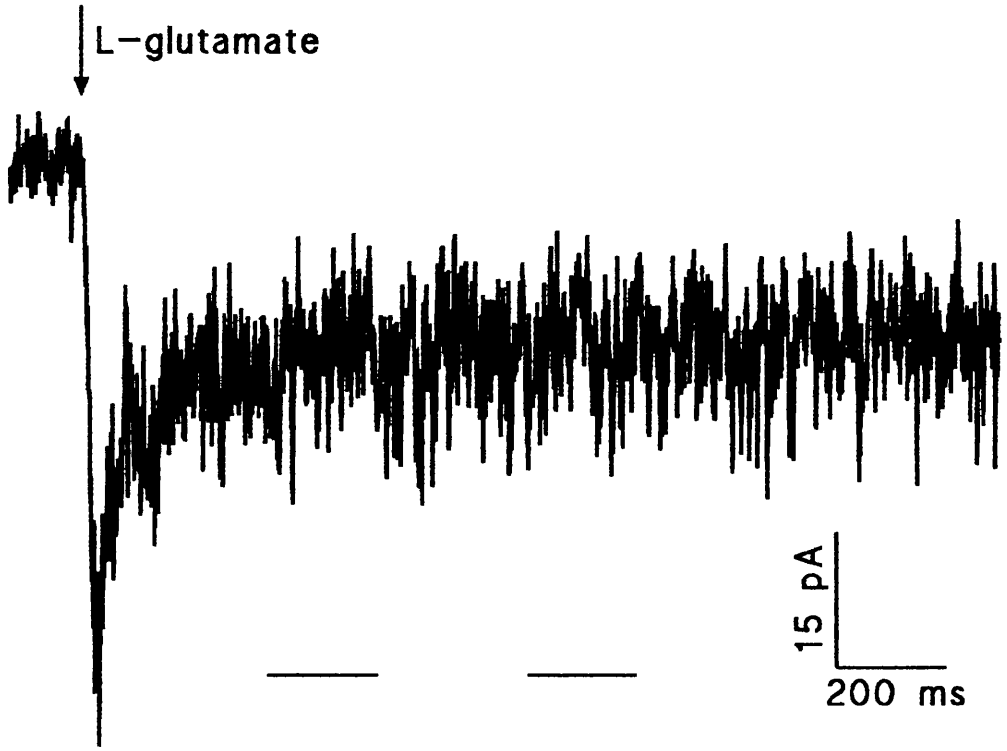

Figure 3.7 1mM caged glutamate did not block the NMDA receptors.

50μM L-glutamate was applied to a voltage clamped cerebellar granule cell in primary culture *via* the bath perfusion in the absence of Mg^{2+} ions. Puffer application of 1mM caged glutamate (indicated by the bars) did not alter the sustained response. Since the majority of current during the sustained response was as the result of activation of the NMDA channels, it was concluded that 1mM caged glutamate was ineffective as a NMDA channel blocker.

HPLC*. Using this method the photolysis yield was estimated to be 35.6% similar to that of caged ATP, and high enough to allow for its use in physiological preparations.

Freshly dissociated dorsal root ganglion cells were used in addition to cerebellar granule cells to study the kinetics of photolysis of caged glutamate. These cells express functional non-NMDA receptors activated by kainate and quisqualate during their first few days in culture (Huettner, 1990) and produce a much larger current in response to application of glutamate (approximately -120 pA at -70 mV) compared to cerebellar granule cells (approximately -40 pA at -70 mV). Following the establishment of whole cell recording the external solution was changed to one containing 1mM caged glutamate and a pulse of UV light was delivered to release 400µM L-glutamate. In 19 cells out of 24 an inward current was detected following a pulse of UV light (Figure 3.8). All 24 cells, however, produced a response when 50µM L-glutamate was applied to them with the puffer. It is possible that during experiments on the 5 cells that did not respond with the UV pulse the flash lamp was miss-aligned. Six dorsal root ganglion neurones were chosen for kinetics analysis. These cells were not exposed to L-glutamate prior to the UV pulse and therefore no desensitisation of the glutamate receptors could have occurred. In these cells the peak current occurred after 107ms (mean, range 78-137 ms), with a half time of 52ms (mean, range 35-80 ms). In the same cells the time taken to obtain a maximal response with puffer application of 50µM glutamate was 14.7 ms (mean, range 5-30 ms).

3.5. Discussion

It is clear from the experiments described that although *N*(1,(2-nitrophenyl)-ethoxycarbonyl)-L-glutamate satisfied many of the criteria required for a caged neurotransmitter its rate of photolysis at physiological pH was too slow to allow the study of rate of receptor activation and the processes involved in synaptic transmission. To be of use, alternative photolabile analogues of L-glutamate need to be synthesised with a faster rate of photolysis. Experiments to be described in the following chapter, however, will demonstrate the use of caged

---

* Glutamate was separated using reverse phase HPLC (Microsorb C18 ODS) and was detected using UV fluorimetry (360/470nm). The mobile phase was isocratic, and contained 80% 75mM KH_2PO_4 buffer and 20% methanol at pH 5.58. The sample was derivatised by the addition of equal volume of opthaldehyde/mercaptopropionic acid and 50µl of the mixture was injected automatically (Gilson 231 autoinjecter) after 1 minute. The amount of glutamate was calculated from a previously obtained standard curve.

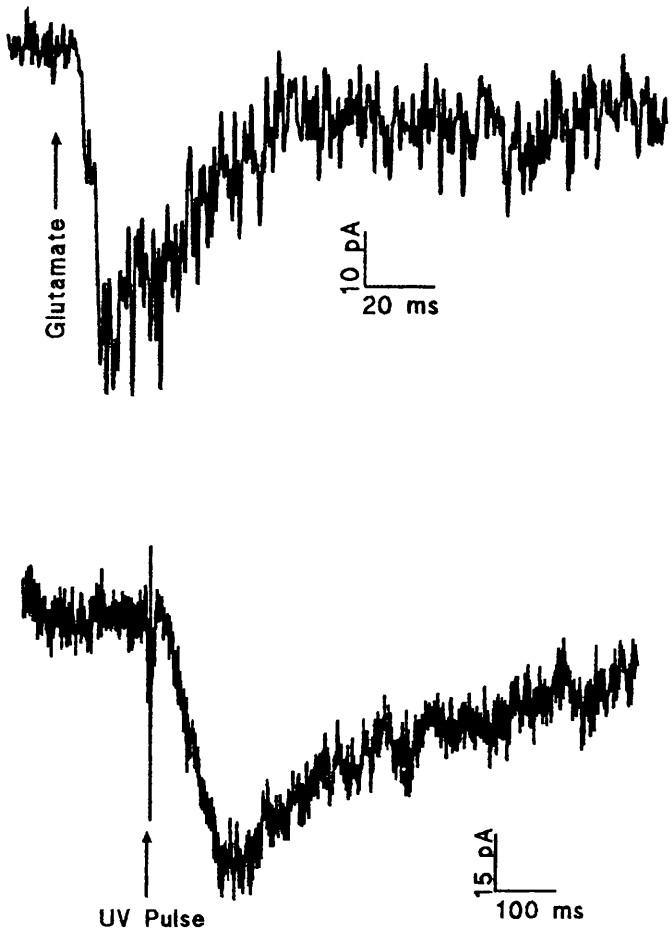

Figure 3.8 Photolytic release of L-glutamate.

The lower trace shows the current of a whole cell voltage clamped cerebellar granule cell bathed in an extracellular solution to which 1mM caged glutamate was added. At the time indicated by the arrow 400μM L-glutamate was photolytically released resulting in the activation of the glutamate activated ion channels. The inward current reached its maximum in 100ms. The top trace shows application of L-glutamate to another voltage clamped granule cell *via* the pressure puffer. Note the difference in the time scales.

glutamate where the ability of the preparation to withstand acidic pH was exploited to increase the rate of photolysis. Under these conditions the rapid application of L-glutamate at the squid giant synapse by photolysis of caged glutamate resulted in the production of action potentials at the 3rd order fibre, a phenomenon which had not been possible to demonstrate by other means due to presence of diffusion barriers, supporting the pharmacological evidence for L-glutamate as a neurotransmitter.

Chapter 4
Glutamate at the squid giant synapse

4. L-Glutamate as the neurotransmitter at the squid giant synapse

Synchronous activation of the motor axons innervating the muscle in the mantle of the squid impart fast jet propulsion to the squid. One set of these motor axons consist of about ten third-order giant axons (Martin and Miledi, 1986) which originate in the stellate ganglion (Young 1938), and receive their input through a single preganglionic nerve, the second-order giant fibre (Young 1939). The 'giant synapse' referred to in this chapter is the synapse of the last branch of the second-order axon with the most medial and thickest of the third-order fibre. The giant synapse is over 1mm long (Martin and Miledi, 1986), and Figure 4.1, Young's drawing of the synapse (Young, 1973), demonstrates the complex structure of this synapse; numerous postsynaptic processes penetrate a tight sheath to make 15000 functional contacts with the presynaptic fibre (Martin and Miledi, 1986) with the synaptic clefts only 12nm wide (Martin and Miledi, 1986).

The nature of the neurotransmitter at this synapse is not yet established with certainty. The strongest candidate, L-glutamic acid, was proposed to be a neurotransmitter due to its depolarising actions (Miledi, 1967). However close postsynaptic application of L-glutamate by ionophoresis, or by bath application of L-glutamate or glutamate agonists fail to elicit action potentials and result only in slow, weak depolarisation of the postsynaptic membrane (Miledi, 1967, 1969; De Santis *et al*, 1975; Adams and Gillespie, 1988; De Santis and Messenger, 1989). This is attributed to the complex structure of the synapse; diffusion of externally applied agents into the synapse is slow resulting in desensitisation of the postsynaptic receptors and a postsynaptic potential rise too slow to discharge action potentials. Further evidence in support of L-glutamic acid as the endogenous neurotransmitter is that continued soaking of the stellate ganglion in solutions containing L-glutamate results in the blockade of transynaptic transmission (Kelly and Gage, 1969), presumably due to desensitisation of the receptors involved in synaptic transmission. Furthermore specific non-NMDA antagonists of glutamate-gated ion channels such as the spider toxins JSTX or argiotoxin$_{636}$ (Kawai *et al*, 1983a; 1983b; Kerry *et al*, 1988; De Santis and Messenger, 1989), and quinoxalinediones CNQX, DNQX (De Santis and Messenger, 1989) are able to block synaptic transmission and L-glutamate induced depolarisation. Antagonists of the NMDA channels do not block either the postsynaptic potentials nor glutamate induced depolarisations (De Santis and Messenger, 1989) and it is thought that the channels activated by glutamate at the stellate ganglion may be similar to those found at the locust (Anwyl, 1977; Bateman *et al*, 1985) and crayfish (Dekin, 1983) neuromuscular junction.

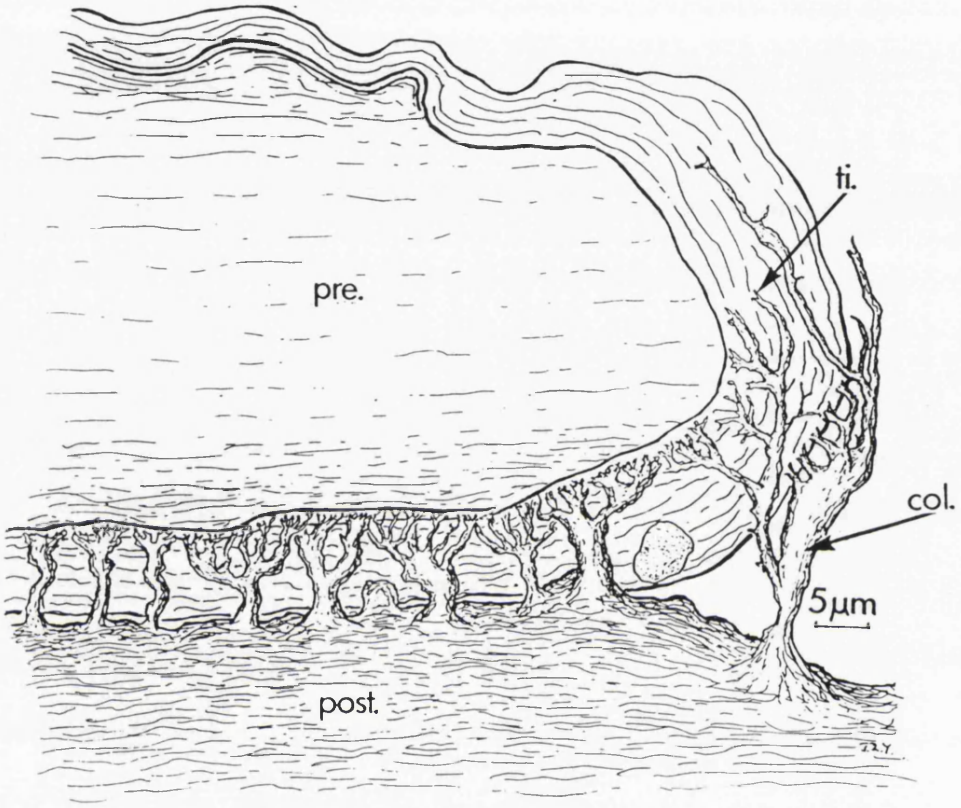

Figure 4.1 The giant synapse

Young's drawing of the giant synapse (Young 1973) demonstrating the complex structure of this synapse. Numerous postsynaptic processes penetrate a tight sheath to make 15000 functional contacts with the presynaptic fibre.

The main difficulty for the role of glutamate as the endogenous neurotransmitter is the that the reversal potential of depolarisations evoked by glutamate is different to that of the postsynaptic potentials (Miledi, 1969; Llinas *et al*, 1974); the postsynaptic potentials reverse at a membrane potential of +13-40 (Miledi, 1969), or +18-25mV (Llinas *et al*, 1974) though that of glutamate induced depolarisation reverse at more negative potentials, -22mV (Miledi, 1969), -30mV (Eusebi *et al*, 1985) or -36mV (Adams and Gillespie, 1988). The possible explanation for the different reversal potentials obtained by various experimenters and the discrepancy between the reversal potential of glutamate induced depolarisations and the transynaptic potentials may be that there is a considerable voltage variation in the postsynaptic membrane due to the complex structure and considerable size of the giant synapse (Miledi, 1969; Dekin *et al*, 1983; Adams and Gillespie, 1988; Messenger *et al*, 1992). It should be noted that the only other contender as the endogenous neurotransmitter at the giant synapse, acetylcholine, (Webb *et al*, 1966; Stanley, 1983) was shown to increase the membrane permeability to a chloride channel and therefore is not the excitatory neurotransmitter (Stanley, 1984).

The complex structure of the giant synapse has resulted in failure of several methods which have attempted to abruptly apply L-glutamate to the synapse to test whether it can elicit postsynaptic action potentials. Experiments reported here were designed to bypass the tortuous access paths to the synaptic cleft; the stellate ganglion was soaked in a solution containing caged glutamate, allowing the compound to equilibrate with the synapse, and L-glutamate was rapidly released *in situ* by flash photolysis. The ability of L-glutamate released abruptly in the giant synapse to elicit postsynaptic action potentials are discussed.

4.1. Depolarisation of the giant synapse with photolytic release of L-glutamate at pH 7.8

Synaptic transmission was demonstrated in the excised stellate ganglion by stimulating the pallial nerve stump at 10 times threshold voltage and recording postsynaptic potentials with a microelectrode inserted close to the synaptic region in the most medial third order giant fibre. The pH of the solution was controlled with 50mM HEPES at pH 7.8 and when stable transmission was established, caged L-glutamate dissolved in artificial seawater was added to the bath to make a final concentration of 5-40mM. The postsynaptic action potential was monitored at 5 min intervals during a 20-40min incubation allowed for diffusion of the caged glutamate into the synaptic region. Synaptic transmission was stable and

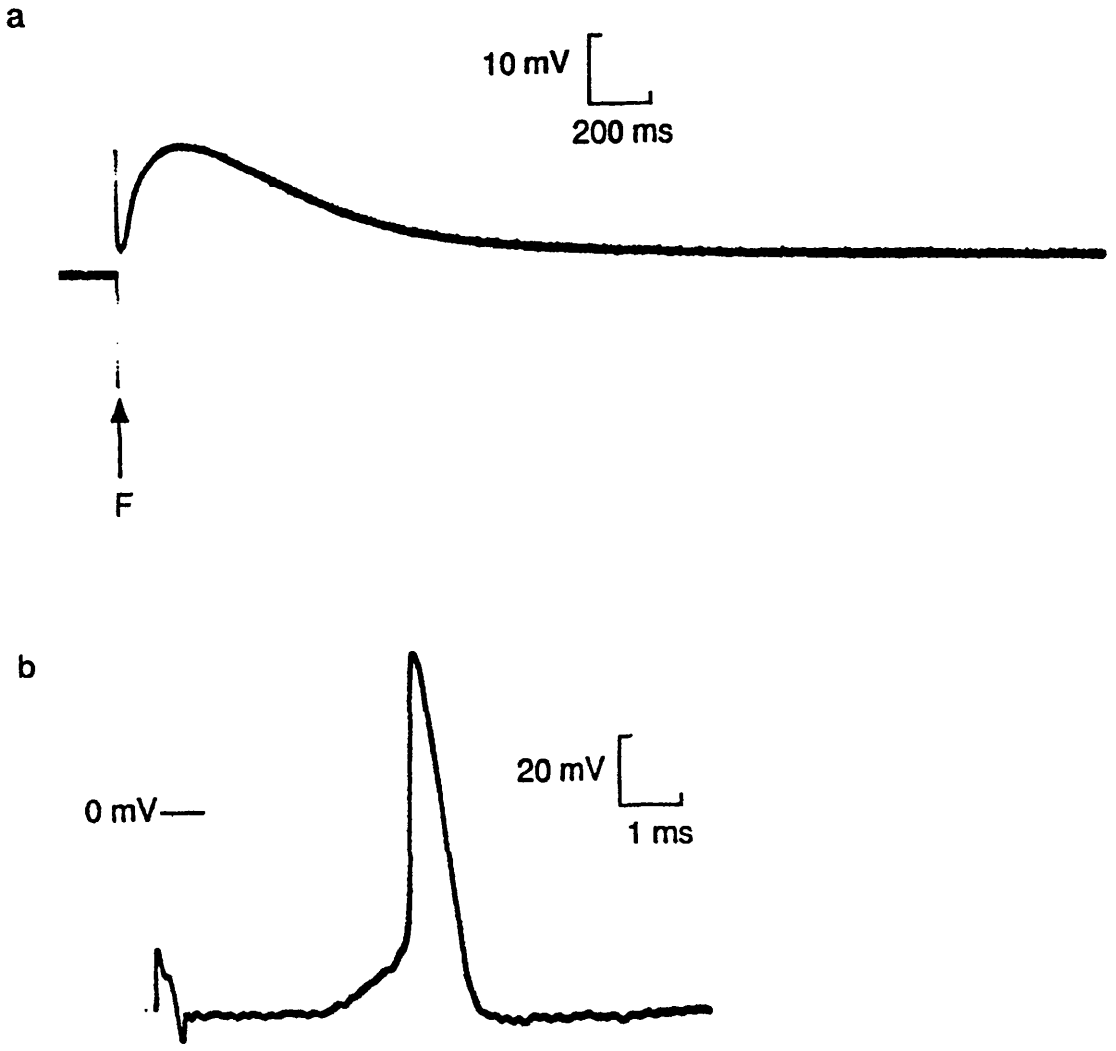

Figure 4.2 Postsynaptic activation by photolytically released glutamate at pH 7.8.

The stellate ganglion was pre-equilibrated for 40 minutes with an artificial seawater containing 20mM caged glutamate at pH 7.8. A full intensity flash (100mJ) produced a 20 mV depolarisation (panel a) of the postsynaptic cell with slow onset (halftime 60ms) and long duration (1.6s). Transynaptic stimulation produced an action potential (panel b) about 1 minute after the photolytic release of glutamate shown in panel a.

was not affected by the presence of caged glutamate. After 40min equilibration in 20mM caged glutamate release of about 5mM free glutamate produced a 20mV depolarisation of the postsynaptic cell with slow onset (halftime 60 ms) and long duration, 1.6s (Figure 4.2a). The size of the depolarisation was much smaller than that seen with electrical stimulation of the presynaptic terminal in presence of TTX (Miledi, 1969), perhaps because the slow release of glutamate at this pH resulted in the desensitization of the glutamate receptors, and the slow change of potential favoured inactivation of the Na^+ conductance. Normal transynaptic action potentials were generated after photolysis once the depolarisation had subsided (Figure 4.2b). The possibility that desensitization of glutamate receptors occured was tetsted by fyrther photolytic release of glutamate at the plateau of the glutamate-evoked depolarization. This produced no further depolarization (data not shown), even though about 75% of the caged glutamate was still available for photolysis. Transynaptic activation was also suppressed during the glutamate depolarization (data not shown), by receptor desensitization or inactivation of the action potential. The slow depolarization with release from caged glutamate at pH 7.8 is similar to that seen with iontophoretic application of L-glutamate and other glutamate receptor agonists to the synapse (Miledi, 1967, 1969; De Santis and Messenger, 1989), although iontophoresis from a microelectrode has the additional problem of not uniformly activating contacts over the whole 1mm length of the synapse (Martin and Miledi, 1986).

4.2. Action potential discharge at the giant synapse with Photolytic release of L-glutamate at pH 5.5

In acid conditions glutamate release from caged glutamate is faster; at pH 5.5 the rate of photolysis is about 200 times that at pH 7.8 (Figure 3.4) and is $95s^{-1}$ at 16°C in artificial sea water. The rate is 0.37 times that shown at pH 5.5 in Figure 3.4 because of the increased ionic strength and lower temperature (McCray and Trentham, 1989). In strongly buffered sea water (50mM MES or 2-phosphoglycerate) transynaptic activation of the ganglion was well maintained at pH 5.5. Figure 4.3a shows postsynaptic action potentials elicited by presynaptic stimulation 19min after replacing the solution around the ganglion with seawater containing 33mM caged glutamate at pH 5.5. After 20min in caged glutamate with release of an estimated 9mM L-glutamate in the synapse the postsynaptic fibre depolarized with a halftime of 10ms and generated a train of 5 action potentials, shown on a fast timescale in Figure 4.3b. The first action potential was identical in amplitude to single spikes elicited

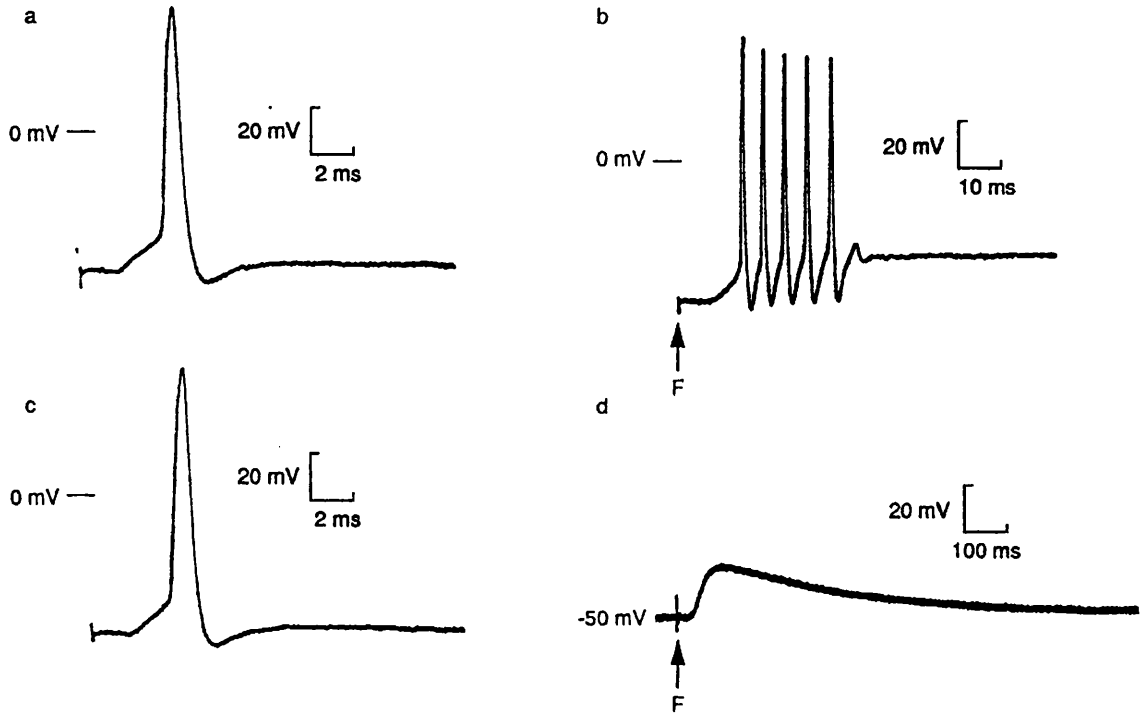

Figure 4.3 Photolytic release of glutamate at pH 5.5.

Synaptic transmission was unaffected when the stellate ganglion was soaked in an artificial seawater containing 33mM caged glutamate at pH 5.5. Panels (a) and (c) show postsynaptic action potentials evoked transynaptically before and after photolysis. Panel (b) shows action potentials evoked on photolytic release of 9mM L-glutamate from caged glutamate equilibrated for 20 minutes. At 16°C in artificial seawater (I=0.68M) photolysis rate constant is $135s^{-1}$. Panel (d) shows a subthreshold depolarisation elicited by a weaker flash releasing about 3mM L-glutamate.

transynaptically. Subsequent amplitudes declined as the depolarization was maintained and the action potential mechanism accommodated, and failed after the fifth spike. Once the fibre had repolarised a full amplitude transynaptic action potential could be elicited (Figure 4.3c). Fig.3d shows the depolarization after a weaker flash, releasing about 3mM L-glutamate, when the rate of change of concentration was too small to elicit an action potential, though a subsequent full intensity flash did. These results show that L-glutamate released quickly at the giant synapse is able to generate a large depolarization fast enough to elicit action potentials in the postsynaptic fibre.

4.3. Discussion

To test a putative transmitter more rigorously and obtain information on mechanisms of postsynaptic processes, an ideal experiment would be one in which photolytic application of transmitter can mimic precisely the form of the synaptic potential. In the giant synapse the postsynaptic potential evoked by transynaptic stimulation rises in 1ms and declines in a further 5ms (Miledi, 1967). In contrast the depolarisation following photolytic release of glutamate at pH 5.5 rises in 10-20 ms and declines in about 1s. The slow rise can be attributed to the rate of photolysis of the cage and it is clear that an alternative photolabile analogue of L-glutamate with faster kinetics at physiological pH is required. The slow decline when compared with the synaptic potential, and the firing of several rather than a single action potential, are probably due to the diffuse photolysis of caged glutamate within the ganglion, resulting in activation of receptors outside the area of synaptic contact, for example in the numerous postsynaptic giant fibre cell bodies. By contrast after normal presynaptic release, transmitter is localized in the synaptic cleft and most likely removed by diffusion and uptake into surrounding neural and glial tissue. Therefore further experiments during which the area of photolysis is restricted only to the synaptic region need to be carried out. The technical requirements of such an experimental apparatus will be discussed in chapter 6.

The generation of postsynaptic action potentials by rapid application of L-glutamate in the synaptic cleft is further evidence supporting its role as a neurotransmitter at the squid giant synapse. However to confirm this hypothesis it should be shown that glutamate is present at appropriate levels in synaptic vesicles at the pre-axon, and that it is released upon stimulation of the pre-axon as shown at the crayfish neuromuscular junction (Kawagoe, 1981). Furthermore using the arterial perfusion

technique (Stanly and Adelman, 1984), which partially overcomes the difficulty for applied compounds to diffuse to the synaptic region, quantitative experiments should be done to compare the blockade of transynaptic action potentials with selective glutamate antagonists with the depolarisation induced by perfusion of glutamate, or action potentials produced by photolytic release of glutamate from a faster caged glutamate.

Chapter 5

Functional Properties of $InsP_3$ receptors in neurones

5. Photolytic release of $InsP_3$ in cultured neurones

Experiments were made to examine whether $InsP_3$ released intracellularly in neurones could alter $[Ca^{2+}]_i$, and if so to determine the concentration range at which $InsP_3$ was effective, and to investigate its mechanism of action and effects on the membrane excitability.

Neurones from primary explant cultures were whole cell voltage clamped at a holding potential of -70mV with a patch pipette containing 200μM Fluo-3 and 10-100μM caged $InsP_3$. The intracellular patch pipette solution was allowed to equilibrate with the cell, and the average somatic intracellular free calcium ion concentration was monitored by measuring the fluorescence emitted from the cell body. A 1ms pulse of near UV light was used to produce photolytic release of $InsP_3$ in the cytosol. The extent of photolysis was estimated with the calibration procedure described in chapter 2. $InsP_3$ released intracellularly did not result in a change of the fluorescence emitted by the dye in the cytosol of cerebellar granule cells, hippocampal or striatal neurones or DRGs with concentrations of $InsP_3$ as high as 40μM (n>30 for each cell type, data not shown).

As a control experiment changes in $[Ca^{2+}]_i$ were made by activating voltage gated calcium channels with 500ms depolarisations from the holding potential of -70mV to 0 or +30mV and monitoring the fluorescence emitted by the indicator. A transient rise in the fluorescence was detected during depolarisation (Figure 5.1). The fact that the experimental apparatus detected a change in the fluorescence emitted by the dye during calcium influx, and that no change was seen following the photolytic release of $InsP_3$, it is concluded that intracellular release of $InsP_3$ did not result in alteration of $[Ca^{2+}]_i$ in these neurones.

Experiments were made to examine whether the wash-out of an intracellular component *via* the patch pipette during whole cell recordings was responsible for the lack of calcium mobilisation evoked by $InsP_3$ in cultured neurones. The membrane under the cell attached patch pipette was permeabilized by α-toxin following the procedure described in chapter 2, allowing the introduction of caged $InsP_3$ and Fluo-3 into the cytosol while restricting wash out of intracellular proteins larger than 1000D. Hippocampal (n=3), striatal (n=5), and DRG neurones (n=13) examined with the perforated whole cell voltage clamp technique showed no calcium mobilisation following photolytic release of 40μM $InsP_3$, indicating that wash out *via* the patch pipette of an intracellular protein was not the reason, or that a molecule smaller than 1000D was important. The inability of $InsP_3$ to mobilise calcium from intracellular stores was seen with pipette solutions containing 50μM GTP, or an ATP-regenerating system, indicating that

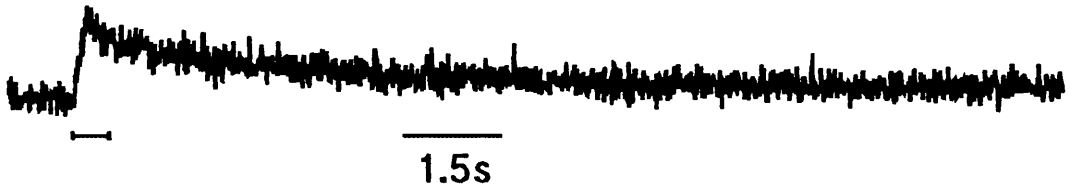

Figure 5.1 The change in the Fluo-3 Fluorescence with depolarisation.

Fluo-3 fluorescence emitted from the soma of a voltage clamped hippocampal neurone in primary explant culture. The bar represents a 500ms step in the membrane potential from -70mV to +30mV.

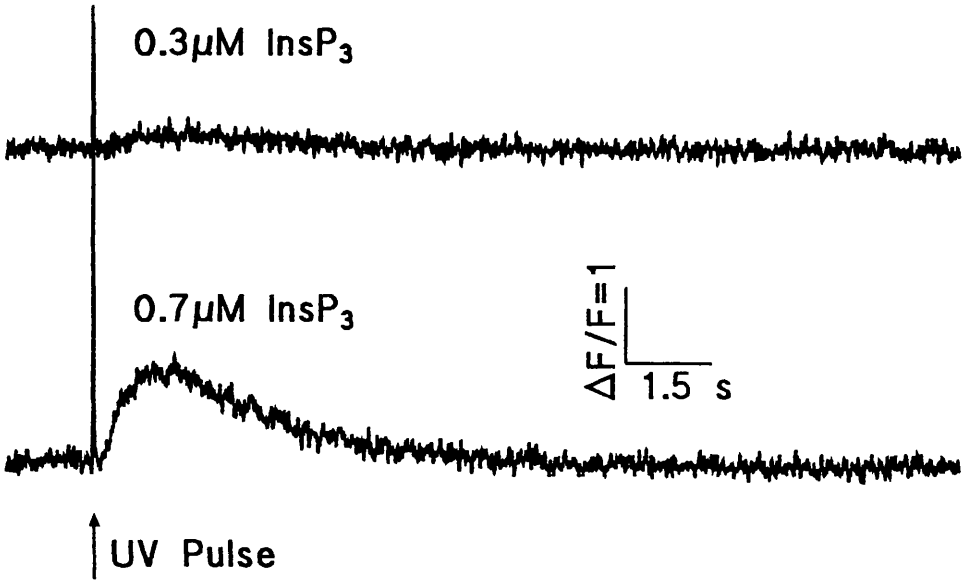

Figure 5.2 Calcium mobilisation by $InsP_3$ released photolytically in an astrocyte.

Fluo-3 fluorescence change following photolytic release of 0.3 and 0.7μM $InsP_3$ in the cytosol of an astrocyte in cerebellar primary culture. The cell was voltage clamped at -40mV.

reduction in the concentration of these compounds due to dialysis *via* the patch pipette was not responsible for the lack of response.

5.1. Calcium mobilisation evoked by $InsP_3$ in astrocytes in culture

Astrocytes from the same primary explant cultures of hippocampus, striatum, and the cerebellum were used to investigate calcium mobilisation by $InsP_3$ with the same procedures used for neurones. In all the cells tested $InsP_3$ at concentrations higher than 0.3μM (n=11) released calcium from intracellular stores in the presence (figure 1) or absence (no added calcium, 0.5mM EGTA) of external calcium. The latency of the onset of the fluorescence change at 0.3μM was about 300ms and decreased with increasing concentration of $InsP_3$ (130ms with 0.7μM in Figure 5.2) so that at high concentrations (about 5μM) the latency was less than 25ms. Increasing the concentration of $InsP_3$ also resulted in an increase in the rate of rise of the fluorescence which was due to a greater efflux of calcium ions from the intracellular stores (Figure 5.2), assuming no change in the rate of removal of calcium. During the experiments astrocytes were voltage clamped at -40mV. At this potential no consistent change in membrane conductance was observed following calcium release evoked by $InsP_3$. It should be noted that calcium mobilisation by $InsP_3$ was seen in astrocytes from the same cultures that had non-responsive neurones.

The mechanism of action of $InsP_3$ in astrocytes was not studied in detail because of the difficulty in identification and classification of astrocytes in tissue culture. Nevertheless the increased efflux of calcium ions from the stores indicated by the rate of rise of fluorescence, and the decreased delay of the rise of the fluorescence signal at higher concentrations of $InsP_3$ in astrocytes are consistent with the direct activation of a calcium permeable channel on the membrane of the intracellular calcium stores by $InsP_3$. Furthermore the range of $InsP_3$ concentrations required to mobilise calcium from the intracellular stores in these cells compared well with that observed in peripheral tissue such as smooth muscle (Somlyo *et al*, 1992), exocrine cells (Gray *et al*, 1989), hepatocytes (Ogden and Capiod, 1990), and vascular endothelial cells (Carter and Ogden, 1992).

5.2. Calcium mobilisation evoked by $InsP_3$ in Purkinje cells in cerebellar slices

Purkinje cells from acutely prepared thin slices of the cerebellum were studied to investigate the ability of intracellular $InsP_3$ to elevate

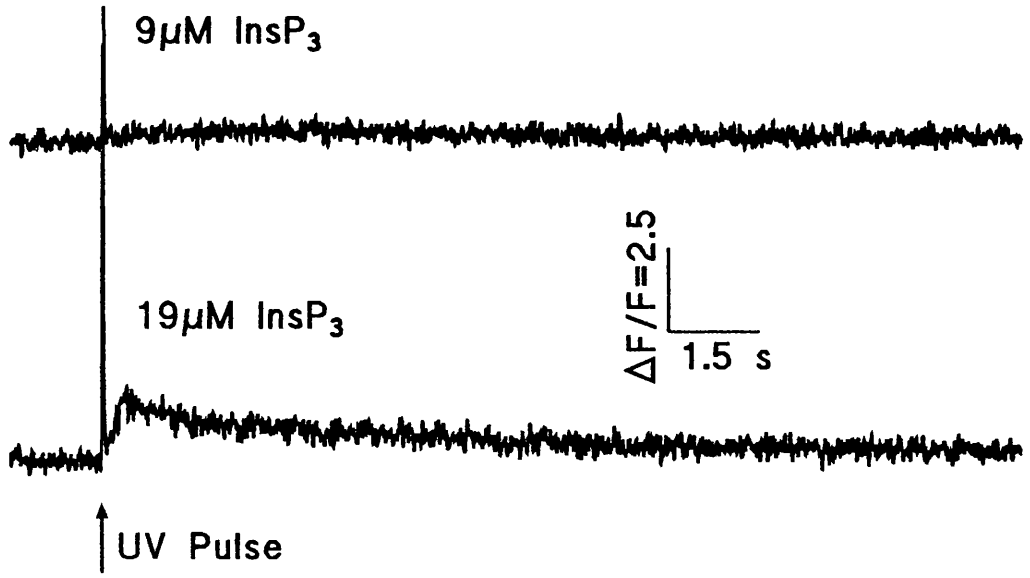

Figure 5.3 Calcium mobilisation by $InsP_3$ released photolytically in a voltage clamped Purkinje cell *in situ*.

Fluo-3 Fluorescence change following the photolytic release of 9 and 19μM $InsP_3$ in the cytosol of a voltage clamped Purkinje cell at a holding potential of -70mV. 50μM caged $InsP_3$ and 200μM Fluo-3 were introduced into the cytosol *via* the patch pipette, and the intensity of the UV pulse was varied to release the concentrations of $InsP_3$ shown.

[$InsP_3$] / μM	9	19	23	25	38
ΔF/F	1.4±0.39 (4)	3.16±0.37 (9)	3.49±0.39 (3)	3.61±0.30 (5)	3.05±0.36 (14)
F latency / ms	93±30.1 (4)	56.1±11.1 (10)	44.6±12.3 (3)	27±6.2 (5)	22.1±3.2 (15)

Table 5.1 Properties of the Fluo-3 light transient following release of $InsP_3$ in the cytosol of voltage clamped Purkinje neurones.

The change in the Fluo-3 fluorescence, and the latency before the onset of the change in the Fluo-3 fluorescence following the photolytic intracellular release of $InsP_3$ in voltage clamped Purkinje neurones. Values are means with the SEM, and the number in parenthesis indicate the number of cells.

$[Ca^{2+}]_i$. The range of concentrations at which $InsP_3$ was capable of mobilising calcium was determined, and attempts were made to elucidate mechanism of $InsP_3$ action and its role in the control of the membrane excitability. The data obtained from use of fluorescent calcium indicators Fluo-3 and Furaptra will be discussed.

5.3. Use of Fluo-3 to follow the changes in $[Ca^{2+}]_i$

Fluorescence emitted from the soma of voltage clamped Purkinje cells (holding potential -70mV) equilibrated with 200µM Fluo-3 and 50-200µM caged $InsP_3$ was recorded to monitor the intracellular free calcium ion concentration. $InsP_3$ concentrations greater or equal to 9µM elevated $[Ca^{2+}]_i$ indicated by an increase in the Fluo-3 fluorescence (Figure 5.3). The term 'light transients' used hereafter refers to the transient changes in the fluorescence emitted by the calcium indicator due to an increase of $[Ca^{2+}]_i$. The peak of the light transients evoked by $InsP_3$ increased with increasing $InsP_3$ concentrations from a value of 2.4±0.39 ($\Delta F/F$, SEM, n=4, range 0.95-3.25) at 9µM $InsP_3$, to 3.05±0.36 (SEM, n=14, range 0.93-5.25) at 38µM $InsP_3$ (Table 5.1, Figures 5.3, 5.4, & 5.7).

Experiments were made to determine whether the elevation of $[Ca^{2+}]_i$ following the photolytic release of $InsP_3$ was due to calcium entry from the extracellular solution, calcium mobilisation from the intracellular stores, or both. The bathing solution was changed to a calcium free solution (calcium ions replaced with magnesium ions and 0.5mM EGTA) and the removal of calcium from the extracellular space monitored with repeated depolarisations. Under conditions at which no change in the intracellular calcium was detected in the soma with depolarisation, $InsP_3$ released photolytically was capable of producing calcium transients. The lack of extracellular calcium during calcium transients evoked by $InsP_3$ confirmed that calcium was mobilised from intracellular stores and had not entered the cytosol through the plasma membrane.

To investigate the mechanism of calcium mobilisation by $InsP_3$ the immediate events following the photolytic release of $InsP_3$ were studied. Following the pulse of UV light there was an optical artifact 20ms long due to phosphorescence of the recording chamber and the objective. This was reduced in some experiments to <6ms by replacing the 515-565nm barrier filter with a 530nm narrow band interference filter. The fluorescence rise following a pulse of UV light was observed after a delay which had a mean of 93±30.1ms (SEM, n=4, range 40-164ms) at the lowest effective concentration of $InsP_3$ (9µM) and decreased with increasing $InsP_3$ concentration to 22.1+3.2ms (SEM, n=15, range 8-50ms) at 38µM $InsP_3$ (Table

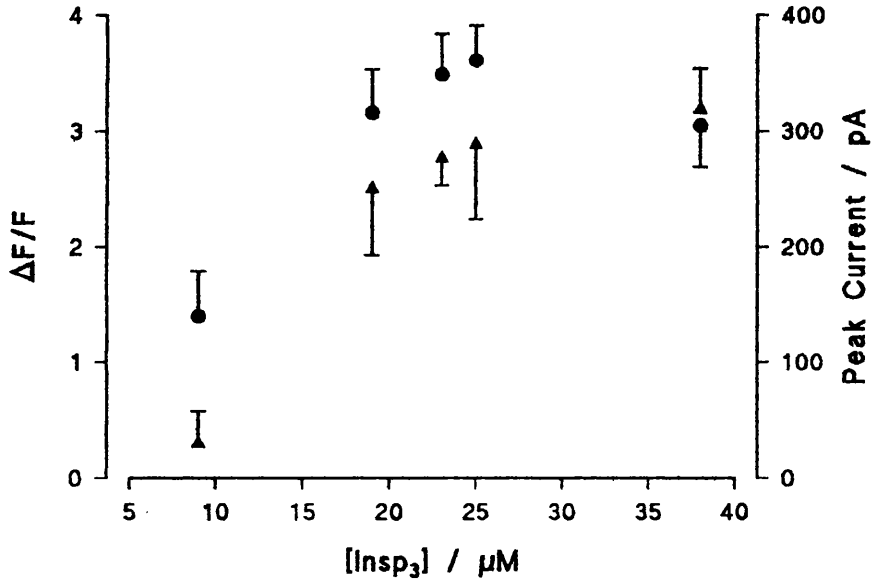

Figure 5.4 The relation between the peak of Fluo-3 and conductance transients with [$InsP_3$] in voltage clamped Purkinje neurones.

The increase with [$InsP_3$] of the maximum Fluo-3 fluorescence change (circles) and the outward current (triangles) following photolytic release of $InsP_3$ in voltage clamped Purkinje neurones. Values are means with their corresponding standard error.

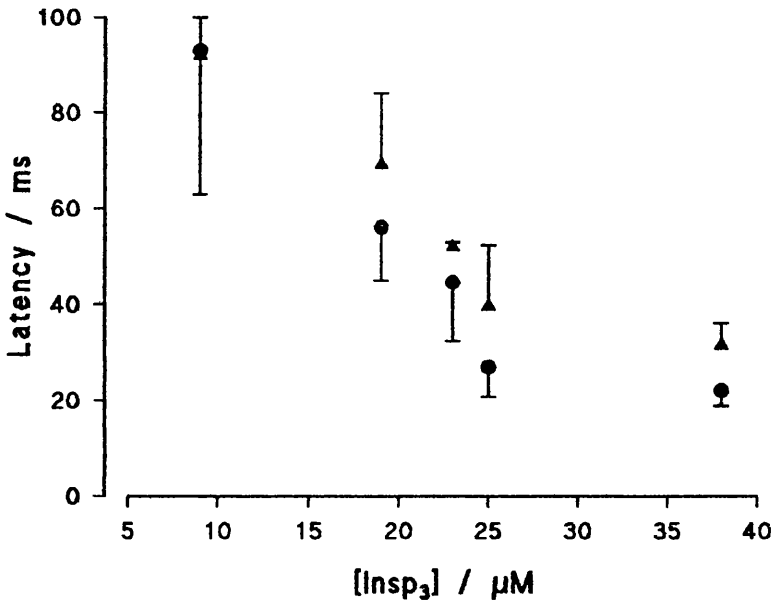

Figure 5.5 The reduction in latency of Fluo-3 fluorescence and conductance with increasing [$InsP_3$] in voltage clamped Purkinje neurones.

The relation between latencies of onset of the Fluo-3 light transient (circles) and the outward current (triangles) following intracellular photolytic release of $InsP_3$ in voltage clamped Purkinje cells with [$InsP_3$]. Error bars represent standard error of the mean.

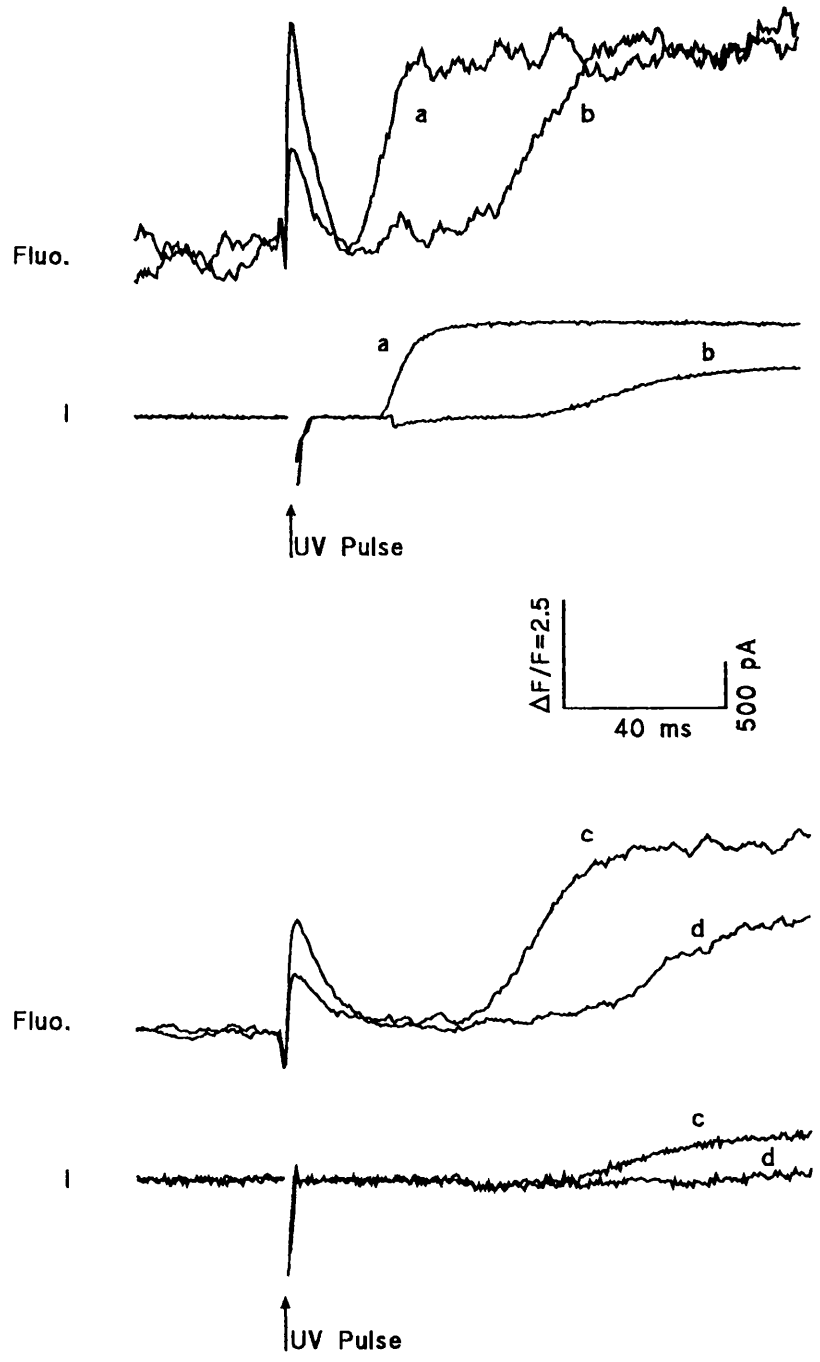

Figure 5.6 Early events following photolytic release of $InsP_3$.

Changes in the Fluo-3 fluorescence of the soma and whole cell conductance of two voltage clamped Purkinje cells following photolytic release of $InsP_3$ are shown (Top and bottom pair of traces). Flash lamp intensity was altered to release; a=38μM, b=c=19μM, and d=9μM $InsP_3$ from caged $InsP_3$ equilibrated in the cytosol of the cells. Following the optical flash artifact there is a delay followed by an increase in the Fluo-3 fluorescence. The latency of the onset of the light transient decreases, and the rate of rise of the transient increases with increasing [$InsP_3$]. The outward current rises shortly after the onset of the fluorescence signal. A reduction in the latency of onset and increase in the rate of rise of the outward current is observed with increasing [$InsP_3$].

5.1, Figures 5.5, & 5.6). Considering the 2-4ms half time for photolytic release of $InsP_3$ (Walker *et al*, 1989), and the time taken for the indicator to report the changes in $[Ca^{2+}]_i$ (1.4ms for Fura-2; Kao and Tsien, 1988), the short latency of the onset of the fluorescence rises at high concentrations of $InsP_3$ favours the idea of direct activation by $InsP_3$ of a calcium permeable ion channel, the $InsP_3$ receptor, and makes the possibility of the presence of an intermediate step between $InsP_3$ release and activation of the $InsP_3$ receptor less likely. The increase in the latency of onset of fluorescence rise at lower concentrations of $InsP_3$ may be explained by the cooperative action of calcium ions on the $InsP_3$ receptor (Finch *et al*, 1991; Bezprozvanny *et al*, 1991); at resting $[Ca^{2+}]_i$, about 0.1μM, binding of $InsP_3$ to its receptor results only in an initial slow release of calcium until the concentration of free calcium adjacent to the receptors rises high enough to increase the open probability of the $InsP_3$ receptor and set up regenerative fast efflux of calcium. Although a slow leakage of calcium through the $InsP_3$ receptors preceding the transients was not detected with the indicator, the mechanism of action of $InsP_3$ may nevertheless require calcium cooperativity if the initial calcium release was small and localised.

Examination of the events immediately following the release of $InsP_3$ also revealed an increase in rate of rise of the Fluo-3 fluorescence with increasing $InsP_3$ concentrations (Figure 5.6). Although saturation of the dye distorts the kinetics and rate of rise of the fluorescence signal, the increase in the rate of rise with higher concentrations of $InsP_3$ can nevertheless be attributed to an increased efflux of calcium ions from the intracellular stores if it is assumed that the rate of calcium removal in the cytosol is not altered. The rate of change of $[Ca^{2+}]_i$ provides a measure of calcium efflux similar to Ca^{45} efflux (Finch *et al*, 1991) and would be proportional to open probability of $InsP_3$ receptor measured in lipid bilayers (Bezprozvanny *et al*, 1991).

Occasionally at low concentrations of $InsP_3$, and always at higher concentrations an outward current accompanied the calcium transient. This current was due to an increase in the membrane conductance (see Figure 5.9) and its reversal potential was not altered when the intracellular anions were changed from the impermeant gluconate to the permeant chloride ions indicating that it was as the result of the efflux of potassium ions out of and not due to the influx of chloride ions into the cell. The outward current accompanied the fluorescence change at the same time or shortly afterwards with its latency decreasing, and its peak increasing with increasing $InsP_3$ concentrations (Table 5.2, Figures 5.4, 5.6, & 5.7), suggesting that the change in the membrane permeability was related to

[$InsP_3$] / µM	9	19	23	25	38
I Peak / pA	32±2.8 (2)	249±57 (7)	276.5±23.5 (2)	288±64.1 (5)	318.6±35.2 (13)
I latency / ms	92±8 (2)	69.1±14.9 (8)	52±1.3 (1)	39.6±12.8 (5)	31.5±4.6 (14)

Table 5.2 Properties of current transients following release of InsP3

Peak outward current and the latency before the onset of the current following the photolytic intracellular release of $InsP_3$ in voltage clamped Purkinje neurones. Cells were held at -70mV. Values are means with the SEM, and the number in parenthesis indicate the number of cells.

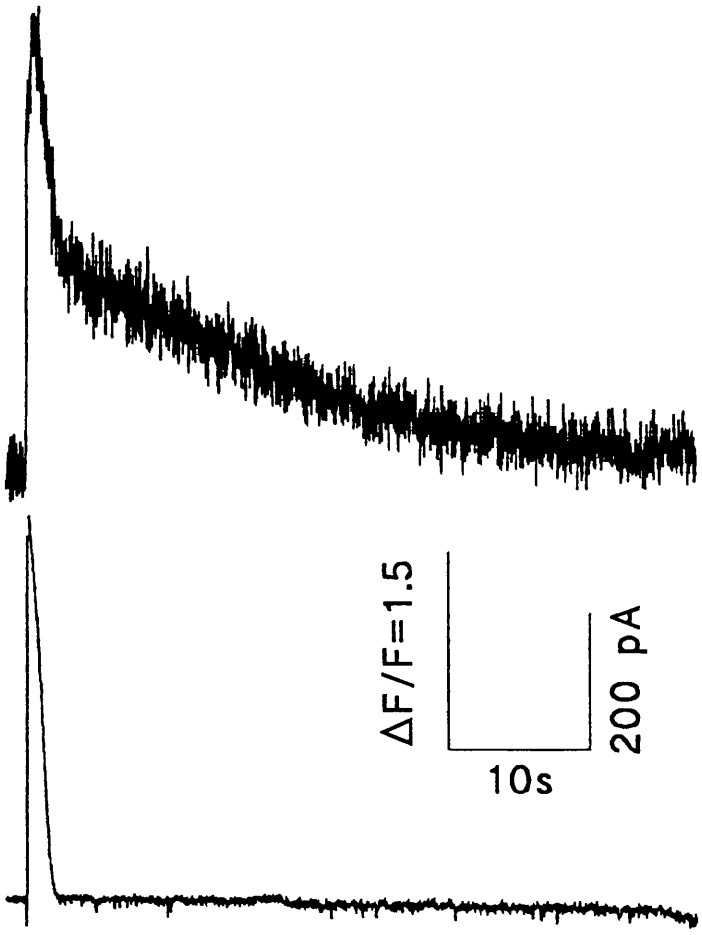

Figure 5.7 Increase in $[Ca^{2+}]_i$ and membrane conductance following photolytic release of $InsP_3$

38µM $InsP_3$ was photolytically released in the cytosol of a voltage clamped Purkinje neurone (holding potential -70mV). Increase in $[Ca^{2+}]_i$ is detected by the increase in Fluo-3 fluorescence signal. The outward current is due to an increase of the membrane conductance to potassium ions (see text).

the $InsP_3$ concentration. This can be either by the direct gating of the potassium channel with $InsP_3$ or an $InsP_3$ metabolite such as $InsP_4$, or *via* a process mediated by $InsP_3$ such as elevation of cytosolic calcium. Although presence of $InsP_3$ (Kuno and Gardner, 1987) and $InsP_4$ (Irvine and Moor, 1986; Luckhoff and Clapham, 1992) gated ion channels at the plasma membrane has been documented, these channels are mainly permeable to calcium ions and not to the monovalent potassium ions. Calcium activated potassium channels, however, have been characterised and exist in most cells studied. These include *Aplysia* neurones (Meech, 1972; Tsien and Zucker, 1986), chromaffin cells (Marty, 1981), photoreceptors (Bolsover, 1981), rat lacrimal glands (Trautmann and Marty, 1984), bullfrog (Adams *et al*, 1982; MacDermot and Weight, 1982) and rat sympathetic neurones (Gurney *et al*, 1987), and hepatocytes (Field and Jenkinson, 1987; Capiod *et al*, 1987; Capiod and Ogden 1989). Therefore it is likely that the outward current recorded are as the result of activation of a calcium activated potassium conductance. It must be emphasised that arguments presented here in favour of activation of the potassium conductance by calcium ions are indirect and the calcium dependence of the conductance should be characterised. The use of inside out and outside out excised patches would allow the accurate control of solutions on both sides of the membrane facilitating investigation of the calcium dependence, and the pharmacology of these channels (cf Marty, 1981; Capiod & Ogden, 1989). Alternatively the presence of calcium activated potassium channels could be demonstrated by rapidly increasing the concentration of intracellular calcium by photolytic release of calcium from nitr series compounds or DM-nitrophen (cf Tsien and Zucker, 1986; Gurney *et al*, 1987) while recording the whole cell conductance.

The effect of $InsP_3$ on short term excitability was tested with current clamp experiments. Under these conditions photolytic release of $InsP_3$ resulted in the hyperpolarization of the membrane potential of the Purkinje cells to -85mV from their initial resting potential of about -60mV (Figure 5.8), thus reducing excitability. Figure 5.9 further shows that action potentials evoked by injection of current are inhibited following calcium mobilisation by $InsP_3$. Subsequently the membrane excitability recovered to its normal levels with a time course similar to the recovery of the intracellular calcium to resting levels.

The recovery to the resting levels of the fluorescence following $InsP_3$ was of two types; either the fluorescence recovered to 50% of its peak level within 2-5 seconds and then more slowly (30-90s) to the resting level, or stayed elevated upto 15s and then recovered more slowly (40-90s) (Figure 5.10). The mechanisms responsible for this will be discussed later.

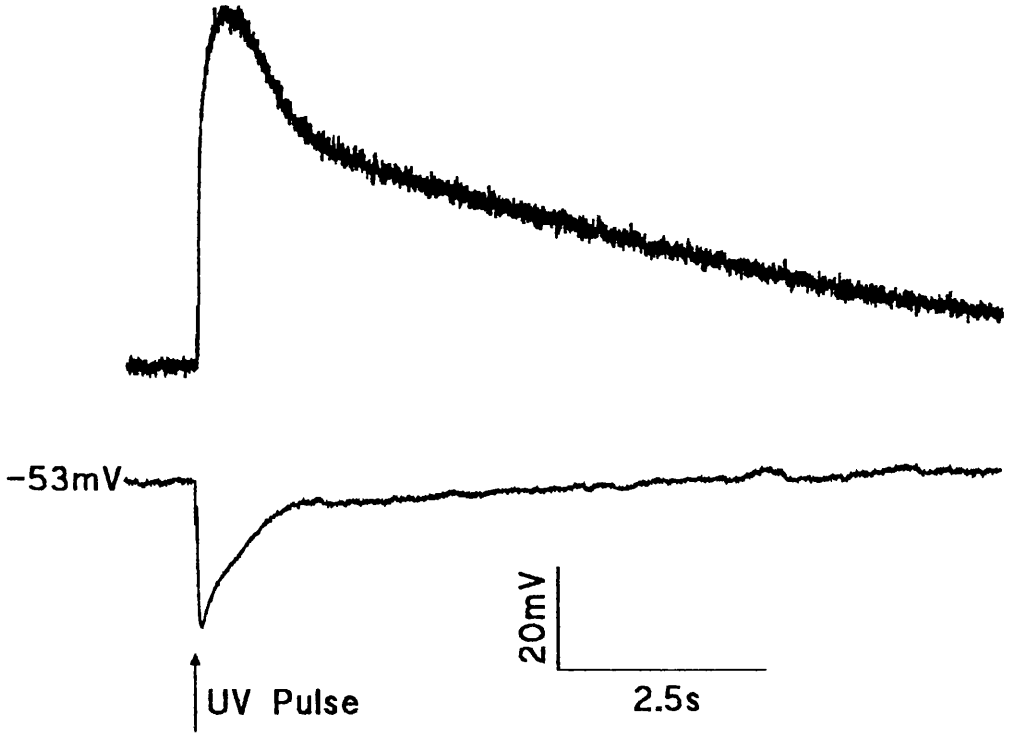

Figure 5.8 Effect of $InsP_3$ on the membrane potential.

Following the photolytic release of $InsP_3$ in the cytosol of current clamped Purkinje neurone the membrane potential hyperpolarised towards the potassium equilibrium potential. The figure demonstrates the light (top trace) and membrane potential change (bottom trace) in a current clamped Purkinje neurone following photolytic release of 38μM $InsP_3$.

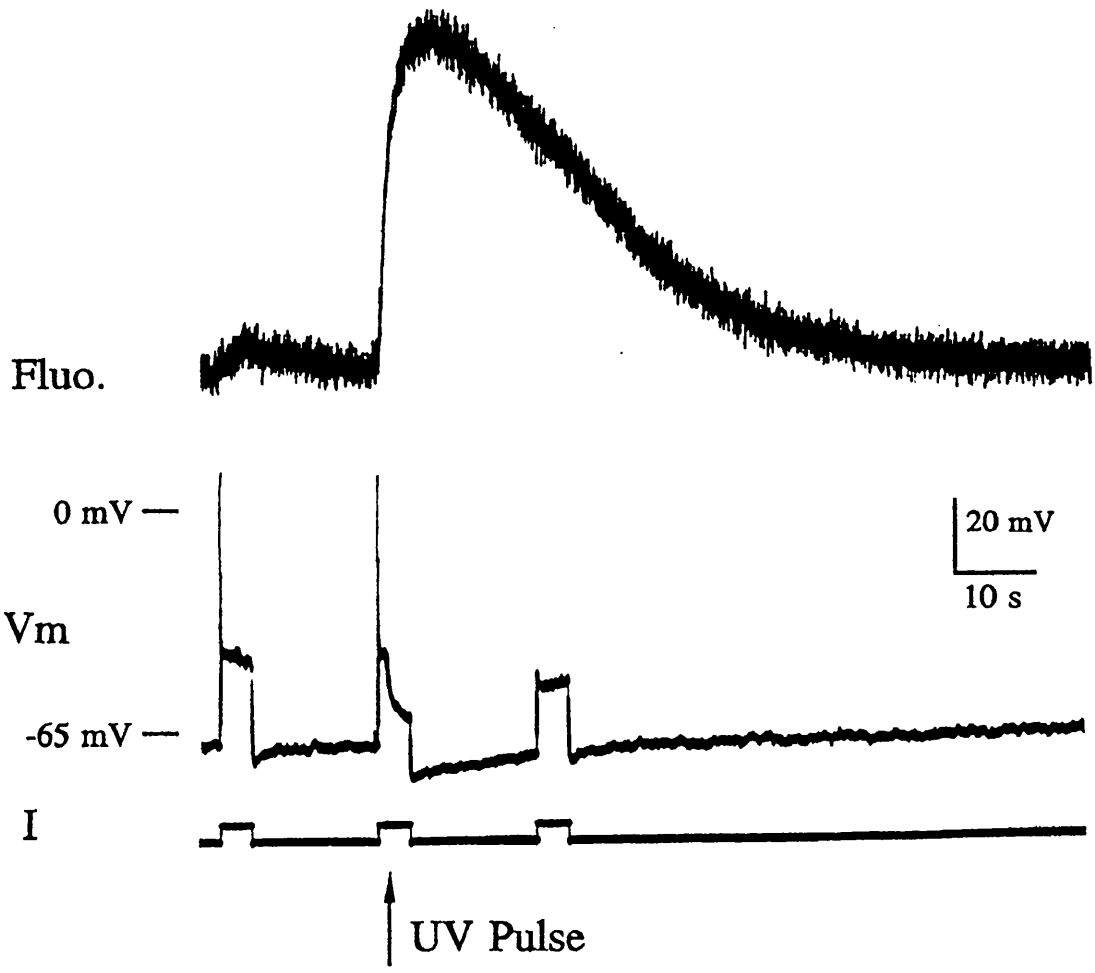

Figure 5.9 Effect of $InsP_3$ on the membrane excitability.

A Purkinje neurone was current clamped and the membrane potential (middle trace) and Fluo-3 fluorescence of the soma (upper trace) recorded. Depolarisation induced by 40pA current pulses gave rise to one full size action potential and one attenuated action potential, accompanied by a small light transient. Photolytic release of 19μM $InsP_3$ (indicated by the arrow) 500ms after the start of the current pulse produced a large light transient accompanied by hyperpolarisation due to increase of the membrane conductance to potassium ions. The following current pulse failed to elicit action potentials, which recovered when tested 30s later (not shown). Note the reduced size of the depolarisation induced by the third current pulse due to the increase in membrane conductance.

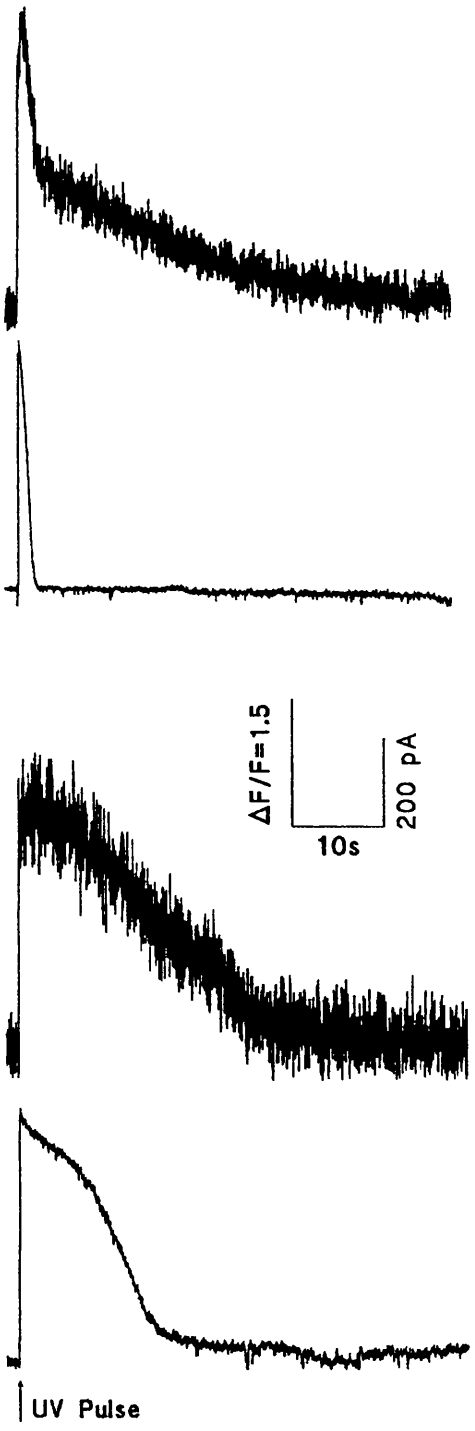

Figure 5.10 The timecourse of calcium transients monitored with Fluo-3.

The timecourse of recovery of the Fluo-3 transient and the whole cell conductance of two Purkinje neurones (different animals) following the photolytic intracellular release of 38μM $InsP_3$ from 100μM caged $InsP_3$. Two types of transients in response to the same concentration of $InsP_3$ released was observed; those with short duration (top traces), and those with longer duration (bottom traces).

The data outlined above were from experiments during which the fluorescence emitted from the soma of cells was recorded. However the main excitatory inputs of Purkinje cells, the parallel and climbing fibres, form synapses on the extensive dendritic tree and dendritic shaft of the Purkinje cells. The ratio of cytosolic volume to the membrane surface area of the dendrites is much less than that of the soma, and therefore attempts were made to collect and measure the fluorescence emitted from the region occupied by the dendritic tree. Higher concentrations of Fluo-3 had to be used as it was difficult to visually locate the dendritic tree of the Purkinje cells by searching for the fluorescence emitted at low Fluo-3 concentrations, in addition to the fact that the signal to noise ratio of the fluorescence measured prevented the use of Fluo-3 with concentrations lower than 1mM. Figure 5.11 shows light transients in the dendritic tree of a Purkinje cell when $InsP_3$ was photolytically released by a full intensity flash with 1.2 mM Fluo-3 and 100μM caged $InsP_3$ in the patch pipette. It was not possible to calculate the concentration of $InsP_3$ photolytically released in the dendritic tree since it could not be assumed that equilibrium between the patch pipette and dendrites had been achieved. In the dendrites the size of the calcium transient was not always greater than that produced by depolarisation. This could be either due to the different surface to volume ratio of the dendrites, or may reflect poor voltage clamp of dendrites far from the patch pipette. Since the very high concentrations of the dye used to monitor calcium in the dendrites increase calcium buffering, and therefore calcium diffusion in the cytosol, and because of problems of voltage clamp in the dendritic tree, it can only be concluded that the intradendritic free calcium increases following photolytic release of $InsP_3$, most probably by calcium mobilisation from stores. To be able to study $[Ca^{2+}]_i$ in the dendrites it would be necessary to allow a longer time for the indicator to diffuse and fully equilibrate with the dendrites (perhaps an hour), and use brighter indicators taking care not to alter cytosolic calcium buffering.

The effect of photolysis byproducts or intermediates in calcium mobilisation or the membrane conductance was tested by photolysis of 100μM 1-(2-nitrophenyl)ethyl phosphate, caged phosphate, introduced into the cell by the whole cell patch pipette following the same procedure used during experiments with caged $InsP_3$. The photolysis by-products and intermediates did not alter the $[Ca^{2+}]_i$ or the membrane conductance (Figure 5.12).

The most striking finding of these experiments was that more than ten times higher concentrations of $InsP_3$ were required to mobilise calcium in Purkinje cells than astrocytes, hepatocytes (Ogden *et al*, 1990) or

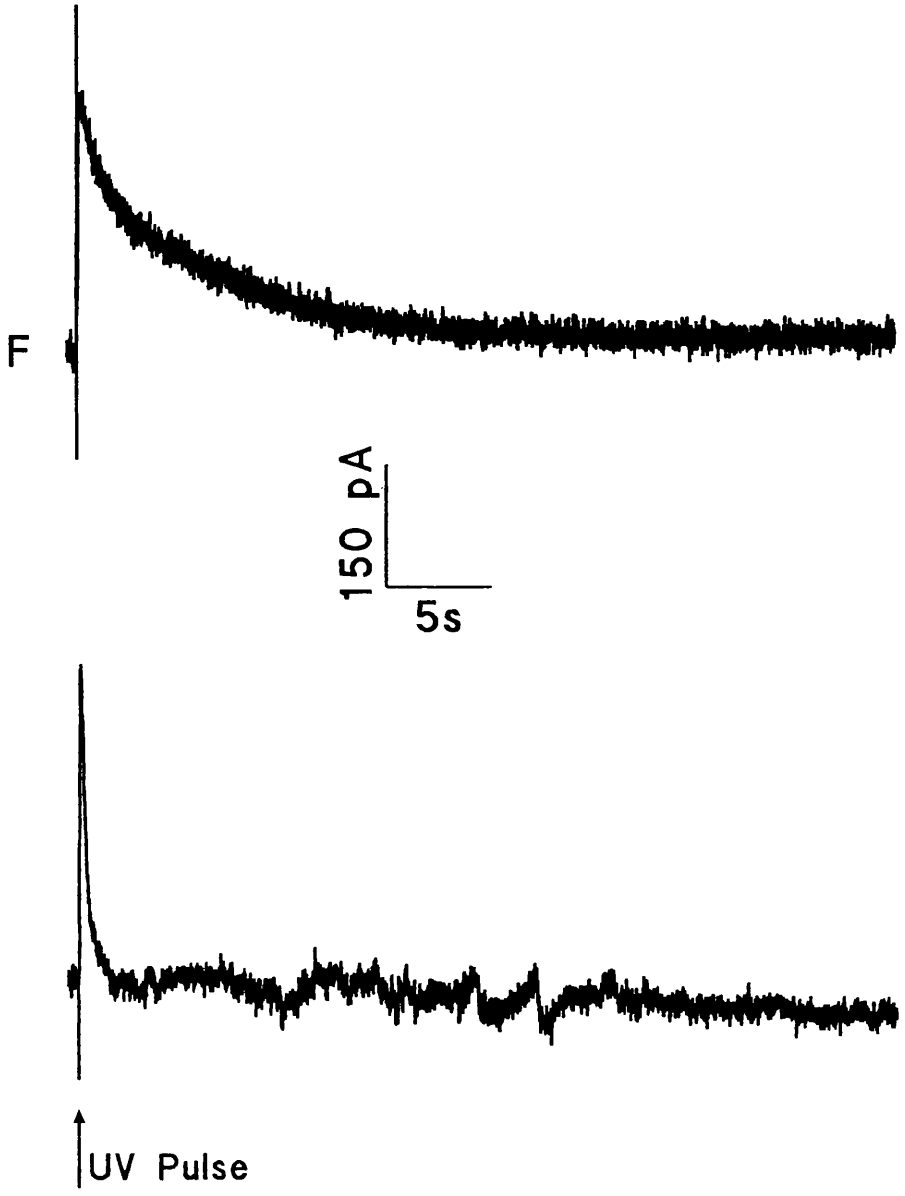

Figure 5.11 Fluo-3 fluorescence of the dendrites a Purkinje cell.

The light from the dendritic tree of a Purkinje cell voltage clamped with a patch pipette containing 1.2mM Fluo-3 and 100μM caged $InsP_3$ was collected (panel A). A full intensity flash of the xenon lamp (100mJ) was used to photolyze the caged $InsP_3$ present in the dendrites. The concentration of $InsP_3$ released cannot be estimated because equilibrium between the patch pipette and the dendritic tree was not achieved but is less than 38μM.

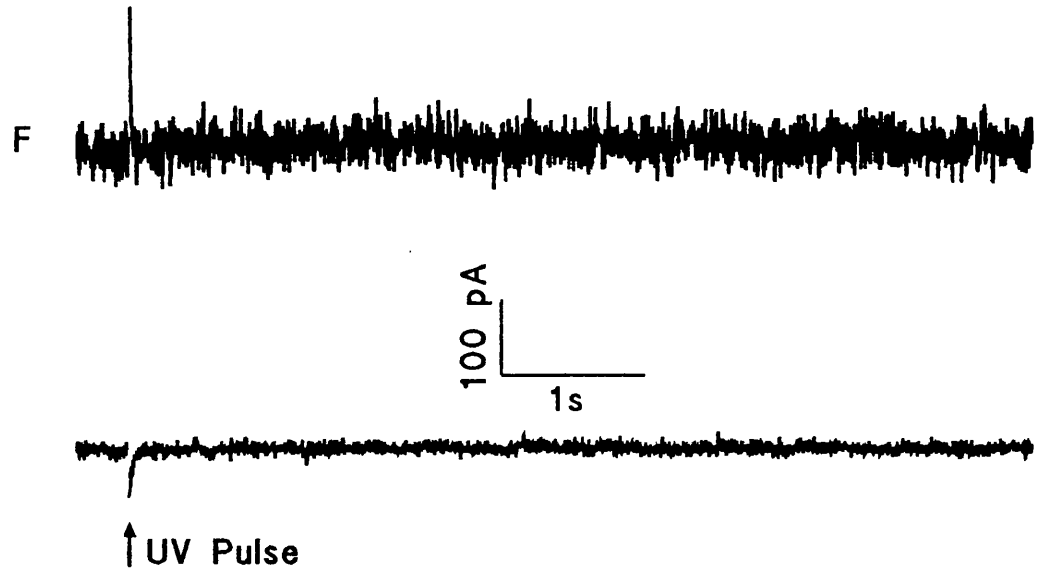

Figure 5.12 Control for the photolysis byproducts and intermediates in photochemical reaction.

Photolysis of 100μM caged phosphate (see text) which results in the release of the same photolysis byproducts as caged $InsP_3$ with a similar quantum yield. No change in the Fluo-3 fluorescence of the soma, or whole cell conductance of a voltage clamped Purkinje neurone (holding potential -70mV) was detected following a full intensity flash of the xenon arc lamp (100mJ).

endothelial cells (Carter & Ogden, 1991, 1992) examined with identical experimental protocols. It is important to consider the possibility that additional calcium buffering introduced into the cytoplasm by the presence of Fluo-3 reduced the $InsP_3$ potency. Calcium buffering by 200μM Fluo-3 is of an order of 400 calcium ions bound to 1 free, compared with an endogenous buffering of 75 bound to 1 free (Neher & Augustine, 1992) assuming a free calcium concentration of 0.1μM. It had to be verified that the additional buffering did not result in 'mopping' of the calcium released adjacent to the $InsP_3$ receptors immediately after photolytic release of $InsP_3$, thus perhaps necessitating a higher concentration of $InsP_3$. Furthermore it would be useful if an estimate of the intracellular calcium concentration evoked by $InsP_3$ could be obtained.

5.4. Use of Furaptra to follow the changes in $[Ca^{2+}]_i$

To address these points it was necessary to use an indicator with a lower affinity for calcium and which could be used at low concentrations to follow the changes in the $[Ca^{2+}]_i$. The fluorescent indicator Furaptra has a much lower affinity for calcium than Fluo-3 and has been successfully used to follow the calcium transients in frog skeletal muscle fibres (Konishi *et al*, 1991). Preliminary experiments indicated that it could be used at a concentration of 500μM to follow the changes of the $[Ca^{2+}]_i$ in the Purkinje cells *in situ*. At this concentration, and assuming the same K_D (44μM) *in vivo* as that *in vitro*, the additional buffering introduced into the cell would be 11 bound calcium ions to 1 free at a free calcium concentration of 0.1μM, which could be neglected compared to that of the endogenous buffers. However Furaptra binds magnesium, although with considerably lower affinity, as well as calcium ions and despite the presence of ATP in the patch pipette solution as a magnesium 'buffer' (see chapter 2) a reduction in the Furaptra fluorescence could be due to an increase in either magnesium or calcium ions (to reduce the fluorescence of Furaptra by half $[Ca^{2+}]_i$ or $[Mg^{2+}]_i$ should rise to their K_Ds, 44μM and 5.3mM, respectively. The later possibility is less likely.). In the absence of a high affinity selective magnesium ion chelator, experiments to directly address this point are difficult to do. The Furaptra light transients recorded following photolytic release of $InsP_3$ were interpreted as alteration in $[Ca^{2+}]_i$ on the basis of experiments described with the high affinity calcium indicator Fluo-3 which has a great selectivity for calcium over magnesium ions. Chapter 2 describes in detail the use of Furaptra as a calcium indicator.

With Furaptra as the fluorescent calcium indicator, occasionally at

9μM $InsP_3$, and always at higher concentrations of $InsP_3$ photolytically released in the cytosol a transient reduction in the light was detected (Figure 5.13), reiterating the requirement of ten fold higher $InsP_3$ concentrations to mobilise calcium in the Purkinje cells compared with that required in astrocytes or peripheral cells. The additional calcium buffering introduced in the cytoplasm by 500μM Furaptra, (11 bound to 1 free at a free calcium concentration of 0.1μM), could be neglected compared to that of the endogenous buffers. The extra buffering by the indicator, particularly with Fluo-3, is an unlikely explanation for the lower potency of $InsP_3$ in mobilising calcium from the intracellular stores in the Purkinje cells. The possible physiological processes which could result in a lower potency of $InsP_3$ in evoking calcium release in these cells will be discussed later.

The low affinity of Furaptra for calcium ions and the large fluorescence change was used to provide a calibration of free $[Ca^{2+}]_i$. F_{min} and F_{max} were estimated for each cell, and $[Ca^{2+}]_i$ calculated assuming K_D=44μM from the *in vitro* calibrations of Konishi *et al* (1991) as described in chapter 2. The calcium concentrations estimated showed that the magnitude of the transients evoked by $InsP_3$ were large, the average cytosolic calcium concentrations often surpassing 30μM (Table 5.3, Figures 5.14, 5.16, & 5.18). Given the rapid efflux of calcium from the intracellular stores following release of $InsP_3$, it is likely that much higher local calcium concentrations existed in areas adjacent to the stores. Therefore it is likely that the average $[Ca^{2+}]_i$ computed is an underestimate of the average cytosolic calcium concentration due to deviation of the binding curve of the indicator from linearity in areas where local calcium concentrations were high.

The immediate events following the photolytic release of $InsP_3$ were obscured in the Furaptra fluorescence signals by an optical artifact about 30ms long. This restricted measurement of the fluorescence latency to delays longer than 30ms. The latencies of the onset of the light transients with 19 and 23μM $InsP_3$ released in the cytosol were 54.7±8.6 and 38±9.1ms (SEM, n=6 and 3) respectively, in close agreement with the latencies obtained using Fluo-3 as the indicator. If a cooperative action of calcium is required for calcium mobilisation *via* the $InsP_3$ receptors, the latency of the onset of the light transient might be expected to get longer if the buffering adjacent to the $InsP_3$ receptors is sufficiently increased. However it is difficult to predict the extra buffering required for such an action, and the absence of a difference between the latencies detected with Fluo-3 and Furaptra at the same $[InsP_3]$ is not conclusive regarding the processes responsible for the delay.

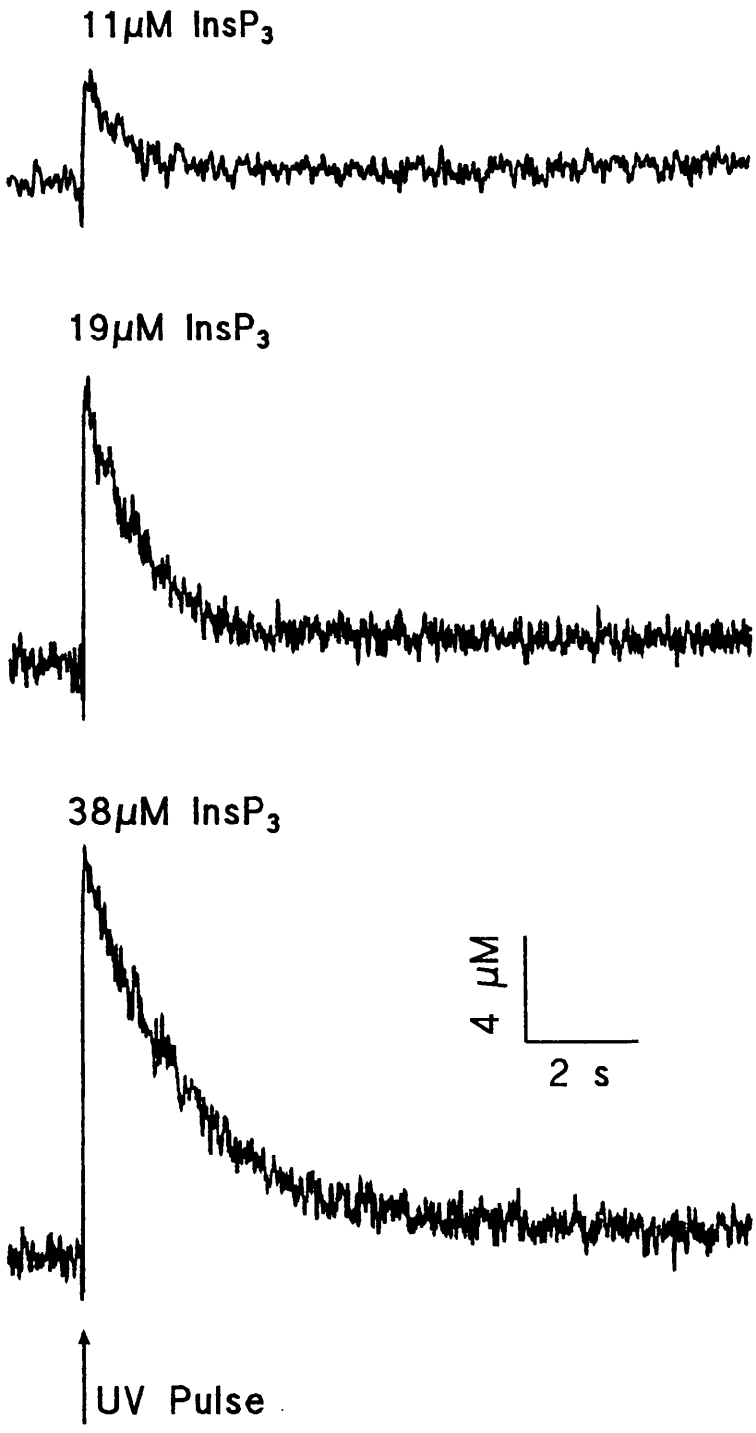

Figure 5.13 Calcium mobilisation by photolytically released $InsP_3$ in voltage clamped Purkinje neurones monitored with Furaptra.

The flash intensity was altered to release 11, 19, and 38μM $InsP_3$ in the cytosol of a voltage clamped (holding potential -70mV) Purkinje neurone *in situ*. Fluorescence of the calcium indicator Furaptra was calibrated as described in methods to estimate the average cytosolic free calcium concentration.

Data obtained with 500 μM Furaptra as the intracellular calcium indicator					
$InsP_3$ / μM	11	19	23	38	76
Fluorescence peak / μM	5±2.4 (3)	10.4±3.6 (12)	9.8±2.4 (8)	33.3±5.9 (18)	28.9±4.5 (18)
Current peak / pA	104±40.4 (3)	138.4±50.3 (12)	148.9±26.7 (8)	365.2±41.9 (18)	296.2±35.6 (18)
Fluorescence latency / ms	85±7.5 (3)	54.7±8.6 (6)	38±9.1 (3)	NA	NA
Current latency / ms	58±12.4 (3)	82±15.3 (8)	44.1±7.7 (8)	26.8±3.1 (18)	16.6±2 (18)
Fluoresence area / μM.s	6.5±5.3 (3)	6.86±2.2 (12)	11.4±5 (8)	89±27.6 (18)	86.8±29 (18)
Current area / pC	65.3±32.4 (3)	78.6±37.6 (12)	132.5±33.3 (8)	1099.3±361 (18)	583±181.5 (18)

Table 5.3 Increase in $[Ca^{2+}]_i$ and outward conductance recorded with Furaptra as the calcium indicator in Purkinje cells.

The change in $[Ca^{2+}]_i$ obtained from the changes in the fluoresnce emiteed by Furaptra in voltage clamped (holding potential -70mV) Purkinje cells following photolytic release of $InsP_3$. Values are means with the SEM.

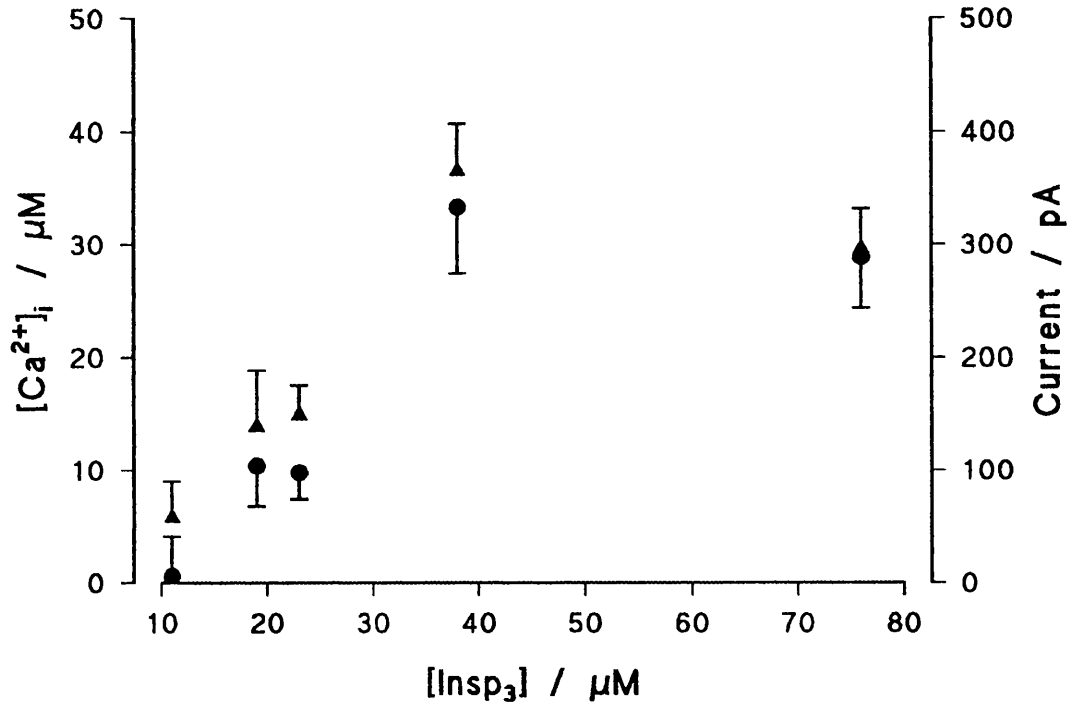

Figure 5.14 The increase with $InsP_3$ released of $[Ca^{2+}]_i$ and whole cell current.

The graph demonstrates the increase in the mean $[Ca^{2+}]_i$ of the soma (circles, estimated form the Furaptra fluorescence) and potassium current (triangles) of voltage clamped (holding potential -70 mV) Purkinje neurones with increasing the concentration of $InsP_3$. Values are means and error bars represent the standard error.

Calcium transients following release of $InsP_3$ were accompanied by an outward current, the peak of which increased in parallel to that of the calcium transient (Table 5.3, Figure 5.14) and compared well with those obtained with similar concentrations of $InsP_3$ released in Fluo-3 experiments.

The latencies of the onset of the conductance change decreased with increasing $InsP_3$ concentration in a similar range as those obtained with Fluo-3 experiments (Figure 5.15, Table 5.3). If the potassium conductance was activated by calcium ions, then calcium has to diffuse from the release site to the plasma membrane. If the delay between the onset of the fluorescence response and the onset of current transient reflects the time taken for calcium to diffuse from the release site to the plasma membrane, the presence of mobile calcium buffers should result in an increase in the rate of diffusion of calcium in the cytosol (discussed in chapter 2), and might be expected to reduce the latency required for the activation of the conductance. However no difference was observed between the conductance latencies obtained from experiments using Fluo-3 or Furaptra. There are at least three arguments which could explain the lack of difference in the latencies and yet support the activation of the potassium channels with calcium. First it might be that a great proportion of Fluo-3 in the cytosol is not mobile and therefore the rate of diffusion of calcium is not greatly altered. Indeed its is reported that about 70% of Fluo-3 used to monitor $[Ca^{2+}]_i$ in frog muscle was bound to myoplasmic constituents (Harkins *et al*, 1991). An alternative explanation might be that the gap between the calcium release site and the plasma membrane was short enough for the alteration in the rate of diffusion of calcium not to significantly alter the latency of the onset of the outward current. In support of this is the demonstration of the existence of calcium stores containing $InsP_3$ receptors close to the plasma membrane in the Purkinje cells (Ross *et al*, 1989; Satoh *et al*, 1990; Otsu *et al*, 1990; Takei, 1992). Third, the origin of the delay between the rise of the potassium conductance and $[Ca^{2+}]_i$ may be a low sensitivity to $[Ca^{2+}]$ and steep activation curve of the potassium conductance, so that calcium adjacent to the membrane needs to rise substantially to activate the conductance.

The recovery of the Furaptra fluorescence to its resting levels following photolytic release of $InsP_3$ was similar to that of Fluo-3 and could be divided qualitatively into two patterns. In the first 80% of the signal recovered within 2-3s of $InsP_3$ release, while in the second this took as long as 15 seconds (Figure 5.16). However, unlike responses with Fluo-3 as the indicator, transients which took longer to recover did not show a plateau following their peak when recorded with Furaptra. The plateau

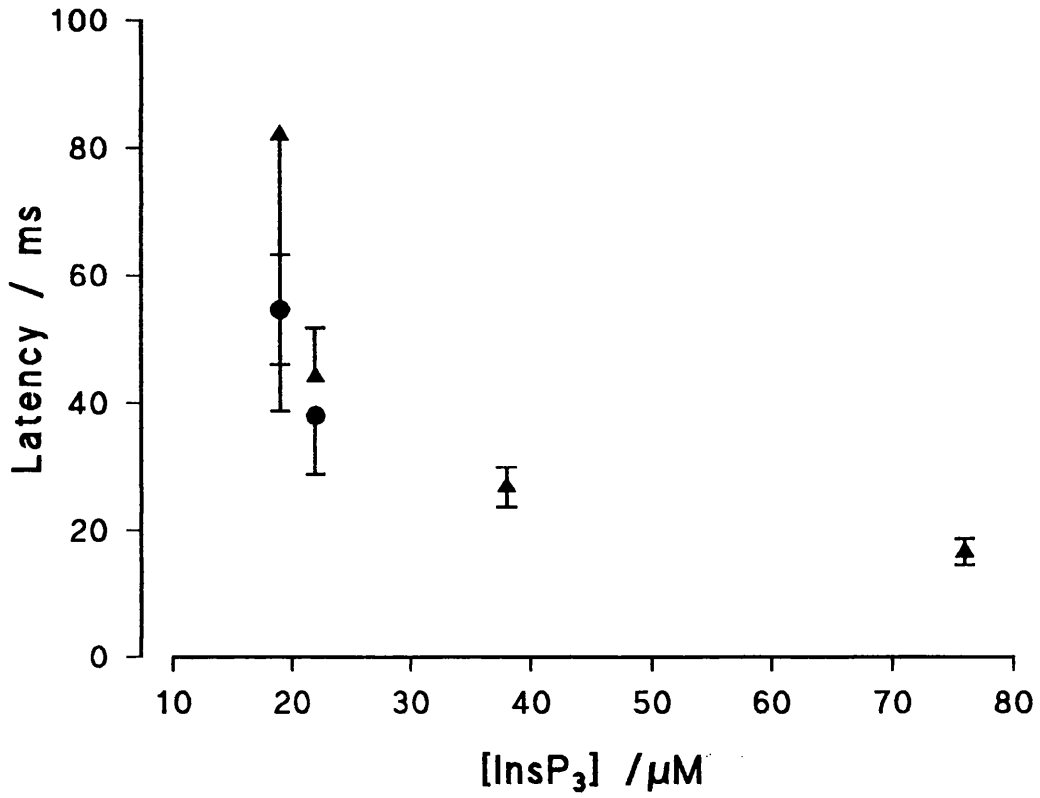

Figure 5.15 The latencies of onset of the Furaptra fluorescence change and the increase in whole cell conductance.

The relation between latencies of onset of the change in the Furaptra fluorescence (circles) and the membrane conductance (triangles) with [$InsP_3$] following photolytic release of $InsP_3$ in the cytosol of voltage clamped Purkinje cells. Due to the optical artifact induced by the flash only fluorescence latencies longer than 30ms would be detected. The latencies obtained with Furaptra are not different from those obtained with Fluo-3 (cf Figure 5.5). Values are mean and standard error.

after the peak of the light transient when Fluo-3 was used as the calcium indicator was probably due to dye saturation at high calcium concentrations. Longer lasting transients were only detected in slices prepared from old animals (30-50g, approximately 21 days postnatal; 16 cells from 3 animals showed this pattern, 6 animals studied), and not in young animals (25-28g, approximately 15 days postnatal; 7 cells from 3 animals, 3 animals studied) (Figure 5.17). Furthermore in cells from young animals the $[Ca^{2+}]_i$ estimated at the peak of the Furaptra transients did not exceed 35μM, although in those prepared from old animals it reached 80μM in some cells at high $[InsP_3]$ (Figure 5.18). However, the longer duration of the longer-lasting calcium transients was not just because of the higher peak $[Ca^{2+}]_i$ concentration; in old animals peak $[Ca^{2+}]_i$ concentrations estimated to be larger than 35μM were associated with either type of response. This is shown in Figure 5.18 where the area under the transient is plotted against the peak $[Ca^{2+}]_i$. The amplitude of the outward current was also dependent on the age of the animals (Figure 5.17), and the area under the current transient changed in the same way as the area under the calcium transient (Figures 5.19, and 5.20). A good correlation (slope=0.87, r=0.96) between the area under the calcium transient and that of the outward current supports the hypothesis that the potassium conductance is activated by calcium ions (Figure 5.20), and not by $InsP_3$ or an $InsP_3$ metabolite, as evidenced by the poor correlation between current area and $[InsP_3]$.

The data described above point to the existence of differences between young and old animals, although the small number of experiments make it difficult to be sure. First, cells studied in 21 day old animals had acquired the ability to elevate the $[Ca^{2+}]_i$ beyond that in Purkinje neurones in young animals. Second, there is a large increase in the area of the calcium transients in some of the older animals at the same concentration of $InsP_3$ or peak $[Ca^{2+}]_i$. Again on the basis of the data presented it is difficult to determine the process responsible. However, transients of large area were only seen with high peak $[Ca^{2+}]_i$ and it may be speculated that the longer duration of the response is due to continued efflux of calcium from stores *via* calcium induced calcium release. The presence of a high density (Ellisman *et al*, 1990) of functional (Bezprozvanny *et al*, 1991) calcium gated calcium channels, the ryanodine receptors, has been shown in the Purkinje cells. There are no developmental studies.

Preliminary experiments were done to examine the possibility that the time course of the recovery of the short-lasting transients was due to $InsP_3$ metabolism. A second pulse of UV light was used to photolytically

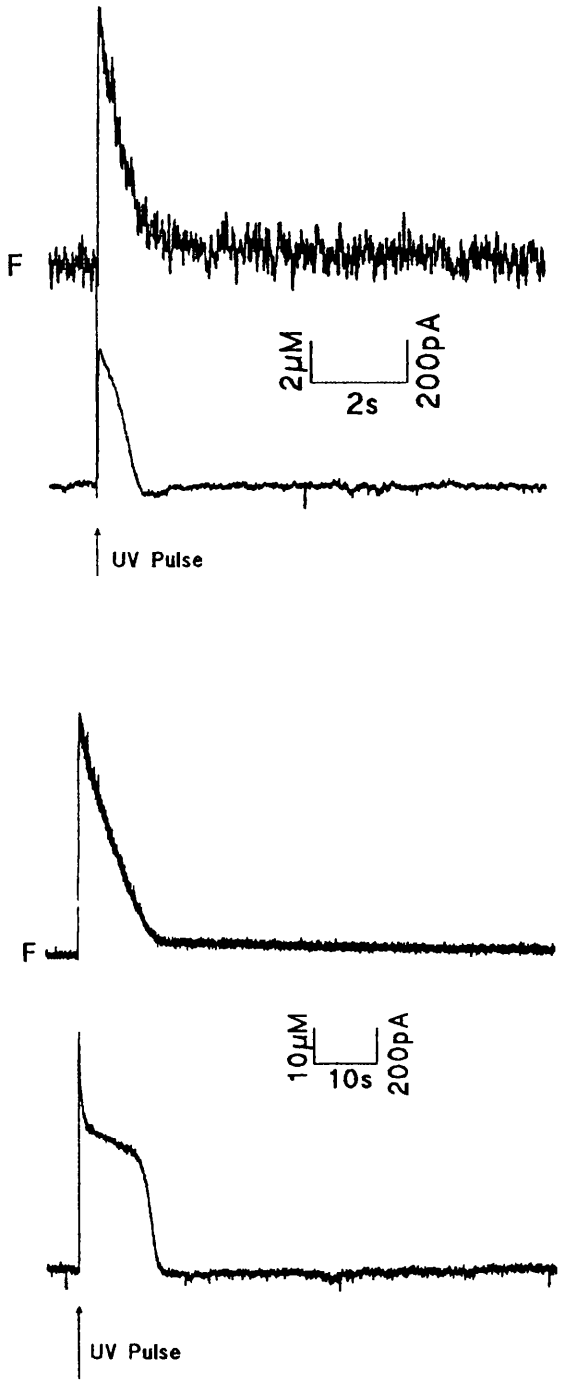

Figure 5.16 The timecourse of calcium transients monitored with Furaptra.

The Furaptra fluorescence signals of two Purkinje neurones following photolytic release of 76μM $InsP_3$ from 200μM caged $InsP_3$ were converted to estimate $[Ca^{2+}]_i$ as described in chapter 2. The top traces relate to a Purkinje cell from a young animal (25g) and the bottom traces relate to one from an old (52g) animal. Note the larger amplitude and duration of the transients in the cell from the older animal. The size and duration of the calcium and current transients were age dependent; large, long transients were only detected in old animals (<30g). Both cells were voltage clamped at a holding potential of -70mV.

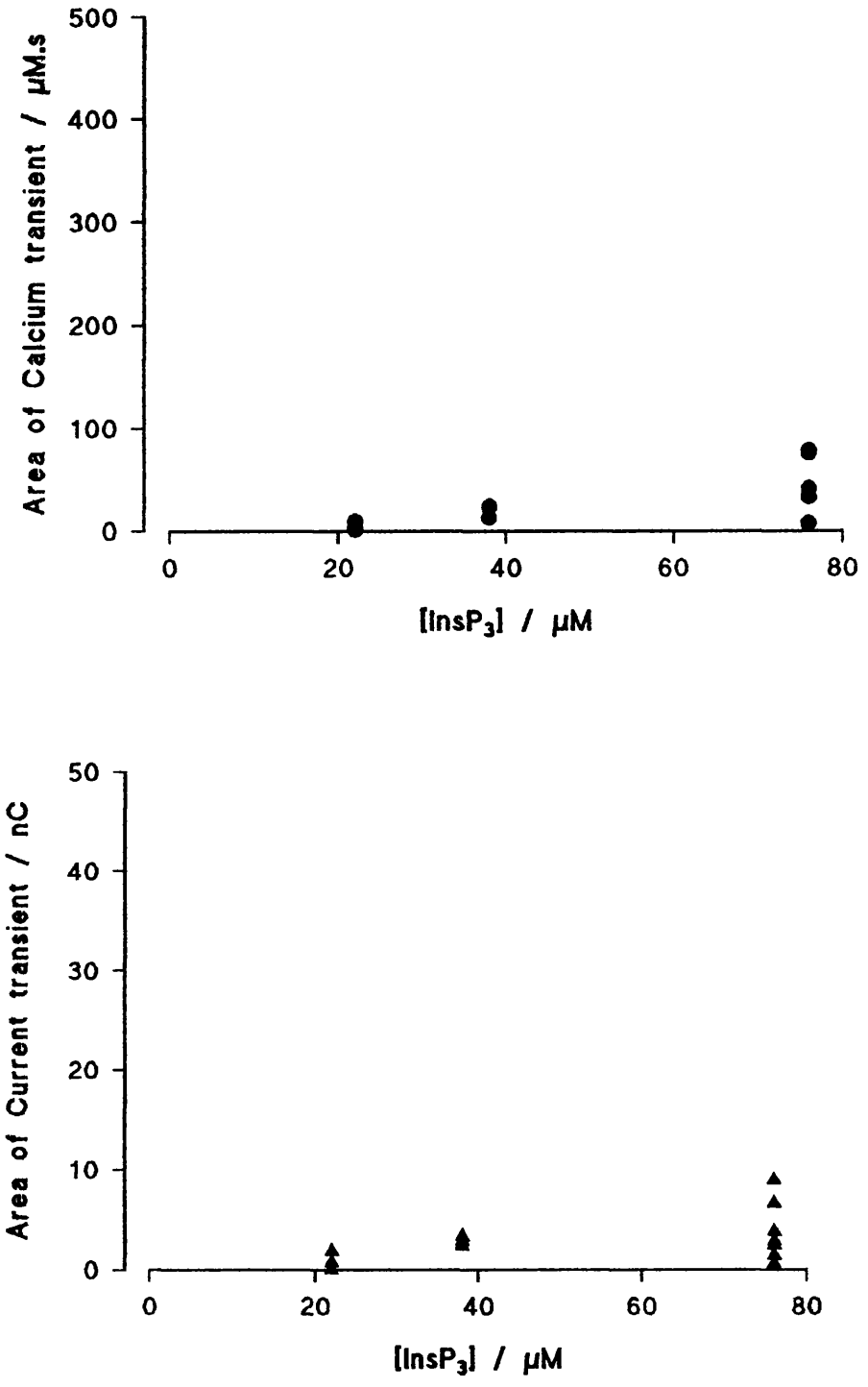

Figure 5.17 Increase with age of the area under the calcium and current transients.

The area under the fluorescence and current transients produced by the photolytic release of $InsP_3$ were calculated and that of the light transient was converted to estimate the area under the calcium transient. The graphs on the left demonstrate the presence of larger areas under the calcium and current transients in old animals (>30g) compared to the those of the young animals (25-28g) demonstrated by the graphs on the right.

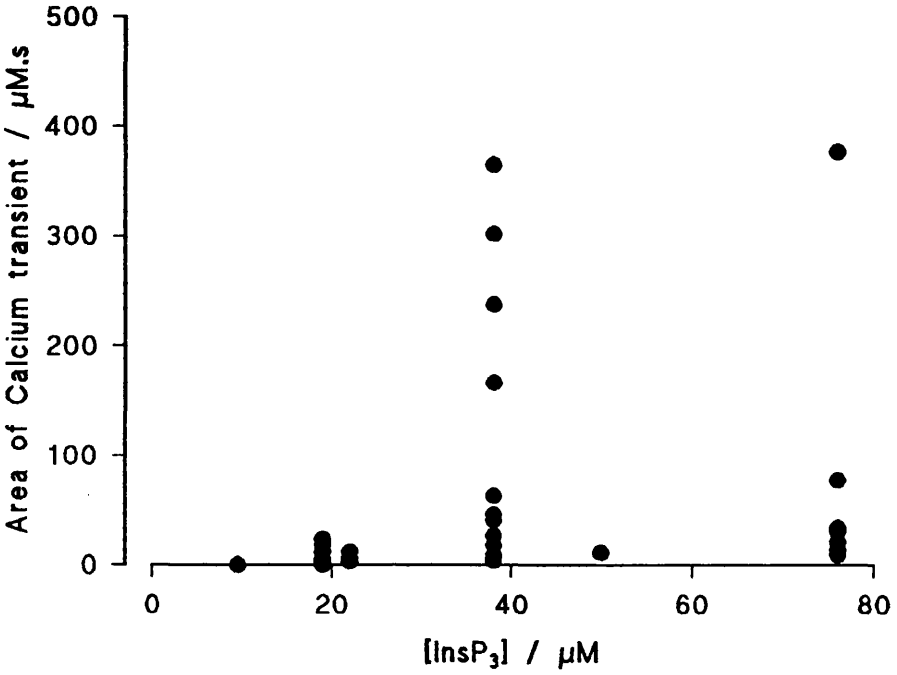
Area of Calcium transient / μM.s
500
400
300
200
100
0
0
20
40
60
80
[InsP3] / μM

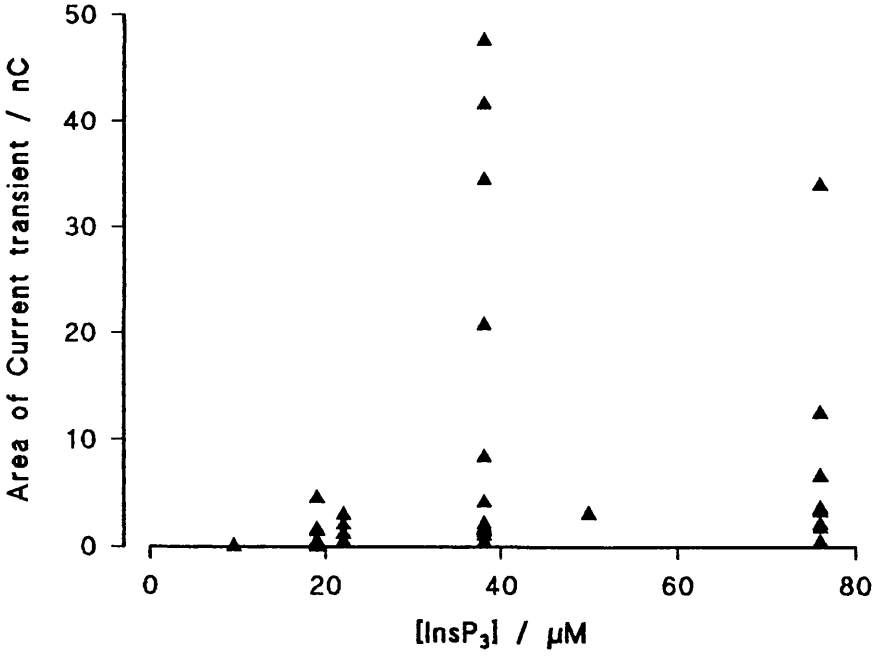
Area of Current transient / nC
50
40
30
20
10
0
0
20
40
60
80
[InsP3] / μM

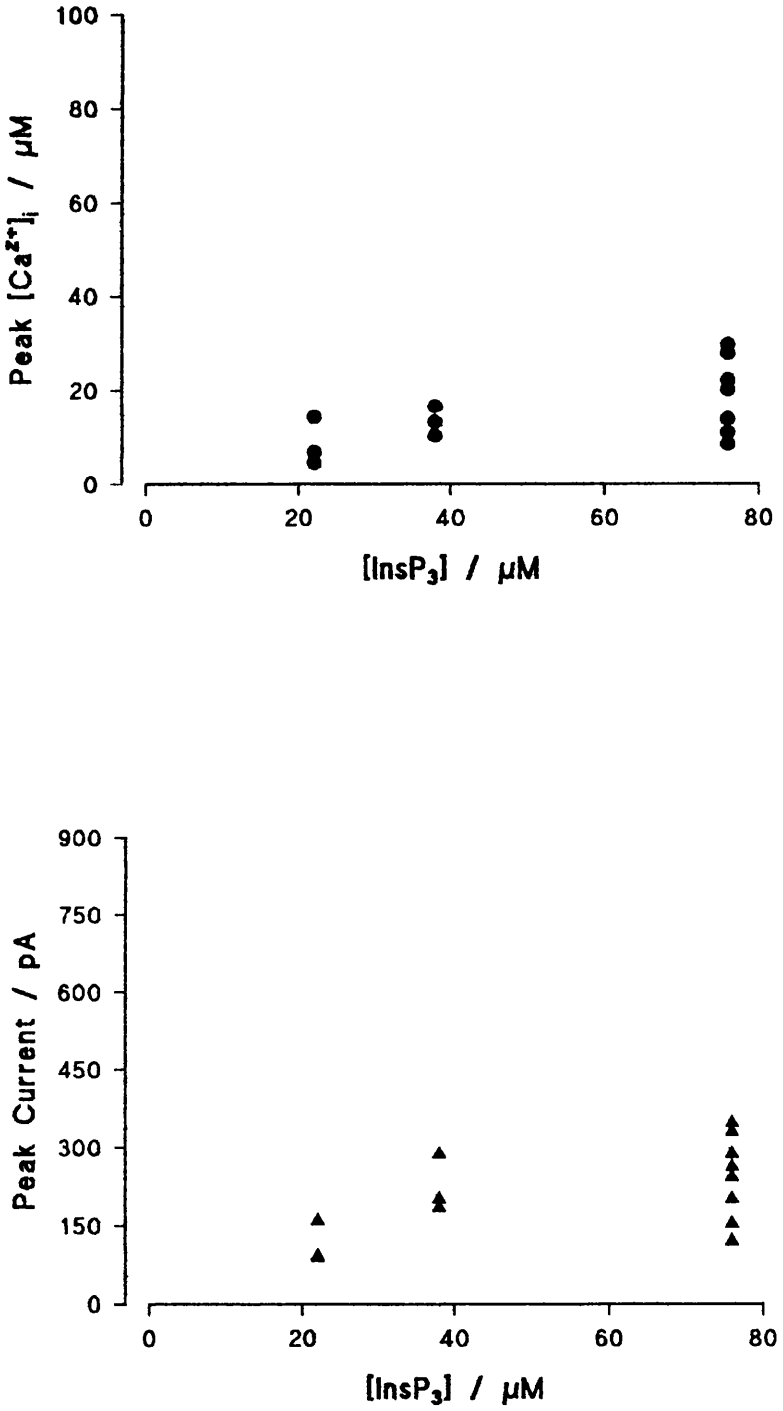

Figure 5.18 Age dependence of the peak $[Ca^{2+}]_i$ and whole cell current transients with $InsP_3$.

Peak calcium estimated from the Furaptra transients and the whole cell conductance induced by intracellular release of $InsP_3$ in voltage clamped Purkinje cells demonstrated age dependence. The graphs on the left show the peak $[Ca^{2+}]_i$ and conductance in young animals (25-28g), and those on the right correspond to old animals (>30g). The cells from older animals could achieve higher $[Ca^{2+}]_i$ and produced larger currents following release of $InsP_3$.

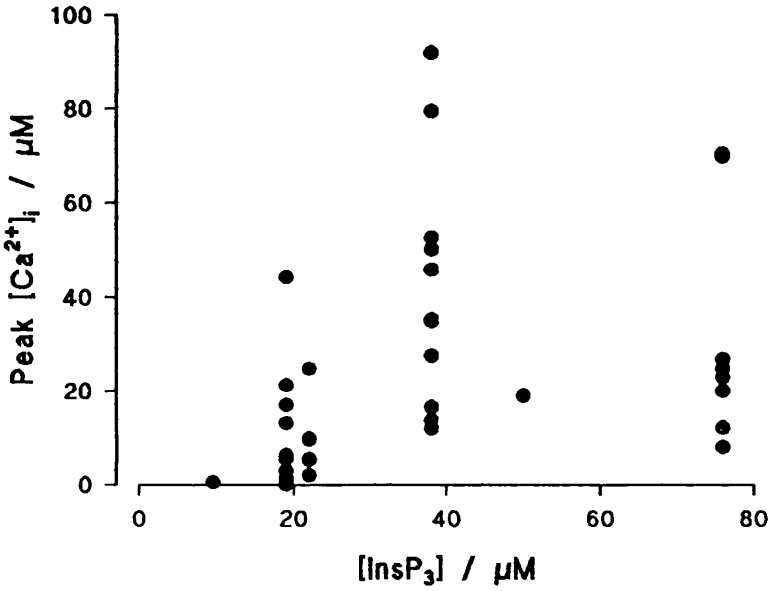
Peak $[Ca^{2+}]_i$ / μM
100
80
60
40
20
0
0
20
40
60
80
$[InsP_3]$ / μM

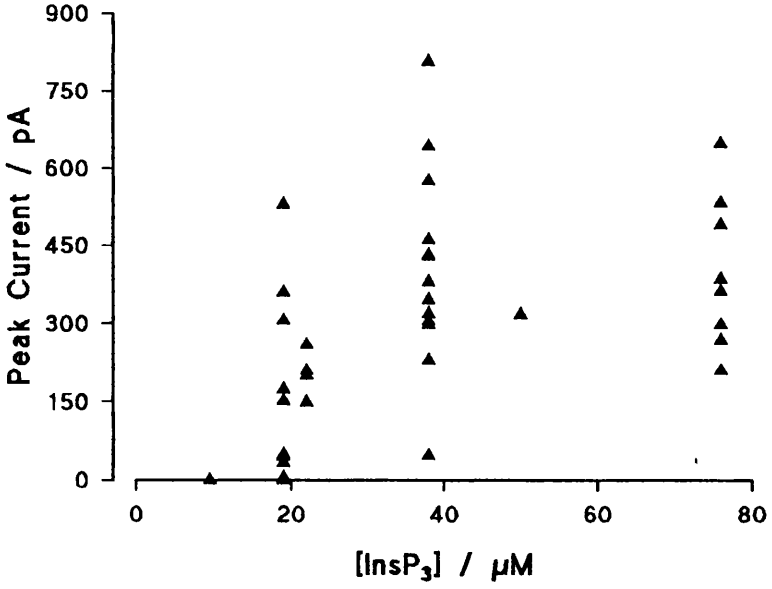
Peak Current / pA
900
750
600
450
300
150
0
0
20
40
60
80
$[InsP_3]$ / μM

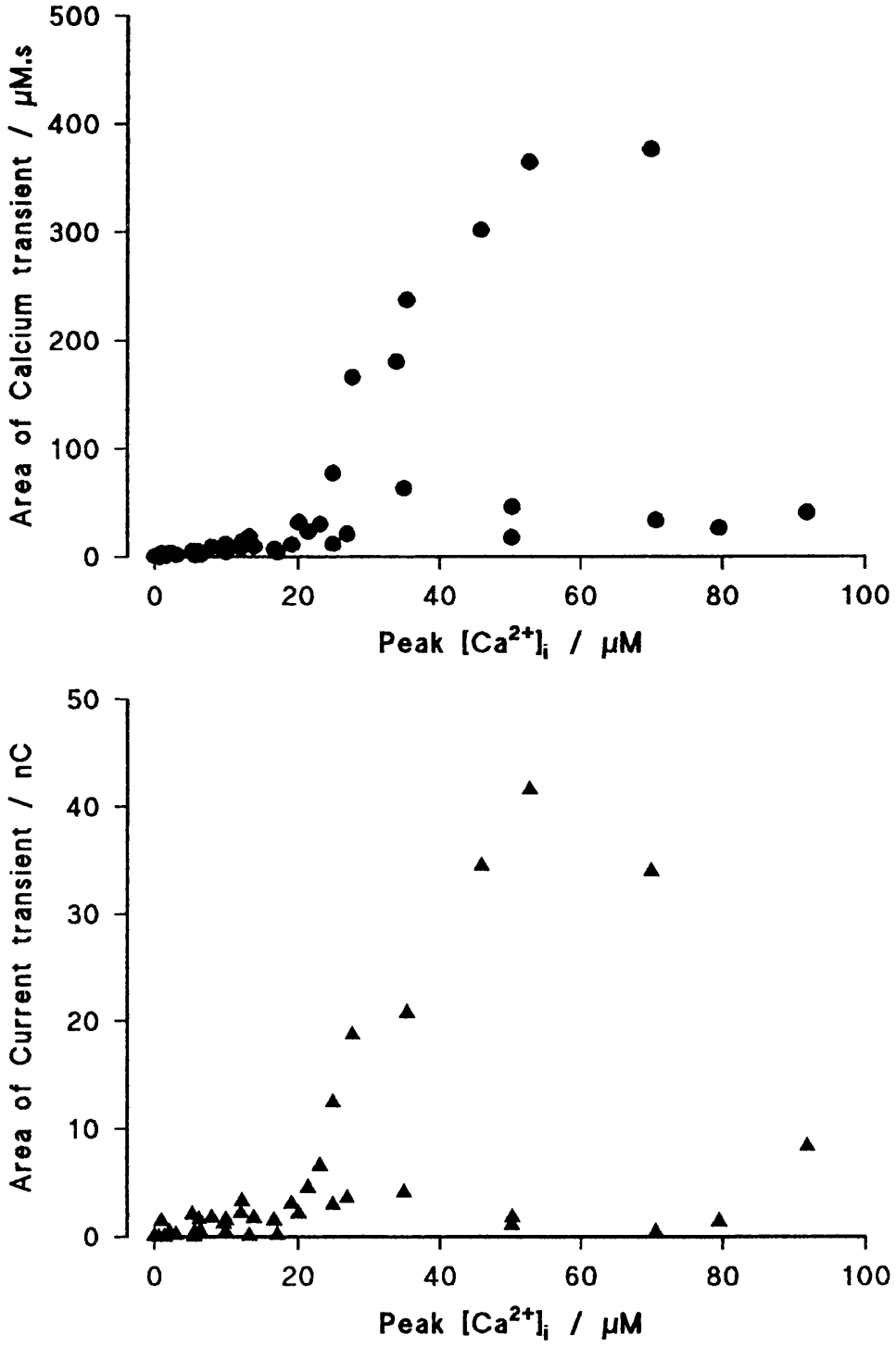

Figure 5.19 Two types of calcium transients are present in the older animals.

The area under the fluorescence transient was calculated and converted to estimate the area under the calcium transient, and is plotted against the peak $[Ca^{2+}]_i$ (top graph). The graph demonstrates the existence of two population of responses; at high $[Ca^{2+}]_i$ (>20μM) photolytically released $InsP_3$ results in either a short or long lasting transient. The area under the current transient also showed a similar distribution.

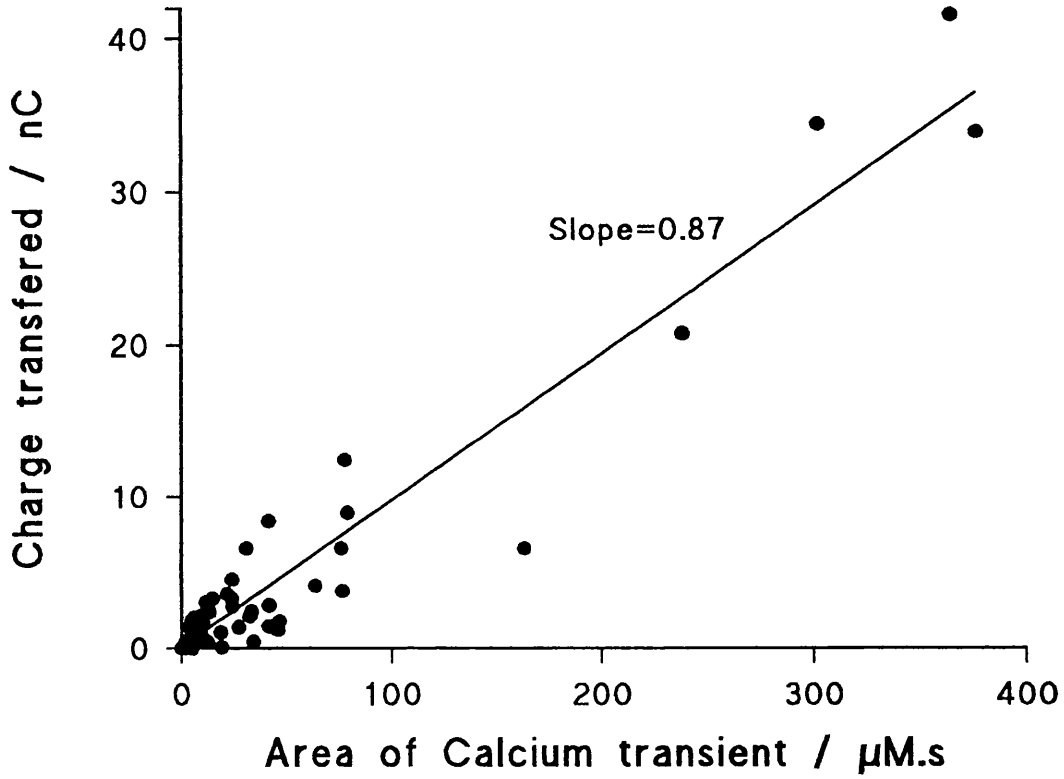

Figure 5.20 Correlation between the area under the current and calcium transients.

The area under the current transient is plotted against the area under the calcium transient estimated from the Furaptra transient. The line is the linear regression of the data points (r=0.96).

release $InsP_3$ during the peak or decline of $[Ca^{2+}]_i$. If the decline was due to metabolism of $InsP_3$ then a the second pulse of $InsP_3$ should have resulted in additional calcium release. Such a phenomena was observed when Fluo-3 was used as the calcium indicator (Figure 5.21), but not with Furaptra (Figure 5.22). If the metabolism of $InsP_3$ was the only factor responsible for the time course of recovery of the transients then a calcium release with the second pulse of $InsP_3$ should have been detected with both indicators. The difference between the results with the two indicators may be due to the greater calcium buffering of the cytoplasm with Fluo-3 compared with Furaptra. It may be argued that the ability of a second pulse of $InsP_3$ to mobilise calcium in the presence of Fluo-3 was due to a reduced inhibition by the lowered calcium concentration adjacent to the $InsP_3$ receptors. Further experiments are required to address this point in more detail. From the data available it is not possible to determine whether the decline of responses in Fluo-3 experiments was due to the partial inhibition of the $InsP_3$ receptors with calcium, metabolism of $InsP_3$, or depletion of the stores sensitive to that concentration of $InsP_3$ (Parker and Ivora, 1990). However experiments in which higher concentrations of the indicator are used to effectively clamp the concentration of free calcium would determine whether inhibition of $InsP_3$ receptors with calcium plays any role in the decline of transients.

5.5. Discussion

The range of concentration of $InsP_3$ effective in calcium mobilisation and its mechanism of action has been studied by application of $InsP_3$ during rapid mixing experiments with permeabilised cells, or with flash photolytic release of $InsP_3$ from its inactive caged analogue pre-equilibrated with the cytosol. Experiments with caged $InsP_3$ in permeabilised smooth muscle (Somlyo *et al*, 1992), in hepatocytes (Ogden *et al*, 1990; Ogedn *et al*, 1991), exocrine cells (Gray *et al*, 1989), and vascular endothelial cells (Carter and Ogden, 1992) have demonstrated the ability of $InsP_3$ to mobilize calcium from intracellular stores in the concentration range 0.2-5μM. The studies have shown a delay in the activation of the calcium efflux of several hundred ms at low $InsP_3$ concentration which become much shorter (<20ms) at high concentrations. The short delay observed in the activation of calcium efflux in these experiments suggest direct activation of the calcium channel by $InsP_3$, in agreement with data obtained from rapid mixing experiments with permeabilised hepatocytes (Champeil *et al*, 1989), or permeabilised rat basophilic leukaemia cells (Meyer *et al*, 1990). The maximum rate of rise of $[Ca^{2+}]_i$ as a function of

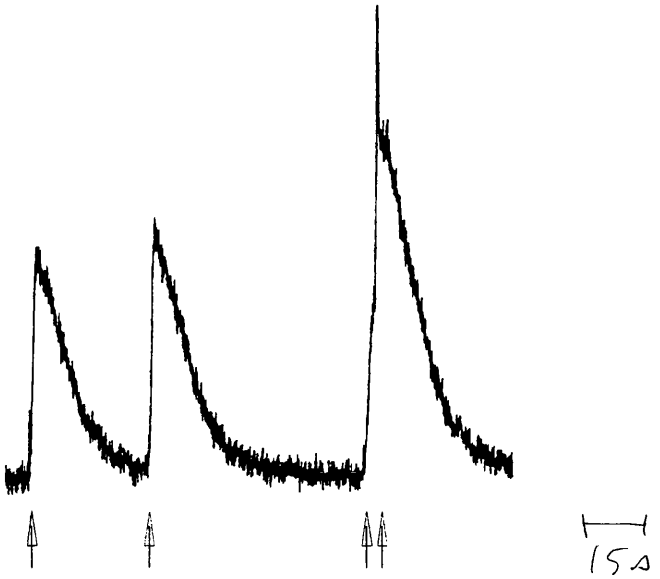

Figure 5.21 Consecutive pulses of $InsP_3$ released in a Purkinje cell loaded with Fluo-3.

The figure demonstrates a Fluo-3 fluorescence record during which consecutive pulses of 19μM $InsP_3$ were photolytically released in the cytosol of a voltage clamped Purkinje neurone at the times indicated by the arrows. No reduction in the amplitude of the light transient evoked by the second pulse of $InsP_3$ was detected. The fourth pulse of $InsP_3$ released immediately after the peak of the light transient resulted in an additional light transient the amplitude of which was greater than the first one.

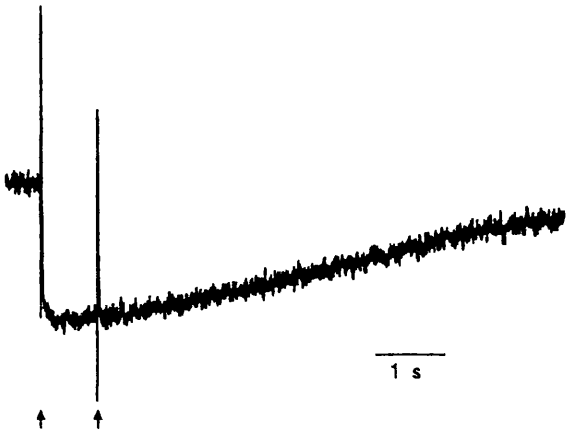

Figure 5.22 Twin pulses of $InsP_3$ in a Purkinje cell loaded with Furaptra.

The figure demonstrates a Furaptra fluorescence record during which 19μM $InsP_3$ was released photolytically with two pulses of UV light. Note that the second pulse failed to mediate further release of calcium. This is probably due to inhibitory effects of the raised calcium concentration on the $InsP_3$ receptors following the first pulse of $InsP_3$.

$InsP_3$ concentration, under conditions where other calcium fluxes into the cytosol are small, provides information relating channel activation as a function of $InsP_3$ concentration. In permeabilised hepatocytes the maximum rates of rise of $[Ca^{2+}]$ increased in the $InsP_3$ concentration range 0.1-10μM with a Hill coefficient of 1.6 (Champeil *et al*, 1989). A much larger Hill slope of 3-4 at low concentrations of $InsP_3$ (4nM) was found in permeabilised rat basophilic leukaemia cells (Meyer *et al*, 1988), suggesting a highly cooperative process. However in rapid mixing experiments with $InsP_3$-sensitive synaptosomes derived from CNS, when the free calcium concentration was buffered the concentration range measured by $^{45}Ca^{2+}$ efflux was 30nM to 10μM with Hill coefficient 1.0 (Finch *et al*, 1991). This study further showed a strong dependence of $InsP_3$ potency on the free $[Ca^{2+}]$; calcium concentrations upto 0.5-1μM potentiated release while higher $[Ca^{2+}]$ was inhibitory. Similar results were found with single channel recordings from $InsP_3$ receptor isolated from cerebellum and incorporated into lipid bilayers (Bezprozvanny *et al*, 1991). The maximum $InsP_3$-evoked open probability (upto 15% at 2μM) was at a free $[Ca^{2+}]$ of 0.3μM and declined with higher calcium concentrations. On the basis of the later two experiments it is likely that the cooperativity observed in other studies is due to the potentiating effects of released calcium and that only a single $InsP_3$ binding is required for the activation of the $InsP_3$ receptor.

The data presented here show that a rise in the $[Ca^{2+}]_i$ of astrocytes in primary cultures of rat cerebellum is detected following photolytic release of $InsP_3$, with the range of concentration of $InsP_3$ effective, and the kinetics of calcium efflux similar to that observed in the periphery. However similar experiments in Purkinje cells from acutely prepared slices of rat cerebellum showed that compared to astrocytes or peripheral tissue more than tenfold higher concentrations of $InsP_3$ are required to produce calcium mobilisation from the intracellular stores. Furthermore the size of calcium mobilisation in the Purkinje cells is larger ($[Ca^{2+}]_i$ in high micromolar), and faster ($[Ca^{2+}]_i$ peaks in less than 15ms with 76μM $InsP_3$) than that observed in the astrocytes or peripheral tissue. The concentration of $InsP_3$ required to mobilize calcium in Purkinje cells is higher than that required to activate $InsP_3$ receptors from canine cerebellum reconstituted in lipid bilayers (Bezprozvanny *et al*, 1991) or mediate calcium efflux from CNS derived tissue (Finch *et al*, 1991). However it should be noted that in neither of these experiments the neuronal origin of the $InsP_3$ receptors can be ascertained, since the possibility that the receptors originated from glia cannot be ruled out.

There are at least three possible explanations for the heterogeneity of $InsP_3$ action observed between the Purkinje cells and the peripheral

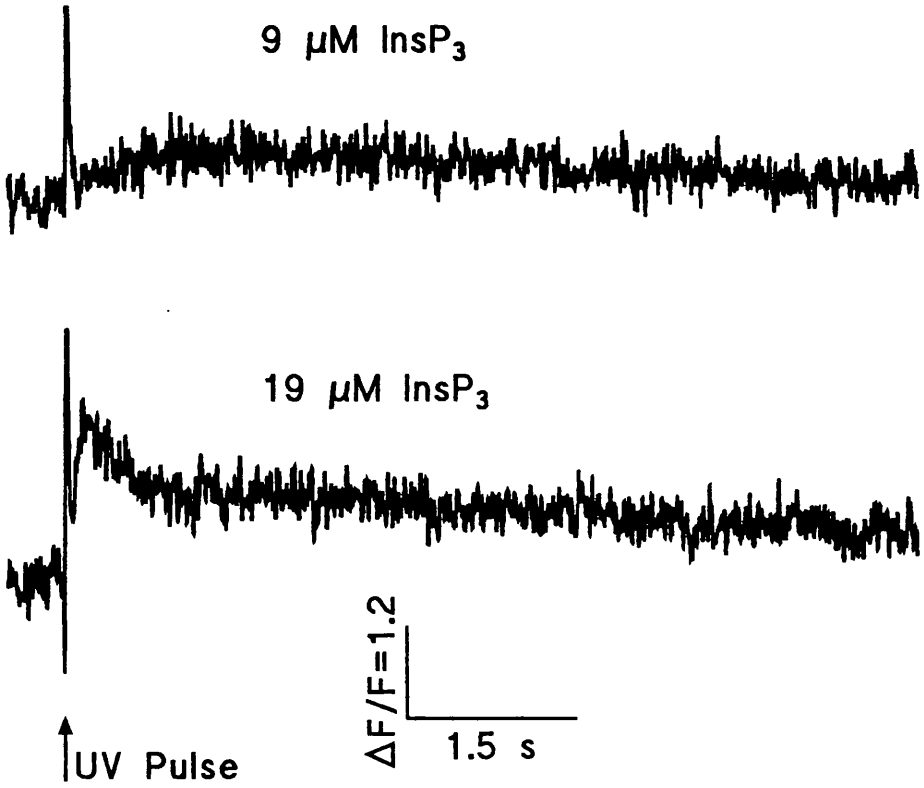

Figure 5.23 Transients in the soma of a Purkinje cell monitored with 1.2mM Fluo-3

The figure shows light transients from the soma of a Purkinje cell voltage clamped with a patch pipette containing 1.2mM Fluo-3 and 50μM caged $InsP_3$. Photolytic release of 9μM $InsP_3$ was capable of mobilising calcium despite the increased buffering (2400:1; bound to free calcium at 0.1μM free calcium) introduced in the cell by Fluo-3.

tissue. First it may be that the endogenous buffering of Purkinje cells tightly regulates the free calcium concentration so that much higher concentrations of $InsP_3$ are required to increase the free calcium concentration to levels necessary for cooperative action of calcium on the $InsP_3$ receptors. Despite the high calcium buffering capacity thought to exist in the Purkinje cells (Vill *et al*, 1991), this seems to be an unlikely explanation on the basis of the large range of calcium buffering used in the experiments described here (Figure 5.23); the calcium buffering introduced by 500μM Furaptra (11 bound to 1 free at 0.1μM free calcium) is small, and that introduced by 1.2mM Fluo-3 (2400 bound to 1 free at 0.1μM free calcium) is large compared to the endogenous buffers (eg 75 bound to 1 free in chromaffin cells, Neher and Augustine 1992). The second possibility is the presence of high density of inactive $InsP_3$ binding sites which result in a rapid reduction of $[InsP_3]$ adjacent to the calcium release sites. Alternatively the third possibility is that the functional $InsP_3$ receptors in the Purkinje cells are different from those present in the peripheral tissue. Indeed in support of this hypothesis alternative splicing and tissue specific expression of the messenger RNA for the $InsP_3$ receptor have been reported (Mignery *et al*, 1990; Nakagawa, 1991; Danoff *et al*, 1991; Ross *et al*, 1992). Furthermore the messenger RNAs alternatively spliced vary in the amino acid sequences encoding for the SI or SII regions, which are thought to be important in the binding of $InsP_3$, and phosphorylation of the $InsP_3$ receptor (Nakagawa *et al*, 1991; Danoff *et al*, 1991), and may determine the potency of $InsP_3$ in calcium release (Nakagawa *et al*, 1991).

Whatever the reason for the heterogeneity of $InsP_3$ action in the Purkinje cells with that of other tissues studied, it is apparent that the requirement for fast signalling in neurones has resulted in a system in which an increase in the cytosolic concentration of $InsP_3$ by stimulation of G protein linked neurotransmitter receptors is capable of rapidly increasing the $[Ca^{2+}]_i$. The elevation of $[Ca^{2+}]_i$ in the short term modifies the excitability of the membrane by activating the calcium gated potassium channels, and in the long term sets in action calcium activated processes such as gene transcription (eg Morgan and Curran, 1988), and protein synthesis (eg Brostorm and Brostorm, 1990).

In experiments described here the changes in the fluorescence emitted by the calcium indicator from a defined region of the cell was measured with a phototube allowing a time, but not spatially resolved study of the changes in the $[Ca^{2+}]_i$. The presence of calcium gradients at different parts of the cell could not be detected. Such gradients may indeed exist and could play an important physiological role. Although

imaging techniques provide spatial resolution, to date their combination with fluorescent indicators have not allowed a time resolved (ms resolution) study of $[Ca^{2+}]_i$. In the view of the fact that the changes in the $[Ca^{2+}]_i$ reported here are extremely fast the present imaging techniques would be unable to provide an accurate indication of the changes in the $[Ca^{2+}]_i$.

Although the elevation of $[Ca^{2+}]_i$ in the Purkinje cells by $InsP_3$ is a compliment of the proposed action of glutamate metabotropic receptors thought to be present in these cells (eg Llano *et al*, 1991), further experiments are required to demonstrate its role in synaptic transmission. For this purpose the thin slice provides a good preparation because a proportion of the synaptic input to a cell in a slice cut at the appropriate orientation is left intact. These pathways may be stimulated in the presence of ionotropic receptor blockers and the changes in $[Ca^{2+}]_i$ monitored. Furthermore the effect of $InsP_3$ released photolytically on action potentials evoked synaptically can be studied. Particular attention should be given to the changes in the $[Ca^{2+}]_i$ of the dendrites because the high membrane surface area to volume may result in altered kinetics of calcium release and removal. However the study of $InsP_3$ action in the dendrites is difficult due to the poor signal to noise ratio of the fluorescence emitted by the calcium indicators to the background fluorescence in this region. Longer 'cell loading' time, and perhaps brighter calcium indicators are required so that the changes in $[Ca^{2+}]_i$ may be studied in the dendrites without disturbing intracellular calcium buffering.

Although the presence of exceptionally high concentrations of $InsP_3$ binding sites and calcium binding proteins made the Purkinje cells the obvious candidate for the study of $InsP_3$ action in neurones, Purkinje cells may not be a good representative of the $InsP_3$ function in the CNS for the same reasons. Furthermore substantial differences in the levels of the alternatively spliced forms of the $InsP_3$ receptor occur in the brain; one form with 15 amino acids deleted accounts for 75-85% of $InsP_3$ receptors in the cerebellum but only for 12% of receptors in the cerebral cortex (Nakagawa *et al*, 1991). Therefore further studies are required to characterize properties of $InsP_3$ signal transduction in neurones other than Purkinje cells to establish whether the adaptation seen in Purkinje cells is a general feature of all neurones.

$InsP_3$ released photolytically in the cytosol of cultured neurones did not mobilise calcium. One explanation may be that the neurones studied, hippocampal pyramidal cells, striatal neurones, cerebellar granule cells, and DRGs do not have functional $InsP_3$ receptors, or the receptors are different from all others studied. This, although possible on the basis of the existence of alternatively spliced forms of $InsP_3$ receptor mRNAs, is the

less likely explanation if the possibility of 'culture artifact' is considered. Numerous alterations in the physiological processes of cells kept in culture have been reported. For example in cultured Purkinje neurones no alteration in the $[Ca^{2+}]_i$ could be detected when the metabotropic receptors were stimulated (Brorson *et al*, 1991). These cells however expressed high $InsP_3$ receptor binding sites and manifested an increase in $[Ca^{2+}]_i$ when they were depolarised, or stimulated with caffeine or glutamate in the absence of glutamate channel blockers (Brorson *et al*, 1991). In contrast to the cultured Purkinje neurones an increase in intradendritic $[Ca^{2+}]_i$ of Purkinje cells in thin slices of the cerebellum following stimulation of the glutamate metabotropic receptors has been reported (Llano *et al*, 1991). In hippocampal pyramidal cells a 'metabotropic' calcium mobilising action of glutamate could only be detected if a depolarising 'conditioning' pulse was used to 'fill up' the stores (Murphy and Miller, 1988). The nature of these artifacts are not clear, but could arise from the lack of proper differentiation of these cell in culture in the absence of the normal synaptic inputs. In order to avoid the possible 'culture artifacts', further experiments on neurones in slices obtained from various regions of the brain should be done to explore the $InsP_3$ function in these cells.

Chapter 6
Overview

6. Overview

Experiments were described during which postsynaptic actions of excitatory amino acids were investigated with flash photolysis. Post synaptically excitatory amino acids exert their actions by opening cation channels, or activating G protein linked 'metabotropic' receptors. The rapid diffusion of the L-glutamate across the synaptic cleft and its rapid binding and opening of glutamate gated channels allow the fast transmission of information from one neurone to the other. The inherent delay in the activation of second messenger systems by the metabotropic receptors, on the other hand, allows for slower, longer lasting modulation of cellular excitability and function.

To study the process of fast synaptic transmission, and the kinetic of activation of receptors, it is informative if the action of neurotransmitter during synaptic activation can be mimicked by exogenous application of compounds. In the central nervous system the specialized structure of synapses makes a diffusion barrier which renders impractical rapid and uniform application of compounds to the postsynaptic membrane by ionophoreses or other conventional methods. One way to overcome this problem is the technique of flash photolysis; an inactive photolabile analogue of the neurotransmitter is allowed to equilibrate with the preparation, and a known concentration of the neurotransmitter released with a pulse of UV light. The result is a spatially uniform rapid concentration step, with kinetics only dependent on the photolysis reaction, and independent of diffusion. Chapter 3 described the experiments required to establish the suitability of a photolabile analogue of a neurotransmitter as a caged neurotransmitter. The only analogue of glutamate tested that satisfied the criteria required for a caged glutamate, *N*(1,(2-nitrophenyl)ethoxycarbonyl)-L-glutamate, had a photolysis half time of about 50ms at pH 7, too slow to allow the study of the kinetics of ion channel activation under physiological conditions. The rate of photolysis of this compound, however, is pH dependent increasing 10 fold with one pH unit drop. Chapter 4 described experiments during which the pH dependence of the kinetics of photolysis, and the ability of the squid giant synapse to withstand acidic conditions allowed the use of caged glutamate to provide good evidence for the glutamatergic nature of the synapse. The squid giant synapse is a good example of a specialized synapse where the peculiar morphology produces an effective diffusion barrier for the exogenously applied compounds and the experiments described in chapter 4 demonstrate the simple principle and practicality of the technique of flash photolysis to overcome the problem of diffusion.

However it is clear that the present caged glutamate does not have fast enough kinetics of photolysis to elucidate mechanism of channel activation, and for the technique to be used effectively a faster caged glutamate is required. In addition the experiments on the squid giant synapse highlighted a general problem with the use of caged neurotransmitters to mimic synaptic transmission utilizing the apparatus described. During synaptic transmission the neurotransmitter is locally released in the synaptic cleft, and removed rapidly by diffusion and active uptake. A pulse of UV light delivered by the experimental apparatus used here, on the other hand, produced photolysis of caged glutamate over a much larger area (about 500μm diameter) resulting in the slower removal of glutamate and activation of several synapses. In the giant synapse this was apparent by the presence of more than one action potential and the long time course of the recovery of the responses. Furthermore if used in slices, abrupt release of glutamate over a large area would result in the activation of all glutamatergic cells present in that area and not just the cell under study (Figures 6.1 and 6.2).

To use the technique of flash photolysis to its full potential when studying synaptic transmission it would be necessary to restrict the area of photolysis. The use of a laser as the light source would provide a columnated beam which is much easier to manipulate. This beam could be focused on the preparation with a high magnification objective either from underneath with the objective used as a condenser, or through the epifluoresence port *via* the objective used for viewing the cell. Alternatively a finely tapered light guide could be used to direct the light to the area of interest. Practical considerations, however, need to be given to the light source, material and effective coupling of optical components so that sufficient energy is provided for photolysis in the preparation. Furthermore the apparatus should be designed so that photolysis is reproducible, and easily and accurately calibrated. One method of producing localized photolysis would be the use of two photon laser scanning fluorescence microscopy (Denk *et al*, 1990) where excitation of a molecule is achieved only when two photons are absorbed simultaneously. Once the technical problems of localized photolysis have been over come, flash photolysis of caged neurotransmitters can be used in thin slices of the brain to investigate the mechanism of such processes as long term potentiation and depression by directly examining the sensitivity of the postsynaptic membranes to the applied neurotransmitter. The technique of flash photolysis can also be employed when studying 'slow' postsynaptic actions of a neurotransmitter. A second messenger system activated by the postsynaptic stimulation of glutamate metabotropic receptors is that of

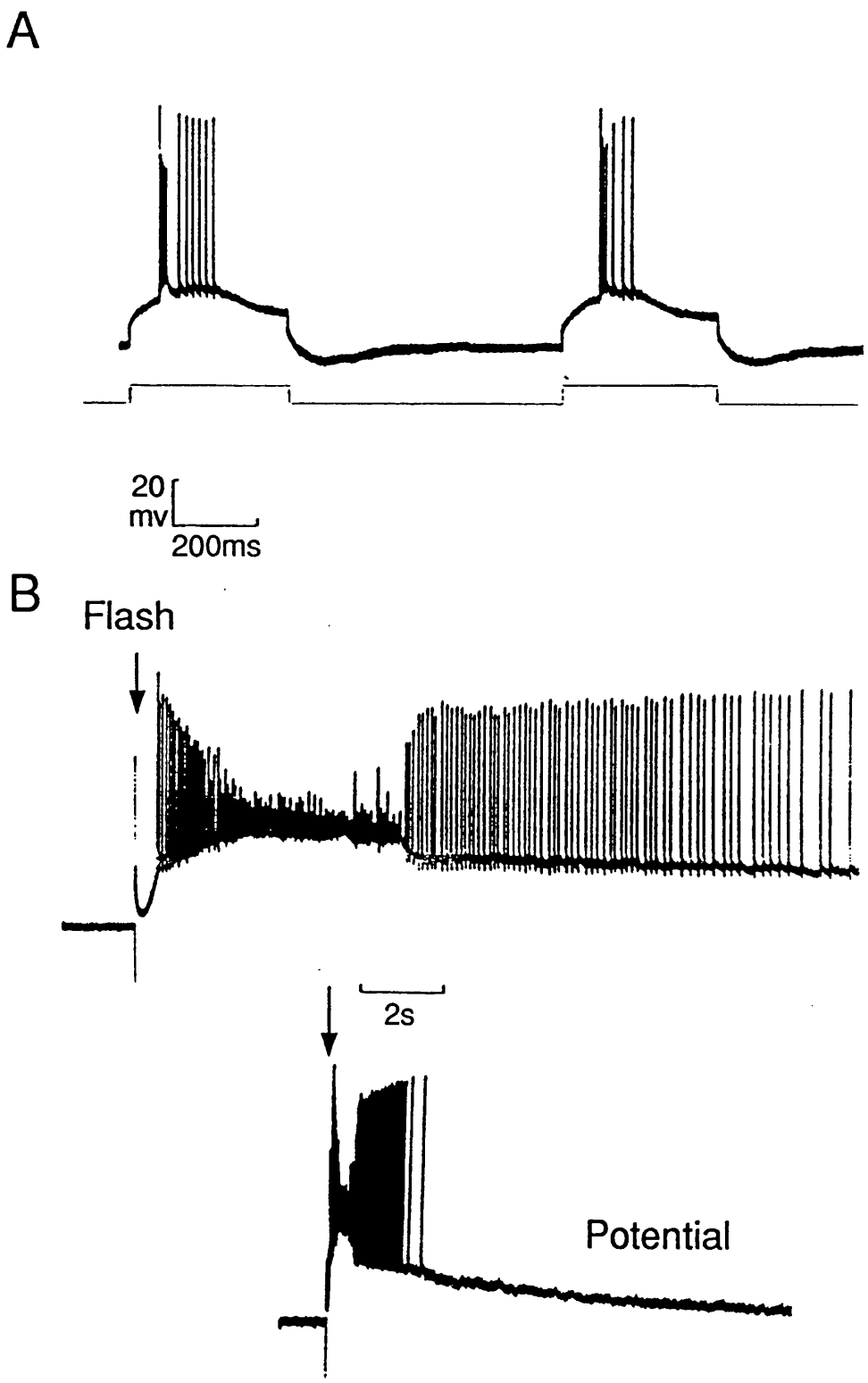

Figure 6.1 Photolytic release of L-glutamate in a cerebellar slice.

A Purkinje cell from a thin slice of the rat cerebellum was patched and following obtaining whole cell configuration current clamped. Panel A demonstrates action potentials produced during current steps. 1.2mM caged glutamate was allowed to equilibrate with the slice for 15 minutes and the xenon arc lamp was fired at the time indicated by the arrow (Panel B). Photolytic release of L-glutamate elicited a train of action potentials which lasted for several seconds.

phosphoinositide turnover and production of $InsP_3$. Chapter 5 described experiments during which the glutamate stimulated processes involved in production of $InsP_3$ were bypassed by intracellular photolytic release of $InsP_3$ from caged $InsP_3$. Microspectroflurimetry of neurones in primary cultures of the striatum, hippocampal pyramidal cells, cerebellar granule cells, and DRGs did not detect calcium mobilization with photolytic release of up to 40μM $InsP_3$. Lack of calcium mobilization with $InsP_3$ in these neurones was not due to 'wash out' of the cytosol *via* the whole cell patch pipette. It is noteworthy that in cerebellar astrocytes from the same cultures as the non-responsive neurones $InsP_3$ resulted in calcium mobilization from intracellular stores. The concentration range of $InsP_3$ effective in calcium mobilization ($[InsP_3]$>0.3μM), and the kinetics of calcium transients were similar to the other non-excitable cells studied. Recent studies have demonstrated the existence of several alternatively spliced forms of $InsP_3$ receptor mRNAs. It is possible that the $InsP_3$ receptors expressed by the neurones in the primary cultures studied are functionally different from that of the astrocytes. Alternatively the reason for the lack of responses in cultured neurones may be due to an artifact of culture condition. This should be examined by investigating the action of $InsP_3$ in the same cell types in acutely prepared slices.

Because of the ease of identification, existence of high densities of $InsP_3$ receptor binding sites and calcium binding proteins, and presence of a metabotropic response in Purkinje neurones these cells were selected to investigate the properties of calcium mobilization by $InsP_3$ in slices. A markedly adapted $InsP_3$ signalling system was demonstrated to exist in Purkinje cells in acutely prepared thin slices of the cerebellum, providing the first direct evidence for the calcium mobilising action of $InsP_3$ in an intact mammalian neurone. Compared to astrocytes and other cells from peripheral tissue, at leat 10 fold higher concentrations of $InsP_3$ was required to mobilise calcium in Purkinje cells. The resulting calcium transients following application of $InsP_3$ were larger, often greater than 30μM, and had much faster kinetics reaching a maximum in less than 35ms with 38μM $[InsP_3]$. Attempts were made to investigate the mechanism responsible for this adaptation. Experiments during which the cytosolic calcium buffering of the cell was manipulated indicated that cytosolic calcium buffering is an explanation for the lower potency of $InsP_3$ in these cells. On the basis of the presence and selective expression of different $InsP_3$ receptor mRNAs in different cells, on the other hand, it is likely that the adaptation seen in the Purkinje cells is due to a difference between the $InsP_3$ receptor present in these neurones with that in the astrocytes and peripheral tissues studied. It is clear that a detailed characterization

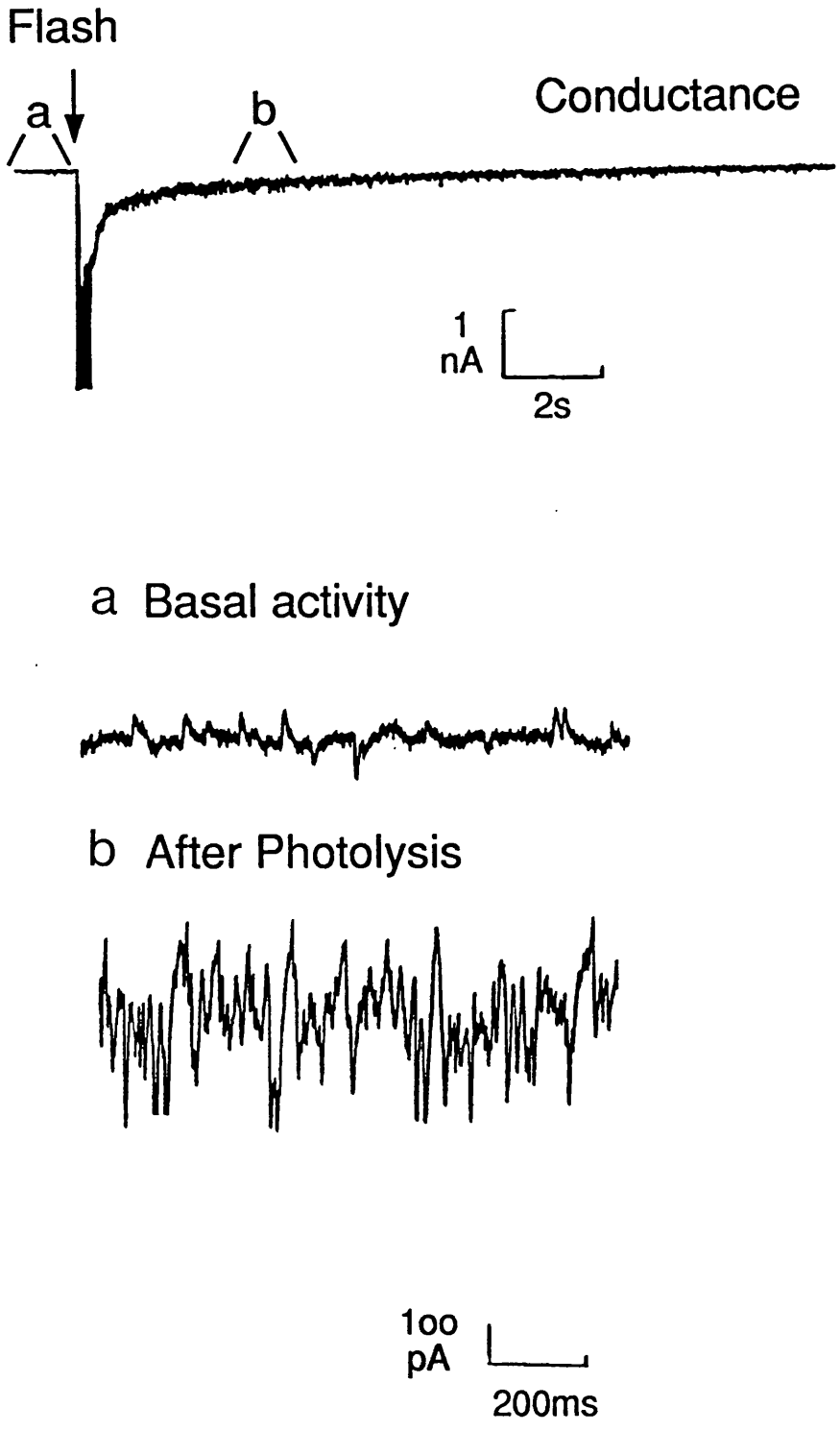

Figure 6.2 Activation of all glutamatergic neurones by flash photolytic release of glutamate in a cerebellar slice.

The same Purkinje cell as that in Figure 6.1 was voltage clamped at a holding potential of -70mV. At the time indicated by the arrow a pulse of near UV light was applied to the slice *via* the condenser, resulting in a large inward current due to activation of glutamate gated channels (the amplifier is saturated immediately after the flash). Note the increase in the number of synaptic inputs to the cell following application of glutamate (part b versus a) due to activation of all the glutamatergic neurones present in the area illuminated by the UV light.

of the functional properties of these receptors is necessary before this hypothesis can be tested rigorously. Whatever the reason for the heterogeneity of $InsP_3$ action in Purkinje cells with that of other tissues studied, it is apparent that the requirement for fast signalling has resulted in a system by which an increase in the cytosolic concentration of $InsP_3$ by stimulation of G protein linked neurotransmitter receptors is capable of rapidly increasing $[Ca^{2+}]_i$. The elevation of $[Ca^{2+}]_i$ in short term modifies the excitability of the membrane by activating the potassium gated potassium channels, and in the long term sets in action calcium activated processes such as gene transcription, protein synthesis, channel phosphorylation and activation of protein kinases.

Experiments are required to examine the physiological conditions under which $InsP_3$ signalling pathway is activated in the Purkinje cells. The well characterized circuitry of the cerebellar slices, and the ease in selective stimulation of various pathways makes thin slices of the cerebellum a good preparation for these experiments. Techniques used in the experiments described may be combined with stimulation of various pathways provide to investigate the short and long term effects of activation of the $InsP_3$ system on the synaptic inputs of the Purkinje neurones. Of particular interest would be a detailed study of $InsP_3$ action in the dendrites, best conducted if time resolved imaging (with ms time resolution) is combined with localized photolysis of $InsP_3$.

The functional properties of $InsP_3$ signalling in Purkinje cells demonstrate an adaptation of this second messenger system to satisfy fast signalling required by these neurones. Further experiments would determine whether this adaptation is only a feature of these cells or is common to all neurones. The combination of the technique of flash photolysis with those of microspectrofluorimetry and patch clamp recording in thin slices of the nervous system provides a powerful tool for the study of postsynaptic actions of neurotransmitters, and second messenger systems.

Appendix 1

The relation between the fluorescence emitted from a fluorescent indicator and concentration of free ion

Appendix 1 The relation between the fluorescence emitted from a fluorescent indicator and the concentration of free ligand

Imagine the equation describing the binding of ligand, L, with dye, D:

$$D+L \leftrightharpoons DL$$

for which at equilibrium it may be written

$$K_D=\frac{L*D}{DL} \qquad (1)$$

where L, d, and DL are the concentration of the free ligand, free dye and bound dye respectively and K_D is the equilibrium dissociation constant. The terms D^*, and DL^*, the fractions of dye in the bound and unbound state, may be defined as:

$$D_T=D+L$$

$$D^*=\frac{D}{D_T} \qquad (2)$$

$$DL^*=\frac{DL}{D_T} \qquad (3)$$

and K_D re-written in terms of D^*, and DL^*:

$$K_D=\frac{L*D^*}{DL^*} \qquad (4)$$

The fluorescence emitted by the dye in the absence of any ligand F_{min}, is the product of the concentration of the dye with its quantum efficiency in the unbound state, ϕ_0:

$$F_{min}=D_T*\phi_0$$

which may be rearranged to:

$$\phi_0 = \frac{F_{min}}{D_T} \tag{5}$$

Similarly, The fluorescence emitted by the dye in the presence of saturating concentrations of the ligand, F_{max}, is the product of the concentration of the dye with its quantum efficiency in the bound state, ϕ_L;

$$F_{max} = D_T * \phi_L$$

which may be rearranged to:

$$\phi_L = \frac{F_{max}}{D_T} \tag{6}$$

In the presence of non-saturating concentrations of the ligand the fluorescence emitted by the dye is the sum of the products of the concentrations of the dye in the bound and unbound form with their respective fluorescence quantum efficiencies:

$$F = D * \phi_0 + DL * \phi_L$$

This equation may be re-written by substituting for the quantum efficiencies from equations (5) and (6):

$$F = F_{min} * D^* + F_{max} * DL^* \tag{7}$$

But

$$D^* = 1 - DL^* \tag{8}$$

and equation (7) may be re-written and rearranged

$$F - F_{min} = -DL^* * F_{min} + DL^* * F_{max}$$

but from equation (1) we have

$$DL^* = \frac{L * D^*}{K_D}$$

therefore

$$F - F_{min} = -\frac{L * D^* * F_{min}}{K_D} + \frac{L * DL^* * F_{max}}{K_D}$$

which may be rearranged to

$$L = K_D * \frac{F - F_{min}}{-D^* * F_{min} + DL^* * F_{max}}$$

and using equation (8)

$$L = K_D * \frac{F - F_{min}}{-D^* * F_{min} - DL^* * F_{max} + F_{max}}$$

which using equation (7) simplifies to:

$$L = K_D * \frac{F - F_{min}}{F_{max} - F} \qquad (9)$$

This allows the calculation of the concentration of free ligand when the fluorescence emitted by the indicator at that concentration, F_{min}, F_{max}, and the K_D are known. Note that this equation may be applied to any fluorescent indicator.

Appendix 2

The minimum detectable response as a measure of relative potency of an agonist

Appendix 2. The minimum detecable response as a measure of relative potency of an agonist

Let us consider a three state model whereby the agonist A binds to the receptor-channel complex and results in the channel opening:

$$A + R \underset{k_-}{\overset{k_+}{\rightleftharpoons}} AR \underset{\alpha}{\overset{\beta}{\rightleftharpoons}} AR^*$$

3 2 1

Where K is the equilibrium dissociation constant for agonist association with the receptor sites and ß and α are rate constants for channel opening and shutting. The probability of being at each state is given by P_1, P_2, and P_3, with the sum of the probabilities being 1. From the law of mass action we have:

$$K = \frac{k_-}{k_+} = \frac{[A][R]}{[AR]} = \frac{[A]P_3}{P_2} \qquad (1)$$

Let [A]/K = c Then from (1): $P_3 = P_2/c$ (2)

$$\frac{\beta}{\alpha} = \frac{[AR^*]}{[AR]} = \frac{P_1}{P_2} \qquad (3)$$

By rearranging (3): $P_2 = P_1 (\alpha/\beta)$ (4)

The sum of the probabilities is 1, therefore:

$$P_3 = 1 - P_1 - P_2$$

Substituting (2): $P_2/c = 1 - P_1 - P_2$

Therefore: $P_2 (1 + c) = c - P_1 c$

Substituting (4): $P_1 (\alpha/\beta)(1 + c) = c - P_1 c$

And rearrange: $P_1 \{(\alpha/\beta)(1 + c) + c\} = c$

But c = [A]/K. Therefore:

$$P_1 \{(\alpha/\beta)(1 + ([A]/K)) + [A]/K\} = [A]/K$$

By rewriting the equation for [A]:

$$[A]=\left(\frac{P_1}{1-P_1-\frac{P_1\alpha}{\beta}}\right)K\frac{\alpha}{\beta} \qquad (5)$$

In the same way for an agonist B with open-shut rate constants α' and β' and probability of P_1' for state 1, and agonist equilibrium dissociation constant K' it can be written:

$$[B]=\left(\frac{P_1'}{1-P_1'-\frac{P_1'\alpha'}{\beta'}}\right)K'\frac{\alpha'}{\beta'}$$

The ratio of the two agonists, [A]/[B] would be:

$$\frac{[A]}{[B]}=\left(\frac{P_1(1-P_1'-\frac{P_1'\alpha'}{\beta'})}{P_1'(1-P_1-\frac{P_1\alpha}{\beta})}\right)\left(\frac{K\alpha\beta'}{K'\alpha'\beta}\right) \qquad (6)$$

Agonists after binding to the receptor-channel complex produce a conformational change in the channel pore so that it becomes permeable to ions. Different agonists produce the same conformational change so that the conductance of the channel is always the same. The difference in the potencies of different agonists, therefore, arises from differences in their equilibrium dissociation constant for agonist binding with the receptor site, and the equilibrium in the channel opening and closing α/β. The channel open-shut equilibrium constant determines the proportion of the channels which would be open if all the receptors were occupied (given by β/(α+β)).

Let us for a moment consider equation (6) where concentrations of agonists [A] and [B] are sufficiently low so that the probability of open channel is very small. Since it is reasonable to assume that α/β and α'/β' are small, we can rewrite equation (6), ignoring the terms P_1, P_1', $P_1'(\alpha'/\beta')$ and $P_1(\alpha/\beta)$:

$$\frac{[A]}{[B]}=\left(\frac{P_1}{P_1'}\right)\left(\frac{K\alpha\beta'}{K'\alpha'\beta}\right) \qquad (7)$$

Equation (7) indicates that the concentration ratio of the two agonists is directly proportional to the ratio of their agonist equilibrium dissociation constant and the ratios of the channel open-shut equilibrium. In another words, the ratio of the two agonists is proportional to the ratio

of their potencies, and the error in the potency ratio arises from the error in estimation of P_1 and P_1'.

In order to have an estimate of the potency ratio of caged glutamate and L-glutamate the minimum concentration of glutamate required to produce a detectable response was obtained. Granule cells from primary cultures of cerebellum were whole-cell voltage clamped (holding potential -70mV) and L-glutamate was applied *via* a pressure puffer in absence of added magnesium. Activation of a few glutamate-gated channels was detected during puffer application of 100nM (6/6 cells), but not 50nM L-glutamate (1/7 cells responded). On the other hand no response could be detected with puffer application of upto 1mM caged glutamate (0/8 cells). If it is assumed that the minimum concentration of L-glutamate to produce a detectable response in the absence of added magnesium ions was 100nM, then a potency ratio of caged-glutamate/L-glutamate of 1mM/100nM is obtained. It is most likely that the channels activated in the absence of magnesium ions are the NMDA channels. Therefore caged glutamate is at least 10000 less potent than glutamate as an agonist at the NMDA channels. Similarly the minimum concentration of L-glutamate to produce a detectable response in the presence of 1mM $MgCl_2$, 50μM, was obtained, and it was concluded that caged glutamate is at least 200 less potent as an agonist at the non-NMDA sites compared to L-glutamate. Errors can arise from the different number of functional receptors expressed on each cell, as well as the criteria set for a detectable response.

References

References

Abe T, Sugihara H, Nawa H, Shigemoto R, Mizuno N, and Nakanishi S (1992). Molecular characterization of a novel glutamate receptor mGluR5 coupled to inositol phosphate/Ca^{2+} signal transduction. J Biol Chem, 267:13361-13368.

Adams D J, and Gillespie J I (1988). The actions of L-glutamate at the postsynaptic membrane of the squid giant syanpse. J Exp Biol, 140:535-548.

Adams P R, Constanti A, Brown D A, and Clark R B (1982). Intracellular Ca^{2+} activates a fast voltage-sensetive K^+ current in vertebrate sympathetic neurones. Nature, 296:746-749.

Alexandre J, Lassalles J P, and Kado R T (1990). Openning of Ca^{2+} channels in isolated red beet root vacule membrane by inositol 1,4,5-trisphosphate. Nature, 343:567-570.

Ames A, Sakanoue M, and Endo S (1964). Na, K, Ca, Mg, and Cl concentrations in choroid plexus fluid and cisternal fluid compared with plasma ultrafilterate. J Neurophysiol, 27:672-681.

Baker P F, and Crawford A C (1972). Mobility and transport of magnesium in squid giant axon. J Physiol, 227:855-874.

Baker P F, Hodgkin A L, and Ridgeway E B (1971). Depolarisation and calcium entery in squid giant axons. J Physiol, 218:709-755.

Barbour B, Brew H, and Attwell D (1988). Electrogenic glutamate uptake in glial cells is activated by potassium. Nature, 335:433-435.

Baskys A, Bernstein N K, Barolet A W, and Carlen P L (1990). NMDA and quisqualate reduce a Ca-dependent K^+ current by a protein kinase mediated mechanism. Neurosci lett, 112:76-81.

Bateman A, Boden P, Dell A, Duce I R, Quicke L J, and Usherwood P N R (1985). Postsynaptic block of a glutamateric synapse by a low molecular weigth fractions of spider toxin. Brain Res, 339:237-244.

Berridge M J and Irvine R F (1989). Inositol phosphates and cell signalling. Nature, 341:197-204.

Berridge M J (1987). Inositol trisphosphate and diacylglycerol: two interacting second messengers. Ann Rev Biochem, 56:159-193.

Bettler B, Boulter J, Hermans-Borgmeyer I, O'Shea-Greenfield A, Deneris E S, Moll C, Borgmeyer U, Hollmann M, and Hinemann S (1990). Cloning of a novel glutamate receptor subunit, GluR5: expression in the nervous system during development. Neuron, 5:583-595.

Bezprozvanny I, Watras J, and Ehrlich B E (1991). Bell-shaped calcium-response curves of Ins(1,4,5)P_3-gated and calcium-gated channels from endoplasmic reticulum of cerebellum. Nature, 351:751-754.

Blaustein M P, and Hodgkin A L (1968). The effect of cyanide on calcium efflux in squid axons. J Physiol, 198:46-48P.

Bolsover S R (1981). Calcium dependent potassium current in barnacle photoreceptor. J Gen Physiol, 78:617-636.

Boulter J, Hollmann M, O'Shea-Greenfield A, Hartley M, Deneris E, Maron C, and Hinemann S (1990). Molecular cloning and functional expression of glutamate receptor subunit genes. Science, 249:1033-1037.

Brinley F J Jr, and Scarpa A (1975). Ionized magnesium concentration in axoplasm of dialyzed squid axons. FEBS Lett, 50:82-85.

Brorson J R, Bleakman D, Gibbons S J, and Miller R (1991). The properties of intracellular calcium stores in cultured rat cerebellar neurones. J Neurosci, 11:4024-4043.

Brostrom C O, and Brostrom M A (1990). Calcium-depenedent regulation of protein synthesis in intact mamalian cells. Annul Rev Physiol, 52:577-590.

Burnashev N, Schoepfer R, Monyer H, Ruppersburg J P, Gunther W, Seeburg P H, and Sakman B (1992). Control by aspargine residues of calcium permeability and magensium blockade in the NMDA receptors. Science, 257:1415-1419.

Burnashev N, Monyer H, Seeburg P H, and Sakmann B (1992). Divalent ion permeability of AMPA receptor channels is dominated by the edited form of a single subunit. Neuron, 8:189-198.

Capiod T, and Ogden D C (1989). The properties of calcium-activated potassium ion channels in guinea-pig isolated hepatocytes. J Physiol, 409:285-295.

Capiod T, Field A C, Ogden D C, and Sandford C A (1987). Internal perfusion of guinea-pig hepatocytes with buffered Ca^{2+} or inositol w4,5-trisphosphate mimics noradrenaline activation of K^+ and Cl^- conductances. FEBS letters, 217:247-252.

Carter T D, and Ogden D C (1992). Kinetics of intracellular calcium release by inositol 1,4,5-trisphosphate and extracellular ATP in porcine cultured aortic endothelial cells. Proc Royal Soci, in press.

Carter T D, and Ogden D C (1991). Calcium release evoked by intracellular inositol 1,4,5-trisphosphate in porcine aortic endothelial cells in tissue culture. J Physiol, 446:558P.

Challiss R A J, Batty I H, Nahorski R (1988). Mass measurments of inositol (1,4,5) trisphosphate in rat cereberal cortex slices using a radioreceptor assay: effects of neurotransmitters and depolarisation. Biochem Biophys Res Commun, 157:684-691.

Champeil P, Combettes L, Berthon B, Doucet E, Orlowski S, and Claret M (1989). Fast kinetics of calcium release induced by myo-inositol trisphosphate in permeabilized rat hepatocytes. J Biol Chem, 264:17665-17673.

Charpak S, Gahwiler B H, Do K Q, and Knopfel T (1990). Potassium conductances in hippocampal neurons blocked by excitatory amino-acid transmitters. Nature, 347:765-767.

Clements J D, Lester R A, Tong G, Jahr C E, Westbrook G L (1992). The time course of glutamate in the synaptic cleft. Science, 258:1498-1501.

Colquhoun D C, Jonas P, and Sakmann B (1993). Action of brief pulses of glutamate on AMPA/kainate receptors in patches from different neurones of rat hippocampal slices. J Physiol, 458:261-287.

Cull-Candy S G, and Usowicz M M (1987). Multiple conductance channels activated by excitatory amino acids in cerebellar neurones. Nature, 325:525-528.

Cull-Candy S G, Howe J R, Ogden D C (1988). Noise and single channels activated by excitatory amino acids in rat cerebellar granule neurones. J Physiol, 400:189-222.

Cull-Candy S G, Dilger P, Ogden D C, and Temple S (1985). Patch clamp of rat cerebellar neurones in culture. J Physiol, 362, 45P.

Curtis D R, Phillis J W, and Watkins J C (1959). Chemical excitation of spinal neurones. Nature, 183:611-612.

Curtis D R, Philis J W, and Watkins J C (1960). The chemical excitation of spinal neurones by certain acidic amino acids. J Physiol, 150:656-682.

Curtis D R, and Watkins J C (1963). Acidic amino acids with strong excitatory actions on mamalian neurones. J Physiol, 166:1-14.

Curtis D R, and Watkins J C (1960). The excitation and depression of spinal neurones by structurally related amino acids. J Neurochem, 6:117-141.

Curutchet P, Bochet P, Prado de Carvalho L, Lambolez B, Stinnakre J, and Rossier (1992). In the GluR1 glutamate receptor subunit a glutamine to histidine point mutation suppresses inward rectification but not calcium permeability. Biochem Biophys Res Commun, 182:1089-1093.

D'Angelo E, Rossi P, Garthwaite J (1990). Dual-component NMDA receptor currents at a single central synpase. Nature, 346:467-470.

Danoff S K, Ferris C D, Donath C, Fische G A, Munemitsu S, Ullrich A, Snyder S H, and Ross C A (1991). Inositol 1,4,5-trisphosphate receptors: distinct neuronal and nonneuronal forms derived by alternative splicing differ in phosphorylation. Proc Natl Acad Sci USA, 88:2951-2955.

Davies J, Francis A A, Jones A W, and Watkins J C (1981). 2-amino-5-phosphonovalerate (2APV), a potent and selective antagonist of amino acid induced and synptic excitation. Neurosci Lett, 21:77-81.

De Santis A, and Messenger J B (1989). New evidence that L-glutamate is a trasnmitter at the squid giant synapse. Quart J Exp Physiol, 74:219-222.

Dekin M S (1983). Permeability changes induced by L-glutamate at the crayfish neuromuscular junction. J Physiol, 341:105-125.

Denk W, Strickler J H, and Webb W W (1990). Two-photon laser scanning fluorescence microscopy. Science, 248:73-76.

Dudel J, Franke CH, Hatt H (1990). Rapid activation, desensitization, and resensitization of synaptic channels of crayfish muscle after glutamate pulses. Biophys J, 57:533-545.

Dufy B, MacDermott A, and Barker J L (1986). Rundown of GH3 cell K^+ conductance response to TRH following patch recording can be obviated with GH3 cell extract. Biochem Biophys Res Commu, 137:388-396.

Ebashi S (1963). Third component of participating in the superprecipitation of 'Natural actomyosin'. Nature, 200:1010.

Edwards F A, Konnerth A, Sakmann B, Takahashi T (1989). A thin slice preparation for patch clamp recordings from neurones of the mammalian central nervous system. Pflugers Arch, 414:600-612.

Egebjerg J, Bettler B, Hermans-Borgmeyer I, and Hinemann S (1991). Cloning of a cDNA for a glutamate receptor subunit activated by kainate and not AMPA. Nature, 351:745-748.

Ellisman M H, Deerinck T J, Ouyang Y, Beck C F, Tanksley S J, Walton P D, Airey J A, and Sutko J L (1990). Identification and localisation of ryanodine binding proteins in the avian central nervous system. Neuron, 5:135-146.

Eusebi F, Miledi R, Parker I, and Stinnakre J (1985). Post-synaptic calcium influx at the giant synapse of the squid during activation by glutamate. J Physiol, 369:183-197.

Fernandez J M, Neher E, and Gomperts B D (1984). Capacitance measurments reveal stepwise fusion events in degranulating mast cells. Nature, 312:453-455.

Ferris C D, Hunganir R L, and Snyder (1990). Calcium flux mediated by purified inositol 1,4,5-trisphosphate receptor in reconstituted lipid vesicles us allostrically regulated by adenine nucleotides. Proc Nat Acad Sci USA, 87:2147-2151.

Field A C, and Jenkinson D H (1987). The effect of noradrenaline on the

ion permeability of isolated mammalian hepatocytes, studied by intracellular recording. J Physiol, 392:493-512.

Finch E A, Turner T J, and Godlin S M (1991). Calcium as a coagonist of Inositol 1,4,5-trisphosphate induced calcium release. Science, 252:443-446.

Foster A, and Fagg G E (1984). Acidic amino acid binding sites in mammalian neuronal membrane: their characteristics and relationship to synaptic receptors. Brain Res Rev, 7:103-164.

Frankenhaeuser B, and Hodgkin A L (1957). The action of calcium on the electrical properties of squid axons. J Physiol, 137:218-244.

Fussle R, Bhakdi S, Sziegoleit A, Tranum-Jenson J, Kranz T, and Wellensiek H-J (1981). On the mechanism of membrane damage by Staphylococcus aureus α-toxin. J cell Biol, 91:83-94.

Garthwaite J, Charles S L, and Chess-Williams R (1988). EDRF as an intracellular messenger in the brain: release following activation of NMDA recptors. Nature, 336:385-388.

Garthwaite J, and Garthwaite G (1987). Cellular origins of cGMP responses to excitatory amino acid agonists in rat cerebellum *in vitro*. J Neurochem, 48:29-39.

Godfrey P P, Wilkins C J, Tyler W, and Watson S P (1988). Stimulatory and inhibitory actions of excitatory amino acids inositol phospholipid metabolism in rat cereberal cortex. Br J Pharmac, 95:131-138.

Gray P T A, Ogden D C, Trentham D R, and Wlaker J W (1989). Elevation of cytosolic free calcium by rapid photolysis of caged inositol trisphosphate in single rat parotid acinar cells. J Physiol, 410:90P.

Graziani L, Kaplan R, Escriva A, and Katzman R (1967). Calcium flux into the CSF during ventricular and venrtriculocisternal perfusion. Am J Physiol, 213(2):629-636.

Gurney A M, Tsien R Y, and Lester H (1986). Activation of a potassium current by a rapid photochemically generated step increase of intracellular calcium in rat sympathetic neurones. Proc Natl Acad Sci USA, 84:3496-3500.

Harkins A B, Kurebayashi N, Hollingworth S, and Baylor S M (1991). Absorbance and fhluorescence signals from the Ca^{2+} indicator Fluo-3 in intact twitch fibers frog muscle. Biophys Abs, 59:Tu-Pos53.

Hayashi T (1952). A physiological study of epileptic seizures following cortical stimulation and its application to human clinic. Jpn J Physiol, 3:46.

Hertz L (1979). Functional interactions between neurones and astrocytes I. Turnover and metabolism of putative amino acid transmitters. Prog Neurobiol, 13:277-232.

Hestrin S, Sah P, and Nicoll R A (1990). Mechanisms generating the time course of dual component excitatory synpatic curremts recorded in hippocampal slices. Neuron, 5:247-253.

Hodgkin A L, and Keynes R D (1957). Movements of labelled calcium is squid giant axons. J Physiol, 138:253-281.

Holmann M, Hartley M, and Heinemann S (1991). Ca^{2+} permeability of KA-AMPA-gated glutamate receptor channels depeneds on subunit composition. Science, 252:851-853.

Honore T, Davies S N, Drejer J, Fletcher E J, Jacobsen O, Lodge D, and Neilsen F E (1988). quinoxalinediones: Potent competetive non-NMDA glutamate receptor antagonists. Science, 241:701-701.

Horn R, and Marty A (1988). Muscurinic activation of ionic current smeasured by a new whole-cell recording method. J Gen Physiol, 92:145-159.

Houamed K M, Kuijper J L, Gilbert T L, Haldeman B A, O'Hara P J, Mulvihill E R, Almers W, and Hagen F S (1991). Cloning, expression, and gene structure of a G protein-coupled glutamate receptor from rat brain. Science 252, 1318-1321.

Howe J R, Cull-Candy S G, and Colquhoun D (1991). Currents through single glutamate receptor channels in outside-out patches frem rat cerebellar granule cells. J Physiol, 432: 143-202.

Howe J R, Colquhoun D, and Cull-Candy S G (1988). On the kinetics of the large conductance glutamate-receptor ion channels in rat cerebellar

granule neurones. Proceed Royal Society B, 233:407-422.

Huettner J E (1990). Glutamate receptor channels in rat DRG neurones: Activation by kainate and quisualate and blockade of desensitisation by Con A. Neuron, 5:255-266

Hume R I, Dingledine R, Heinemann S F (1991). Identification of a site in glutamate receptor subunits that controls calcium permeability. Science, 253:1028-1031.

Irvine R F, and Moor R M (1986). Micro-injection of inositol 1,3,4,5-tetrakisphosphate activates sea urchin eggs by a mechanism dependent on external calcium. Biochem L, 240:917-920.

Jahr C (1992). High probability opening of NMDA receptor channels by L-glutamate. Science, 255:470-472.

Johnson J W, and Ascher P (1987). Glycine potentiates the NMDA response in cultured mouse brain neurones. Nature, 325:529-531.

Johnston G A R, Curtis D R, Davies J, and McCulloch R M (1974). Nature, 248:804-805.

Jonas P, and Sakmann B (1992). Unitary stimulus evoked excitatory postsynaptic current sin CA3 pyramidal cells of rat hippocampal slices as resolved by patch clamp technique. J Physiol, 446:515P.

Kao J P Y, and Tsien R Y (1988). Ca^{2+} binding kinetics of Fura-2 and Azo-1 from temperauture-jump relaxation measurements. Biophys J, 53:635-639.

Kaplan J H, and Ellis-Davies G C (1988). Photolabile chelator for the rapid photorelease of divalent cations. Proc Nat Acad Sci USA, 55:6571-6575.

Kawagoe R, Onodera K, and Takeuchi A (1981). Release of glutamate at the crayfish neuromuscular junction. J Physiol, 312:225-236.

Kawai N, Yamagishi S, Saito M, and Furuya K (1983b). Specific antagonism of the glutamate receptor by an extract from the spider Araneus ventricosus. Toxicon, 21:438-440.

Kawai N, Yamagishi S, Saito M, and Furuya K (1983a). Blockade of synaptic

transmission in the squid giant synapse by a spider toxin (JSTX). Brain Res, 278:346-349.

Keller B U, Konnerth A, Yaari Y (1991). Patch clamp analysis of excitatory synaptic currents in granule cells of rat hippocampus. J Physiol, 435:275-293.

Kelly J S, and Gage P W (1969). L-Glutamate blockade of transmission at the giant synapse of the squid stellate ganglion. J Neurobiol, 1:209-219.

Kerry C J, Ramsey R L, Sansom M S P, and Usherwood P N R (1988). Single channel studies of non-competitive antagonism of a quisqualate-sensetive glutamate receptor by argiotoxin$_{636}$- a fraction isolated from orb-web spider venom. Brain Res, 459:312-327.

Keynes R D, and Lewis P R (1956). The intracellular calcium contents of some invertebrate nerves. J Physiol, 134:399-407.

Khodakhah K, Carter T D, Torok K, Ogden D, and Smith S M (1992). Patch permeabilisation with *Staphylococcal* α-toxin in whole cell recording. J Physiol, 452:160P.

Kitazawa T, Kobayashi S, Horituti K, Somlyo A V, and Somlyo A P (1989). Receptor-coupled, permeabilised smooth muscle. J Biol Chem, 264:5339-5342.

Kjems E (1963). Two variants of staphylococcus aureus Wood 46 (NCTC 7121) differing in respect to alpha toxin productionl. J Bact, 86:1127-1128.

Kleckner N W, and Dingledine R (1988). Requirment for glycine in activation of NMDA receptors expressed in *xenopus* oocytes. Science, 241:835-837.

Konishi M, Hollingworth S, Harkins A B, and Baylor S M (1991). Myoplasmic calcium transients in intact skeletal muscle fibers monitored with the fluorescent indicator Furaptra. J Gen Physiol, 97:271-301.

Korn S J, and Horn R (1989). Influence of sodium-calcium exchange on calcium current rundown and the duration of calcium-dependent chloride currents in pituitary cells, studied with whole cell and perforated patch recording. J Gen Physiol, 94:789-812.

Krnjevic K and Phillis J W (1963). Ionophoretic studies of neurones in the

mamalian cerebral cortex. J Physiol, 165:274-304.

Kuffler S W, and Yoshikami D (1975). The distribution of acetylcholine sensitivity at the postsynaptic membrane of vertebrate skeletal twitch muscles: Iontophoretic mapping in the micron range. J Physiol, 244:703-730.

Kumer K N, Tilakaratne N, Johnson P S, Allen A E, and Michaelis E K (1991). Cloning of the cDNA for the glutamate-binding subunit of an NMDA receptor complex. Nature, 354:70-73.

Kuno M, and Gardner P (1987). Ion channels activated by inositol 1,4,5-trisphosphate in plasma membrane of human T-lymphocytes. Nature 326:301-304.

Kutsuwada T, Kashiwabuchi N, Mori H, Sakimura K, Kushiya E, Araki K, Meguro H, Masaki H, Kumanishi T, and Arakawa M (1992). Molecular diversity of the NMDA receptor channel. Nature, 358:18-19.

Lind I, Ahnert-Hilger G, Fuchs G, and Gratzel M (1987). Purification of alpha toxin from staphylococcus areus and application to cell permibilisation. Analyt Biochem, 164:84-89.

Llano I, Dreessen J, Kano M, and Konnerth A (1991). Intradendritic release of calcium induced by glutamate in cerebellar Purkinje cells. Neuron, 7:577-583.

Llano I, Marty A, Armstrong C M, and Konnerth A (1991). Synaptic and agonist-induced excitatory currents of Purkinje cells in rat cerebellar slices. J Physiol, 434:183-213.

Luckhoff A, and Clapham D E (1992). Inositol 1,3,4,5-tetrakisphosphate actiavtes an endothelial Ca^{2+}-permeable channel. Nature, 355:356-358.

MacDermott A B, and Weight F F (1982). Action potential repolarisation involve a transient, Ca^{2+}-sensetive outward current in a vertebrate neurone. Nature, 300:185-188.

Maclennan D H (1970). Purification and properties of an adenosine trisphosphate from sarcoplasmic reticulum. J Biol Chem, 250:4508-4518.

Maeda N, Kawasaki T, Nakade S, Yokomoto N, Taguchi T, Kasai M, and

Mikoshiba K (1991). Structural and functional characterization of inositol 1,4,5-trisphosphate receptor channel from mouse cerebellum. J Biol Chem, 266:1109-1116.

Martell A E, and Smith R M (1985). Critical stability constants. Volume 5: First supplement. Plenum press, London. page 283.

Martin R, and Miledi R (1986). The form and dimensions of the giant synapse of the squid. Phil Trans R Soc Lond B, 311:355-377.

Marty A (1981). Ca-dependent K channels with large unitary conductance in chromaffin cell membranes. Nature, 291:497-499.

Marty A, and Neher E (1983). Tight-seal whole cell recording. In single channel-recording. B Sakmann, and E Neher, editors. Plenum Publishing Corp., New York, NY. 107-122.

Masu M, tanabe Y, Tsuchida K, Shigemoto R, and Nakanishi S (1991). Sequence and expression of a metabotropic glutaamte receptor. Nature, 349:760-765.

Mayer M L, and Westbrook G L (1987). Permeation and block of *N*-methyl-D-aspartic acid receptor channels by divalent cations in mouse central neurones. J Physiol, 394:501-527.

Mayer M L, MacDermott A B, Westbrook G L, Smith S J, and Baker J L (1987). J Neurosci, 7:3230.

Mayer M L, Westbrook G L, and Guthrie P B (1984). Voltage dependent block of Mg^{2+} of the NMDA responses in spinal cord neurones. Nature, 309:261-263.

McCray J A, and Trentham D R (1989). Properties and uses of photoreactive caged compounds. Annu Rev Biophys Chem, 18:239-270.

Meech R W (1972). Intracellular calcium injection causes increased potassium conductance in *Aplysia* nerve cells. Comp Biochem Physiol, 42A:493-499.

Meguro H, Mori H, Araki K, Kushiya E, Kutsuwada T, Yamazaki M, Kumanishi T, Arakawa M, Sakimura K, and Mishina M (1992). Functional

characterizarion of a hetromeric NMDA receptor expressed from cloned cDNAs. Nature, 357:70-74.

Messenger J B, De Santis A, and Ogden D C (1992). Chemical transmission at the squid giant syanpse. In 'Cephalopod Neurobiology'. Abbott N J, and Williamson R, Oxford Univ Press, in press.

Meyer T, Holowka D, and Stryer L (1988). Highly cooperative openning of calcium channels by inositol 1,4,5-trisphosphate. Science, 240: 653-656.

Mignery G A, Sudhof T C (1990). Structure and expression of the rat inositol 1,4,5-trisphosphate receptor. J Biol Chem, 265:12679-12685.

Miledi R (1967). Spontaneous synaptic potentials and quantal release of transmitter in the stellate ganglion of the squid. J Physiol, 192:370-406.

Miledi R (1969). Transimitter action in the giant synapse of the squid. Nature, 223:1284-1286.

Minta A, Kao J P Y, and Tsien R Y (1989). Fluorescent indicators for cytosolic calcium based on rhodamine and fluorescein chromophores. J Biol Chem, 264(14):8171-8178.

Mishina M, Sakimura K, Mori H, Kushiya E, Harabayashi M, Uchino S, and Nagahari K (1991). A single amino acid residue dteremine the Ca^{2+} permeability of AMPA-selective glutamate channels. Biochem Biophys Res Commun, 180:813-821.

Morgan J I, and Curran T (1988). Calcium as a modulator of the immediate-early gene cascade in neurones. Cell Calcium, 9:303-311.

Mori H, Masaki H, Yamakura T, and Mishina M (1992). Identification by mutagenesis of a Mg^{2+}-block site of the NMDA receptor channel. Nature, 358:673-675.

Moriyoshi K, Masu M, Ishii T, Shigemoto R, Mizuno N, and Nakanishi S (1991). Molecular cloning and characterization of the rat NMDA receptor. Nature, 354:31-37.

Murphy S N, and Miller R J (1988). A glutamate receptor regulates Ca^{2+} mobilisation in hippocampal neurones. Proc Natl Acad Sci USA, 85:8737-8741.

Nakanishi S (1992). Molecular diversity of glutamate receptors and implications for brain function. Science, 258:597-603.

Nakanishi S, Axel R, and Shneider N A (1992). Alternative splicing generates functionally distinct NMDA receptors. Proc Natl Acad Sci USA, 89:8552-8556.

Nakanishi N, Shneider N A, and Axel R (1990). A family of glutamate receptor genes: evidence for formation of hetromultimeric receptors with distinct channel properties. Neuron, 5:569-581.

Nicoletti F, Magri G, Ingrao F, Bruno V, Catania M V, Dell'Albani P, Condorelli D F, and Avola R (1990). Excitatory amino acids stimulate inositol phospholipid hydrolysis and reduce proliferation in cultured astrocytes. J Neurochem, 54:771-777.

Nicoletti F, Meek J L, Iadarola M J, Chuang D M, Roth B L, and Costa E (1986a). Coupling of inositol phospholipid metabolism with excitatory amino acid recognition sites in rat hippocampus. J Neurochem, 46:40-46.

Nicolettis F, Wroblewski J T, Novelli A, Alho H, Guidotti A, amd Costa E (1986b). The activation of inositol phospholipid metabolism as a signal transducing system for excitatory amino acids in primary cultures of cerebellar granule cells. J Neurosci, 6:1905-1911.

Nishizuka Y (1988). The molecular heterogeneity of protein kinase and its implications for cellular regulation. Nature, 334:661-665.

Nowak L, Bregestovski P, and Ascher P (1984). Magnesium gates glutamate-activated channels in mouse centeral neurones. Nature, 307:462-465.

Nowycky M C, Fox A P, and Tsien R W (1985). Three types of neuronal calcium channels with different calcium agonist sensitivity. Nature, 316:440-443.

Ogden D C, Capiod T, and Carter T D (1991). The delay in activation of plasmalemmal K conductance by Ca ions released by inositol trisphosphate in guinea-pig hepatocytes. J Physiol, 434:39P.

Ogden D C, Colquhoun D, Marshal C G (1987). Activation of nicotinic ion channels by acetylcholine analohues. In cellular and molecular basis of

cholinergic function, Ed Dowdall M J, and Hawthorne J N. Ellis Horwood, Chichester.

Ogden D C, and Capiod T (1990). Kinetics of the conductance evoked by noradrenaline, inositol trispohosphate or Ca^{2+} in guinea-pig isolated hepatocytes. J Physiol, 422:585-602.

Okamoto S (1951). Epileptogenic action of glutamate directly applied into the brain of animals and inhibitory effects of proteins and tissue emulsions on its action. J Physiol Soc Jpn, 13:555.

Otsu H, Yamamoto A, Maeda N, Mikoshiba K, and Tashiro Y (1990). Immunogold localisation of inositool 1,4,5-trisphosphate ($InsP_3$) receptor in mouse cerebellar Purkinje cells using three monoclonal antibodies. Cell Struc Func, 15:163-173.

Parker I and Ivora I (1990b). Inhibition by Ca^{2+} of inositol trisphosphate-mediated Ca^{2+} libration: a possible mechanism for oscillatory release of Ca^{2+}. Proc Natl Acad Sci USA, 87:260-264.

Parker I, and Ivora I (1990a). Localized all-or-none calcium liberation by inositol trisphosphate. Science, 250:977-979.

Patel J, Moore W C, Thompson C, Keith R A, and Salama A I (1990). Characterisation of the quisqualate receptor linked to phosphoinositide hydrolysis in neurocortical cultures. J Neurochem, 54:1461-1466.

Pearce B, Albrecht J, Morrow C, and Murphy S (1986). Astrocyte glutamate receptor activation promotes inositol phospholipid turnover and calcium flux. Neurosci Lett, 72:335-340.

Raju B, Murphy E, Levy L A, Hall R D, London R E (1989). A fluorescent indicator for measuring cytosolic free magnesium. Am J Physiol, 256:C540-C548.

Recasens M, Sassetti I, Nourigat A, Sladczek F, and Bockaert J (1987). Characterization of subtypes of excitatory amino acid receptors involved in the stimulation of inositol phosphate synthesis in rat brain synaptoneurosomes. Eur J Neursci, 141:87-93.

Reuter H, and Seitz N (1968). The dependence of calcium efflux from

cardiac muscle on temperature and external ion composition. J Physiol, 195:451-470.

Ross C A, Danoff S K, Schell M J, Snyder S H, and Ullrich A (1992). Three additional inositol 1,4,5-trisphosphate receptors: molecular cloning and different localisation in brain and peripheral tissue. Proc Natl Acad Sci USA, 89:4265-4269.

Ross C A, Meldoelsi J, Milner T A, Satoh T, Supattapone S, and Snyder S (1989). Inositol 1,4,5-trisphosphate receptor localized to endoplasmic reticulum in cerebellar Purkinje neurones. Nature, 339:468-470.

Sakurada K, Masu M, and Nakanishi S (1993). Alteration of Ca^{2+} permeability and sensitivity to Mg^{2+} and channel blockers by a single amino acid substitution in the NMDA receptor. J Biol Chem, 268:410-415.

Satoh T, Ross C A, Antonello V, Supattapone S, Pozzan T, Snyder S H, and Meldolesi J (1990). The inosiotol 1,4,5-trisphosphate receptor in cerebellar Purkinje cells: quantitative immunogold labeling reveals concentration in an ER subcompartment. J Cell Bio, 111:615-624.

Schatzmann H J (1966). ATP-dependent Ca^{++}-extrusion from human red cells. Experientia, 22:364-68.

Schoepp DD, and Johnson B G (1988). Selective inhibition of excitaory amino acid-stimulated phosphoinositide hydrolysis in the rat hippocampus by activators of protein kinase C. Biochem Pharmac, 37:4299-4305.

Shinozaki H, and Konishi S (1970). Actions of several antihelminthics and insectisides on rat cortical neurones. Brain Res, 24:368-371.

Silver R A, Traynellis S F, and Cull-Candy S G (1992). Rapid-time-course minature and evoked excitatory currents at the cerebellar synapses *in situ*. Nature, 355, 163-166.

Somlyo A V, Horiuti K, Trentham D R, Kitazawa T, and Somlyo A P (1992). Kinetics of Ca^{2+} release and contraction induced by photolysis og caged D-myo-inositol 1,4,5-trisphosphate in smooth muscle. The effects of heparin, procaine, and adenine nucleotides. J Biol Chem, 267:22316-22322.

Somlyo A V, Horiuti T, Katazawa T, Trentham D R, and Somlyo A P (1990).

Kinetics of $InsP_3$-induced calcium release in smooth muscle isolated from guinea pig portal vein. J Physiol, 429, 14P.

Stallcup W B, Bulloch K, and Baetge E E (1979). Coupled transport of glutamate and sodium in a cerebellar nerve cell line. J Neurochem, 32:57-65.

Stanley E F, and Adelman W J (1984). Direct access of ions to the squid stellate ganglion giant synapse by aortic perfusion: effects of calcium-free medium, lanthanum, and cadmium. Biol Bull, 167:467-476.

Stern P, Edwards F A, Sakmann B (1992). Fast and slow components of unitary EPSCs on stellate cells elicited by focal stimulation in slices of rat visual cortex. J Physiol, 449:247-278.

Stratton K R, Worley P F, and Baraban J M (1989). Excitation of hippocampal neurons by stimualtion of glutamate Q_P receptors. Eur J Pharm, 173:235-237.

Sugihara H, Moriyoshi K, Ishii T, Masu M, and Nakanishi S (1992). Structures and properties of seven isoforms of the NMDA receptor generated by alternative splicing. Biochem Biophys Res Commun, 185:826-832.

Sugiyama H, Ito I, and Hrrono C (1987). A new type of glutamate receptor linked to inositol phospholipid metabolism. Nature, 325:531-533.

Takahashi (1978). Intracellular recording from visually identified motoneurones in rat spinal cord slices. Proc R Soc Lond B, 202:417-421.

Takei K, Stukenbrok H, Metcalf A, Migery G A, Sudhof T C, Volpe P, and De Camilli P (1992). Ca^{2+} stores in Purkinje neurones: endoplasmic reticulum subcompartments demonstrated by the hetrogeneous distribution of the $InsP_3$ receptor, Ca^{2+}-ATPase, and calseqestrin. J Neurosci, 12:489-505.

Takemoto T, Takagi N, Nakajima T, Arihara S, and Koike K (1972). In 16th Symp Chem Nat Prod, Osaka, Japan.

Tanabe Y, Masu M, Ishii T, Shigemoto R, and Nakanishi S (1992). A family of metabotropic glutamate receptors. Neuron, 8:169-179.

Tang C M, Dichter M, and Morad M (1990). Modulation of the *N*-methyl-D-

aspartate by extracllular H^+. Proc Natl Acad Sci USA, 87;6445-6449.

Torok K, Patel J R, and Ferenzi M A (1990). Permeabilisation of isolated frog skeletal muscle fibres with α-toxin results in fibres with a competent sarcoplasmic reticulum. J Physiol, 434:6P.

Trautmann A, and Marty A (1984). Activation of Ca-dependent K channels by carbamoylcholine in rat lacrimal glands. Proc Natl Acad Sci USA, 81:611-615.

Traynelis S F, and Cull-Candy S G (1990). Proton inhibition of *N*-methyl-D-aspartate receptors in cerebellar neurones. Nature, 345:347-350.

Tsien R Y (1980). New calcium indicators and buffers with high selectivity against magnesium and protons: design, synthesis, and properties of prototype structures. Biochemistry, 19:2396-2404.

Tsien R Y, and Zucker R S (1986). Control of cytoplasmic calcium with photolabile tetracarboxylate 2-nitrobenzhyrol chelators. Biophys J, 50:843-853.

Verdoorn T A, Burnashev N, Monyer H, Seeburg P H, and Sakmann B (1991). Structural determination of ion flow through recombinant glutamate receptor channels. Science, 252:1715-1718.

Walker J W, Reid G P, McCray J A, and Trentham D R (1988). Photolabile 1-(2-nitrophenyl)ethyl phosphate esters of adenine nucleotide analohues. Synthesis and mechanism of photolysis. J Am Chem Soc, 110:7170-7177.

Walker J W, Somlyo A V, Goldman Y E, Somlyo A P, and Trentham D R (1987). Kinetics of smooth and skeletal muscle activation by laser pulsephotolysis of caged 1,4,5-trisphosphate. Nature, 327:249-252.

Walker J W, Reid G P, and Trentham D R (1989). Synthesis and properties of caged nucleotides. Meth Enzymol, 172:288-301.

Walker J W, Feeney J, and Trentham D R (1989). Photolabile precusrsors of inositol phosphates. Preparation and properties of 1-(2-nitrophenyl)ethyl esters of *myo*-inositol 1,4,5-trisphosphate. Biochemsitry, 28:3272-3280.

Watkins J C and Evans R H (1981). Excitatory amino acid trasnmitters.

Annual Rev Pharm and Toxic, 21:165:204.

Widdowson E M, and Dickerson J W T (1964). In Mineral Metabolism, ed Comar C L, Bronner F, 2:1-274. New York: Academic.

Worly P F, Baraban J M, Snyder S H (1989). Inositol 1,4,5-trisphosphate receptor binding: autoradiographic localization in rat brain. J Neurosci, 9:339-346.

Worly P F, Baraban J M, Colvin J S, Snyder S H (1987). Inositol trisphosphate localization in brain: variable stoichiometry with protein kinase C. Nature, 325:159-161.

Wyllie D J A, Traynelis S F, and Cull-Candy S G (1992). Multiple non-NMDA glutamate receptors in rat cerebellar granule neurones in explant cultures. J Physiol Proceed (in press).

Young J Z (1973). The giant fibre synapse of *Loligo*. Brain Res, 57:457-460.

Young J Z (1938). The functioning of the giant nerve fibres of the squid. J exp Biol, 15:170-185.

Young J Z (1939). Fused neurones and synaptic contacts in the giant nerve fibres of the cephalopods. Phil Trans R Soc Lond B, 229:465-503.